UNIVERSITY OF COPENHAGEN
FACULTY OF HEALTH AND MEDICAL SCIENCES

PhD Thesis

Jonas Vind

Chemical and Functional Characterization of Propolis and Its Potential in Type 1 Diabetes

22nd of May 2026

Preface

Author:	Jonas Vind
Title:	Chemical and Functional Characterization of Propolis and Its Potential in Type 1 Diabetes
Affiliations:	Bartholin Institute, Department of Pathology, Rigshospitalet Graduate School of Health and Medical Sciences, University of Copenhagen Graduate Programme in Immunology and Infectious Diseases
Principal supervisor:	Professor Dan Stærk, PhD
Primary co-supervisor:	Senior Researcher Knud Josefsen, MD, PhD
Co-supervisor:	Professor Søren Balling Engelsen, PhD
External Assessor:	Henrik Munch Jørgensen, MSc Eng, BSc

Project Website

Publications (peer- and non-peer-reviewed) and dissemination material associated with this PhD project, including a documentary illustrating the scientific process and research development, are available at www.propolisinitiative.dk.

Funding

This PhD project was funded under the scheme *Projekter i sektoren for biavlsprodukter 2023-2026*, administered by the Danish Agricultural Agency and co-financed by the European Union under the Common Agricultural Policy.

This thesis has been submitted to the Graduate School of Health and Medical Sciences, University of Copenhagen, on the 22nd of May 2026 for evaluation for the degree of PhD.

Acknowledgements

This thesis would not have been possible without the support and contributions of many people, to whom I am sincerely grateful.

I would like to begin by thanking Knud Josefsen for his consistently helpful and approachable nature, as well as his high scientific ambitions. Throughout my PhD, Knud created an environment that offered both freedom and motivation to grow while maintaining a calm, constructive atmosphere. I greatly appreciate the openness of our discussions, both scientific and non-scientific, and the freedom to express differing views, which I admittedly used to the full extent.

I also thank Søren Balling Engelsen for his consistently constructive and direct input, and for the challenging discussions that pushed me to think more critically and broaden my scientific perspective. His willingness to engage with unconventional ideas and challenge assumptions encouraged deeper reflection and has been an important part of my academic development.

I am grateful to Camilla Hartmann Friis Hansen for sharing her expertise and support in mice and immunology work, which were essential for this thesis. I also thank Dan Stærk for being part of my supervisory team and for supporting the project framework.

My sincere gratitude also goes to Henrik Munch Jørgensen, who co-initiated this project and laid its foundation. Although he is no longer with us and did not see the project's completion, his engagement and visions were instrumental in shaping its direction.

A special thanks also goes to Violetta Aru. Un sincero ringraziamento va a te per il tuo prezioso supporto e per tutto il tempo che hai speso ad aiutarmi durante questo dottorato. Il tuo contributo alla spettroscopia NMR, all'acquisizione e all'analisi dei dati e alla condivisione della tua competenza scientifica è stato fondamentale per questo lavoro. Ti sono inoltre molto grato per aver condiviso la cultura italiana e per il tuo aiuto nel farmi vivere la cultura sarda. Hai sempre offerto tutto con grande disponibilità. Grazie.

Finally, I would like to thank my friends and family for their continued presence. A special thank you goes to my fiancée and future wife, Alberte, for her constant support, understanding, and calm presence throughout everything. Your support for me has always been unwavering, and I am deeply grateful.

Table of contents

Manuscripts included

Manuscript I. Vind J, Aru V, Jørgensen HM, Antvorskov JC, Tekin H, Josefsen K, Engelsen SB. ***Comparative Spectroscopic Analysis of Bee Propolis: NIR, FT-IR, FT-Raman, and 1H NMR. Focus on Provenance and Antioxidative Correlation***.
Pharmacological Research - Natural products. DOI: 10.1016/j.prenap.2026.100578.
Corresponding author: Vind J

Manuscript II. Vind J, Engelsen SB, Jørgensen HM, Antvorskov JC, Josefsen K, Aru V. ***Comparative ^{1}H NMR Metabolomics between Scandinavian Propolis and Australian Propolis: The Quest to Identify Radical Scavenging Compounds***.
Magnetic Resonance in Chemistry. DOI: 10.1002/mrc.70082.
Corresponding author: Vind J

Manuscript III. Steintún M*, Vind J*, Hansen CHF, Larsen J, Duelund L, Bahij R, Jørgensen HM, Antvorskov JC, Markussen B, Aru V, Engelsen SB, Josefsen K. ***Linking propolis chemical composition and geographical origin to immunomodulatory effects in human immune cells***.
Journal of Ethnopharmacology. DOI: 10.1016/j.jep.2026.121867.
*Shared first authorship
Corresponding author: Vind J

Manuscript IV. Vind J, Hansen CHF, Steintún M, Krych L, Jørgensen HM, Antvorskov JC, Aru V, Engelsen SB, Josefsen K. ***Immunomodulatory Effects of Perorally Administered Propolis in Autoimmune Diabetes: A Preclinical Study in NOD Mice***.
Applied Food Research. Manuscript under review (AFRES-D-26-00715).
Corresponding author: Vind J

List of abbreviations

CD	Cluster of differentiation
DPPH	2,2-diphenyl-1-picrylhydrazyl
GAD65	Glutamic acid decarboxylase 65
HPLC	High-performance liquid chromatography
IA-2	Insulinoma-associated antigen-2
IFN	Interferon
IL	Interleukin
IR	Infrared
LPS	Lipopolysaccharide
MAPK	Mitogen-activated protein kinase
NF-κB	Nuclear factor kappa B
NIR	Near-infrared
NOD	Non-obese diabetic
PBMC	Peripheral blood mononuclear cell
PCA	Principal component analysis
PLS	Partial least squares
rPLS	Recursive weighted PLS
RSA	Radical scavenging activity
Th	T helper cells
TLR4	Toll-like receptor 4
TNF	Tumor necrosis factor
T1D	Type 1 diabetes
UV-Vis	Ultraviolet-visible
ZnT8	Zinc transporter 8
^{1}H NMR	Proton nuclear magnetic resonance

Abstract

Introduction: Type 1 diabetes is a chronic autoimmune disease characterized by progressive dysfunction and destruction of insulin-producing pancreatic β-cells. Although immunotherapies can delay disease progression, additional strategies that safely modulate immune processes during early disease development are still needed. Propolis, a resinous honey bee product rich in bioactive compounds, is widely used for its curative properties and has been reported to exhibit both antioxidative and immunomodulatory effects. However, its pronounced chemical complexity and variability hinder standardization and reproducibility of its biological effects, thereby complicating its potential clinical integration. The aim of this thesis was to establish a framework linking propolis composition to its functional properties, and to determine whether dietary propolis can modulate immune processes relevant to type 1 diabetes development.

Methods: The chemical composition of propolis from different geographical origins and bee species, including cerumen from stingless bees, and its link with antioxidative activity were investigated using non-targeted spectroscopic techniques, including infrared, near-infrared, Raman, and proton nuclear magnetic resonance spectroscopy, combined with chemometric modeling. Immunomodulatory effects were evaluated in human immune cells, while liquid chromatography was used to identify compounds associated with these responses. Finally, the impact of dietary propolis supplementation on autoimmune diabetes development was investigated in the non-obese diabetic mouse model.

Results: Distinct geographical chemotypes were identified, with Scandinavian propolis enriched in aromatic compounds and exhibiting greater antioxidative and anti-inflammatory properties than Australian samples, while cerumen displayed a distinct terpenoid-rich profile. Spectroscopic and chemometric analyses enabled prediction of antioxidative capacity from chemical fingerprints, with near-infrared spectroscopy providing the most accurate predictions and demonstrating strong potential as a rapid standardization tool. Further analyses identified *p*-coumaric acid and ferulic acid as descriptors of antioxidative activity, and chrysin as an independent contributor to anti-inflammatory effects. *In vivo*, dietary supplementation delayed autoimmune diabetes onset, modulated T cell distribution and immune signaling, and altered gut microbiota composition. Together, these findings demonstrate that the biological activity of propolis is reflected by its chemical fingerprint and support its further evaluation as a dietary immunomodulatory strategy in autoimmune disease contexts.

Resumé

Introduktion: Type 1-diabetes er en kronisk autoimmun sygdom karakteriseret ved progressiv dysfunktion og destruktion af de insulinproducerende β-celler i bugspytkirtlen. Selvom immunterapi kan forsinke sygdomsprogressionen, er der fortsat behov for strategier, der sikkert kan modulere immunprocesser i de tidlige stadier af sygdomsudviklingen. Propolis, et harpikslignende produkt fra honningbier rigt på bioaktive forbindelser, er bredt anvendt for sine helbredende egenskaber og er rapporteret til at have både antioxidative og immunmodulerende effekter. Dets markante kemiske kompleksitet og variation vanskeliggør dog standardisering og reproducerbarhed af dets biologiske effekter, og forhindrer dermed potentiel klinisk integrering. Formålet med denne afhandling var at udvikle et analytisk grundlag, der kobler den kemiske sammensætning af propolis til de funktionelle egenskaber samt at undersøge, om diætær propolis kan modulere immunprocesser relevante for udviklingen af type 1-diabetes.

Metoder: Den kemiske sammensætning af propolis fra forskellige geografiske oprindelser og biarter, inklusiv *cerumen* fra brodløse bier, og dens sammenhæng med antioxidativ aktivitet blev undersøgt ved hjælp af ikke-målrettede spektroskopiske teknikker, herunder infrarød, nær-infrarød, Raman og protonkernemagnetisk resonans spektroskopi, kombineret med kemometrisk modellering. Immunmodulerende effekter blev undersøgt i humane immunceller, mens væskekromatografi blev anvendt til at identificere forbindelser associeret med disse responser. Effekten af diætær propolis på udviklingen af autoimmun diabetes blev desuden undersøgt i *non-obese diabetic* musemodellen.

Resultater: Der blev identificeret tydelige geografiske kemotyper, hvor skandinavisk propolis var beriget med aromatiske forbindelser og udviste stærke antioxidative og anti-inflammatoriske egenskaber sammenlignet med australsk propolis, mens *cerumen* havde en distinkt terpenoidrig profil. Spektroskopiske og kemometriske analyser muliggjorde forudsigelse af antioxidativ kapacitet ud fra kemisk fingeraftryk, hvor nær-infrarød spektroskopi udviste de mest præcise forudsigelser og et stort potentiale til standardisering af propolis. *p*-Coumarinsyre og ferulinsyre blev identificeret som beskrivende stoffer for den antioxidative aktivitet, og chrysin som en uafhængig bidragsyder til antiinflammatoriske effekter. *In vivo* forsinkede diætær propolis sygdomsdebut af autoimmun diabetes, modulerede T-celle distribution og immunologiske signalveje samt ændrede tarmens mikrobiota. Samlet set viser disse resultater, at den biologiske aktivitet af propolis afspejler dets kemiske fingeraftryk, og understøtter dets videre evaluering som en diætær immunmodulerende strategi i forbindelse med autoimmune sygdomme.

1 Introduction

Type 1 diabetes (T1D) is a chronic autoimmune disease characterized by progressive dysfunction and destruction of insulin-producing pancreatic β-cells, resulting in loss of endogenous insulin production[1, 2]. More than 9 million people worldwide live with T1D, with approximately half a million new cases diagnosed annually[3, 4]. Although exogenous insulin therapy is well established following clinical onset, individuals with T1D face a life expectancy reduced by more than a decade compared to the general population, rendering diagnosis a life-altering event with substantial impacts on quality of life and healthcare-related costs[5, 6].

Prior to clinical onset, T1D develops over a prolonged phase marked by persistent immunological dysregulation and pancreatic inflammation[7]. Clinical interventions targeting these autoimmune processes before disease onset have demonstrated that modulation of disease progression is possible. Notably, the anti-cluster of differentiation 3 (anti-CD3) monoclonal antibody teplizumab was shown to significantly delay progression to stage 3 T1D and has subsequently become the first marketed immunotherapy for this indication[8, 9]. However, such treatments are not universally effective and may be associated with adverse events, highlighting the need for alternative or supplementary strategies that can safely modulate autoimmune disease development, particularly in the preclinical stages[8, 9]. In this context, complementary immunomodulatory strategies, including naturally derived remedies with potential for safe long-term use, may represent valuable approaches. Propolis is a resinous substance produced by honey bees and constitutes a chemically complex matrix, rich in bioactive compounds, particularly polyphenols[10]. It has a long history of use in traditional medicine[11] and has been reported to exhibit antioxidative and immunomodulatory properties, suggesting potential to modulate processes involved in autoimmune disease development[12, 13].

A major challenge in propolis research is its pronounced chemical complexity and variability arising from differences in botanical source, geographical origin, and bee species[14]. This variability complicates comparisons between studies, limits the reproducibility of functional effects, and hinders standardization. Since specific compounds have been repeatedly linked to the pharmacological activity of propolis, most compositional studies focus on the identification of these already well-characterized polyphenolic constituents using targeted analytical techniques[15-17]. High-performance liquid chromatography (HPLC) is often employed for this purpose, as it offers high selectivity and enables straightforward quantification of polyphenolic compounds[17, 18]. However, its targeted nature

provides limited insight into the holistic chemical fingerprint of propolis. Thus, while identification of specific molecules may serve as an indicator of pharmacological potential, the absence of a comprehensive view of chemical composition risks overlooking important contributors to biological activity. An approach to address this limitation is to use spectroscopic techniques, including vibrational spectroscopy such as infrared (IR), Raman, and near-infrared (NIR) spectroscopy, as well as proton nuclear magnetic resonance (^{1}H NMR) spectroscopy, which enable holistic, non-targeted chemical profiling of complex matrices[19-22]. When combined with chemometric modeling, chemical fingerprints can be linked to functional assays, providing an unbiased connection between chemistry and functionality[23]. However, associations derived from *in vitro* data do not necessarily translate into accurate predictions of biological effects *in vivo*, underscoring the importance of evaluation in disease-relevant animal models. For T1D, the non-obese diabetic (NOD) mouse is a well-established model that enables investigation of whether oral administration of propolis can modulate inflammatory processes and delay or inhibit disease onset[24].

The present thesis therefore integrates chemical and functional characterization with *in vivo* disease evaluation to systematically investigate the potential of propolis as a dietary immunomodulatory strategy in the context of T1D development.

1.1 Hypothesis and objectives

It is hypothesized that propolis, when administered as a dietary supplement, can modulate immune responses, thereby delaying the development and progression of T1D.

To address this hypothesis, the objectives of this thesis were to:

i. Characterize the chemical fingerprint of propolis using non-targeted spectroscopic techniques and chemometric analysis, and link chemical composition to functional properties, providing the basis for subsequent immunological and *in vivo* investigations.
ii. Assess the immunomodulatory effects of propolis in human peripheral blood mononuclear cells (PBMCs) by evaluating propolis' influence on inflammatory cytokine responses and identifying compounds associated with these effects.
iii. Evaluate the effect of dietary propolis supplementation on T1D development *in vivo*, using the NOD mouse model to determine whether propolis can inhibit or modulate immune processes involved in the development of T1D and potentially delay disease onset.

2 Theoretical background

2.1 Type 1 diabetes

T1D is an autoimmune disease in which immune-mediated dysfunction and destruction of insulin-producing pancreatic β-cells[2] results in insulin deficiency and the need for lifelong exogenous insulin therapy. The disease most commonly develops in children and young adults[25] and has a substantial impact on the quality of life[3, 4].

The following sections describe the immunopathogenesis and clinical stages of T1D and outline current and emerging pharmacological strategies to modulate disease progression.

2.1.1 Immunopathogenesis of type 1 diabetes

Both genetic susceptibility[26] and environmental exposures[27] contribute to the initiation of T1D, whereas disease progression is primarily driven by immune-mediated inflammatory processes within the pancreatic islets[28]. This section outlines the anatomical and functional characteristics of the islets, the initiation of islet autoimmunity, and the immune mechanisms responsible for β-cell dysfunction and loss.

2.1.1.1 Pancreatic islet structure and β-cell vulnerability

The pancreas consists of an exocrine compartment involved in digestion, and an endocrine compartment composed of the islets of Langerhans[29]. These islets contain several hormone-producing cell types, predominantly insulin-secreting β-cells, which play a central role in glucose homeostasis[29].

Due to their high metabolic activity, β-cells are particularly susceptible to cellular stress[30]. Moreover, the rich vascularization of the islets, which enables rapid hormone release, also increases exposure to circulating immune cells[30]. Under conditions of immune dysregulation in early T1D, this anatomical and functional environment may facilitate immune recognition of β-cell antigens and amplify local inflammatory responses, thereby contributing to disease progression[31].

2.1.1.2 Initiation of islet autoimmunity

T1D is initiated by a breakdown of immune tolerance to pancreatic β-cell antigens, leading to activation of autoreactive T cells[32]. The earliest detectable markers of islet autoimmunity are autoantibodies directed against insulin, glutamic acid decarboxylase 65 (GAD65), insulinoma-associated antigen-2 (IA-2), and zinc transporter 8 (ZnT8)[7]. These autoantibodies may be detected

months to years before diagnosis and strongly predict disease progression, particularly when multiple autoantibodies are present[33]. Although they reflect ongoing autoimmunity, β-cell damage is predominantly mediated by cellular immune mechanisms[28]. Notably, β-cell destruction has traditionally been considered central to T1D pathogenesis, accumulating evidence in humans indicates that a considerable fraction of β-cells persists even in long-standing disease[34]. These residual cells often exhibit impaired insulin secretion, dedifferentiation, or functional exhaustion rather than complete elimination, suggesting that β-cell dysfunction, alongside immune-mediated cytotoxicity, contributes to disease progression[34].

Nevertheless, immune-mediated β-cell injury remains central to T1D pathogenesis. Progressive loss of functional β-cell mass leads to clinical insulin deficiency. The immune mechanisms underlying this process are outlined below.

In T1D, β-cell damage is driven primarily by antigen-specific cellular immune responses rather than by humoral mechanisms[35]. Autoreactive T cells recognize epitopes derived from β-cell autoantigens, including stress-induced antigens generated during β-cell dysfunction, and mediate direct cytotoxicity (Figure 1)[36].

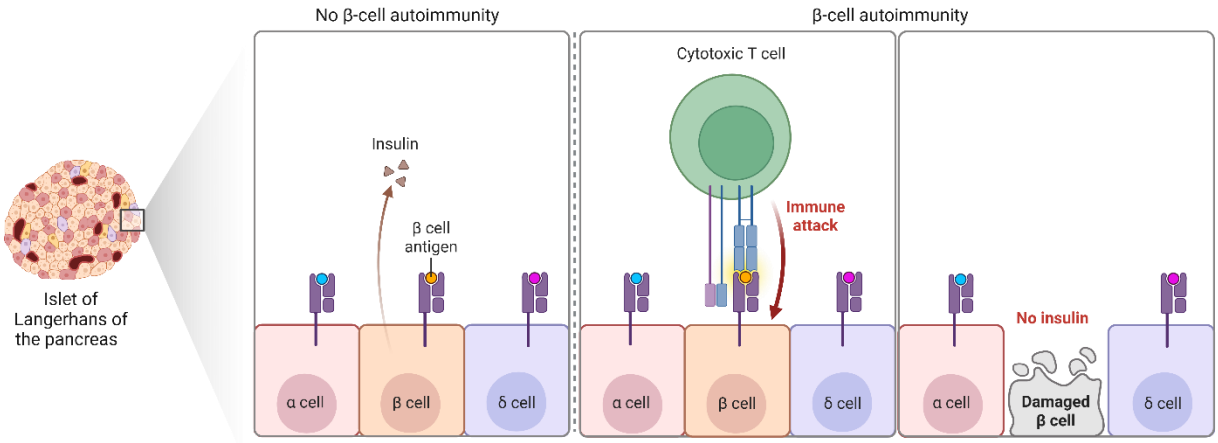

Figure 1. Autoimmune-mediated β-cell damage in pancreatic islets of Langerhans. Cytotoxic T cells target and damage insulin-producing β-cells, resulting in reduced insulin secretion and hyperglycemia[36]. Created with BioRender.com

Innate immune cells such as macrophages further contribute to local inflammation through antigen presentation and production of pro-inflammatory cytokines, which increase the susceptibility of β-cells to immune recognition[37]. Together, these immune mechanisms drive progressive β-cell

dysfunction and loss, leading to declining insulin secretion and progression toward clinically manifest diabetes.

2.1.1.3 Clinical stages of disease progression

Following the initiation of islet autoimmunity, individuals may remain normoglycemic for prolonged periods despite ongoing immune activation and progressive β-cell injury[7]. This phase corresponds to stage 1 T1D, defined by the presence of islet autoantibodies in the absence of dysglycemia or clinical symptoms[7]. During this stage, residual β-cell mass and functional reserve are sufficient to maintain glucose homeostasis.

As β-cell impairment progresses, insulin secretory capacity declines, leading to reduced glucose regulation and progression to stage 2 T1D, characterized by asymptomatic impaired glucose tolerance[33]. Continued loss of β-cell function ultimately results in stage 3 T1D, marked by sustained hyperglycemia and clinical diagnosis[33].

2.1.2 Clinical immunomodulatory strategies

Given that T1D progression is driven by autoimmune β-cell impairment[2], pharmacological strategies have focused on modifying the underlying immune response. These approaches include broad immunosuppression and targeted immune modulation[38].

2.1.2.1 Broad immunosuppression

Early clinical efforts relied on broad immunosuppressive agents such as cyclosporine, a calcineurin inhibitor that suppresses T cell activation, in individuals with newly diagnosed stage 3 T1D. These studies provided proof-of-concept that immune intervention can transiently preserve C-peptide levels (a marker of endogenous insulin production)[39, 40] and increase rate and length of remissions[41]. However, limited specificity and potential toxicity restricted long-term applicability[38].

2.1.2.2 Targeted immune modulation

Subsequent therapeutic strategies shifted toward more selective immune modulation, particularly targeting T cell activation. These include anti-CD3 monoclonal antibodies such as teplizumab, which has become the first approved disease-modifying therapy for individuals with stage 2 T1D to delay progression to clinical (stage 3) disease[8, 9]. CD3 is a key signaling component of the T cell receptor complex required for T cell activation[42]. Thus, by binding to CD3, teplizumab modulates T cell responses, reducing the autoimmune damaging of β-cells and thereby delaying progression to clinical T1D[43]. More recently, frexalimab, evaluated in the FABULINUS trial, has targeted the CD40L

pathway[44]. CD40L is a critical costimulatory molecule required for full T-cell activation and disruption of CD40-CD40L interactions thus limiting pathogenic immune activation[45].

Overall, pharmacological modulation of T1D progression remains an evolving field. Although targeted immune therapies demonstrate that disease modification is achievable, substantial challenges remain. Robust disease control may require early intervention and complementary strategies that modulate autoreactive immune responses. These challenges highlight the need for novel approaches capable of selective immune modulation and supporting β-cell function without broad immunosuppression. In this context, naturally derived products with immunomodulatory properties, such as propolis, may represent complementary strategies worthy of investigation.

2.2 Propolis

Propolis, derived from the Greek words *pro* ('before' or 'in defense of') and *polis* ('city'), is a resinous substance produced by bees, most commonly the honey bee (*Apis mellifera*)[11] (Figure 2). Within the hive, propolis serves structural and protective functions by sealing crevices, reinforcing hive structure, and acting as a chemical defense against microbial threats[46].

Figure 2. Representative samples of raw propolis from Denmark (left), Norway (middle), and Australia (right).

Propolis has been used for centuries in traditional medicine due to its purported curative properties[11]. However, its adoption into modern clinical medicine has been limited partly by its chemically complex and variable composition, which hinders standardization[47, 48], as well as by a relative lack of high quality randomized controlled clinical trials to establish consistent efficacy.

The following section describes the chemical composition of honey bee propolis, its key pharmacological properties, and the challenges associated with standardization and clinical integration. The section focuses on poplar-type propolis, the predominant chemotype in Denmark and Europe in general[49] as this has been most extensively investigated in the present work.

2.2.1 Chemical composition

The chemical composition of propolis is complex; however, it can be divided into two main fractions; a wax fraction and a resin fraction, the latter containing the biologically active compounds[11, 50].

While beeswax is synthesized by bees via specialized abdominal glands[51], the resin fraction is derived from plant materials such as bark, buds, and sap collected by forager bees[52]. These components are subsequently combined with salivary secretions to form propolis[52]. Beeswax is composed mainly of saturated hydrocarbons along with their ester and acid derivatives[53, 54]. In contrast, the resin fraction represents the chemically complex and biologically active component of propolis[52]. It is particularly rich in terpenoids and polyphenolic compounds, primarily flavonoids and phenolic acids, including characteristic constituents of poplar-type propolis (i.e., propolis derived primarily from *Populus* species) such as chrysin, pinocembrin, galangin, ferulic acid, *p*-coumaric acid, and caffeic acid (Figure 3)[55, 56].

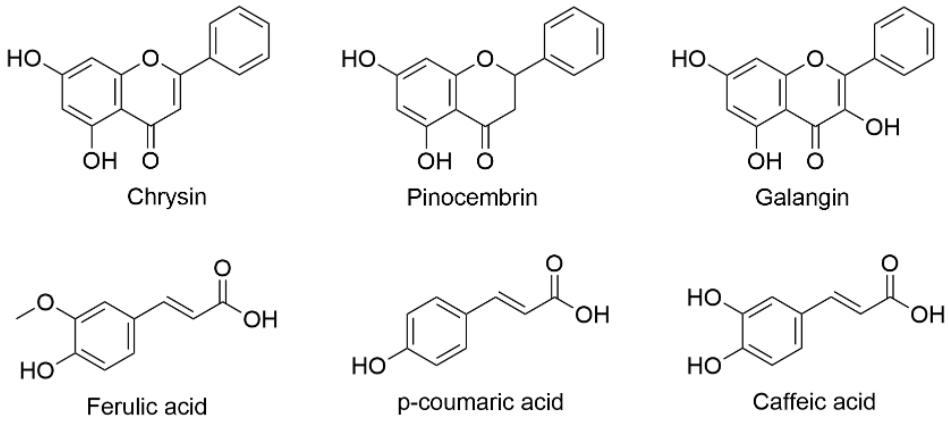

Figure 3. Representative polyphenolic compounds identified in poplar-type propolis.

While poplar-type propolis is comparatively well characterized, the chemical composition varies considerably depending on geographic origin, local flora, and bee species[57-59]. The polyphenolic fraction is often the primary focus of variation analyses due to its pharmacological relevance[11]. Both total polyphenol content and the relative abundance of individual compounds have been shown to differ between samples, even when collected in close geographic proximity[60, 61]. Such variability is therefore an important consideration when evaluating propolis for potential therapeutic applications.

2.2.2 Pharmacological and immunomodulatory properties

While terpenoids have demonstrated biological activity[62], the pharmacological properties of propolis are largely attributed to its high content of polyphenolic compounds[63], and these will therefore be the focus of the following sections.

2.2.2.1 Antioxidative mechanisms

Polyphenols contribute to the antioxidative properties of propolis through their ability to scavenge reactive oxygen species by donating hydrogen atoms or electrons, thereby stabilizing free radicals and limiting oxidative stress[64, 65]. This activity is structurally driven by their aromatic ring systems and conjugated π-electron networks, which enable delocalization of unpaired electrons following radical formation[64]. Such electron delocalization increases the stability of the resulting phenoxyl radicals[66] and underlies the intrinsic radical-scavenging capacity of polyphenolic compounds.

2.2.2.2 Anti-inflammatory and immunomodulatory mechanisms

In addition to their antioxidative effects, polyphenols contribute to the anti-inflammatory activity of propolis through modulation of key inflammatory signaling pathways. A central mechanism involves inhibition of nuclear factor kappa B (NF-κB)[12], a pivotal transcription factor activated downstream of Toll-like receptor 4 (TLR4), the receptor for lipopolysaccharide (LPS)[67] (Figure 4). Activation of TLR4 initiates signaling cascades that lead to NF-κB-mediated transcription of pro-inflammatory genes, including cytokines and components required for inflammasome priming[67].

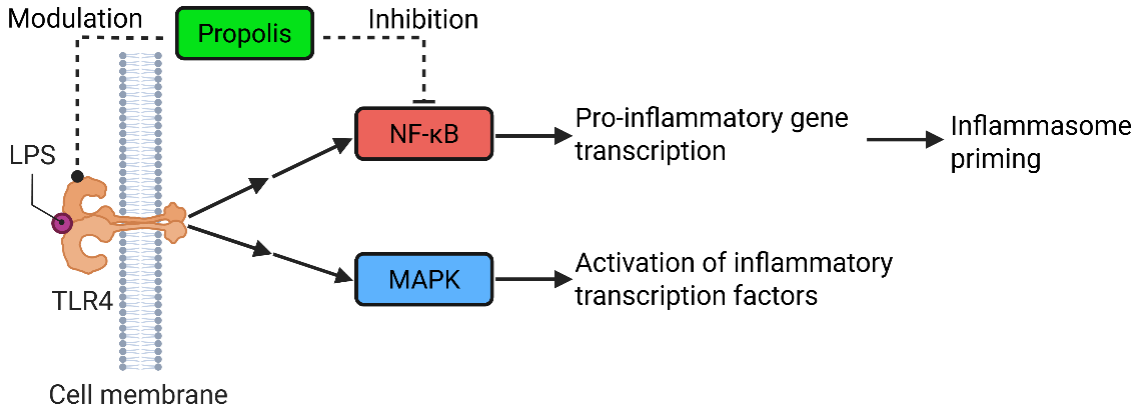

Figure 4. LPS binding to TLR4 activates NF-κB and MAPK signaling pathways. NF-κB drives pro-inflammatory gene transcription, including inflammasome priming, while MAPK contributes to inflammatory responses. Propolis is proposed to modulate TLR4 signaling and modify downstream inflammatory signaling. Created with BioRender.com.

Propolis has also been reported to modulate TLR4 signaling directly[68, 69], affecting other downstream pathways such as mitogen-activated protein kinases (MAPKs)[70]. However, the direction of this modulation is not uniformly suppressive, as increased TLR4 expression and NF-κB activation have also been reported following propolis exposure[68], highlighting that its immunomodulatory effects may be context- and composition-dependent.

Through these mechanisms, propolis exhibits multi-target immunomodulatory activity and thus considerable pharmacological potential. This broad biological activity reflects its chemically diverse composition. However, as discussed previously, inherent variability in chemical profiles between propolis samples may lead to corresponding differences in biological effects. Consequently, issues related to standardization and reproducibility remain significant challenges for its integration into modern clinical practice.

2.2.3 Challenges in standardization and clinical integration

The clinical integration of propolis remains limited, and a major challenge is its inherent chemical variability, which complicates standardization and reproducibility[11, 48]. Efforts to address this include the development of standardized extracts[71] and the introduction of the international standard ISO 24381:2023, which provides specifications for bee propolis. However, propolis is marketed as a dietary supplement rather than as a medicinal product[72], which entails less stringent regulatory scrutiny regarding safety and efficacy compared to pharmaceutical drugs[73]. Although clinical trials have been conducted, variability in composition, the absence of harmonized standards, and less rigorous regulation remain key barriers to broader clinical adoption[47, 74].

Given this chemical complexity and variability, comprehensive characterization of propolis requires analytical approaches capable of capturing holistic compositional profiles rather than targeting individual compounds in isolation. The following section introduces the spectroscopic and chemometric techniques applied in this thesis for that purpose

2.3 Analytical techniques

To characterize the chemical fingerprints of propolis and to identify specific constituents of interest, this thesis employed a range of complementary analytical techniques. This section provides an overview of the applied spectroscopic and chromatographic methods, outlining their theoretical principles and analytical relevance.

2.3.1 Spectroscopy

Spectroscopy is based on the interaction between electromagnetic radiation and matter[75]. Spectroscopic techniques are generally rapid, non-destructive, and highly sensitive, providing information about the chemical composition and structural characteristics of a sample[76]. Commonly used spectroscopic methods include vibrational spectroscopy techniques, such as IR, NIR and Raman, as well as ^{1}H NMR spectroscopy, all of which have been extensively applied in this thesis.

2.3.1.1 Principles of spectroscopic analysis

When electromagnetic radiation interacts with matter, absorption or scattering may occur depending on both the properties of the radiation and the molecular characteristics of the sample[77]. Atoms and molecules possess discrete, quantized energy levels (v), and transitions between these levels occur when the photon energy matches the energy difference between them[78]. The nature of the transition is thus governed by the photon energy of the incident radiation, and accordingly different regions of the electromagnetic spectrum probe different molecular energies (Figure 5).

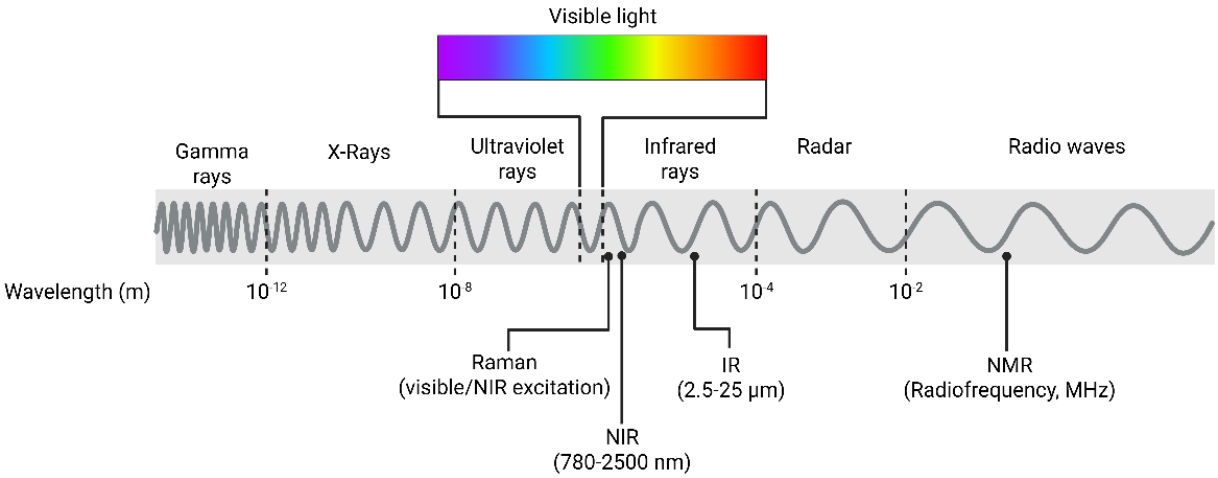

Figure 5. The electromagnetic spectrum[79] highlighting the spectral regions relevant to the spectroscopic methods used in this thesis. Created with BioRender.com.

IR and NIR radiation interact primarily with molecular vibrational energy levels, whereas Raman spectroscopy probes the same vibrational energy differences through inelastic scattering of light[80]. NMR spectroscopy, in contrast, utilizes radiofrequency radiation to induce transitions between nuclear spin states in the presence of an external magnetic field[81]. Each spectroscopic technique thus scrutinizes distinct molecular properties and provides complementary structural information. Each of these techniques is described in greater detail below.

2.3.1.2 Vibrational spectroscopy

Vibrational spectroscopy probes the vibrations of atoms within a molecule as they oscillate around their equilibrium bond lengths and angles[80]. These vibrations occur as characteristic stretching and bending modes that are often associated with specific chemical bonds or functional groups. IR, NIR, and Raman spectroscopy detect these vibrational transitions through different physical mechanisms[80].

Infrared spectroscopy

In IR spectroscopy, absorption occurs when the energy of the incident radiation matches the energy difference between two quantized vibrational states[82]. When this resonance condition is fulfilled, the electric field of the radiation can interact with a molecular vibration that produces a change in the dipole moment of the molecule[82]. A vibrational mode is therefore IR-active only if its dipole moment varies during the vibration. The most intense transitions typically correspond to the fundamental vibrational transition ($v = 0 \rightarrow 1$), which involves excitation from the vibrational ground state to the first excited vibrational level[82] (Figure 6a). Vibrations involving polar bonds, such as carbonyl (C=O) groups, usually generate large changes in dipole moment and therefore give rise to strong IR absorption bands[83]. Consequently, IR spectroscopy is particularly sensitive to functional groups with significant charge separation or uneven electron distribution[83].

Near-infrared spectroscopy

NIR spectroscopy likewise relies on absorption processes, occurring when the energy of the incident radiation matches the energy difference between quantized vibrational states. However, in contrast to IR spectroscopy, NIR predominantly probes overtone (e.g., $v = 0 \rightarrow 2$, $0 \rightarrow 3$) and combination band transitions rather than the fundamental transition[84] (Figure 6a). These transitions arise because real molecular vibrations deviate from ideal harmonic oscillator behavior[85]. In an ideal harmonic system, only fundamental transitions ($\Delta v = \pm 1$) are allowed[85]. However, molecular vibrations are anharmonic, meaning that the potential energy curve deviates from perfect quadratic form and the vibrational energy levels are not evenly spaced[85]. This anharmonicity relaxes the strict selection rules and permits overtone and combination transitions to occur[85]. However, these higher-order transitions involve smaller changes in dipole moments and are therefore much weaker than fundamental absorptions. Consequently, NIR bands are broader and less well resolved than those in mid-IR spectroscopy, resulting in overlapping features that reflect integrated vibrational contributions from multiple molecular groups rather than isolated functional modes. The most intense overtones

arise from the most anharmonic bond vibrations, particularly O-H (omnipresent in carbohydrates and water), N-H (predominantly found in proteins), and C-H (omnipresent in fats). This makes NIR spectroscopy particularly suited for quantitative analysis of bulk properties of biological samples.

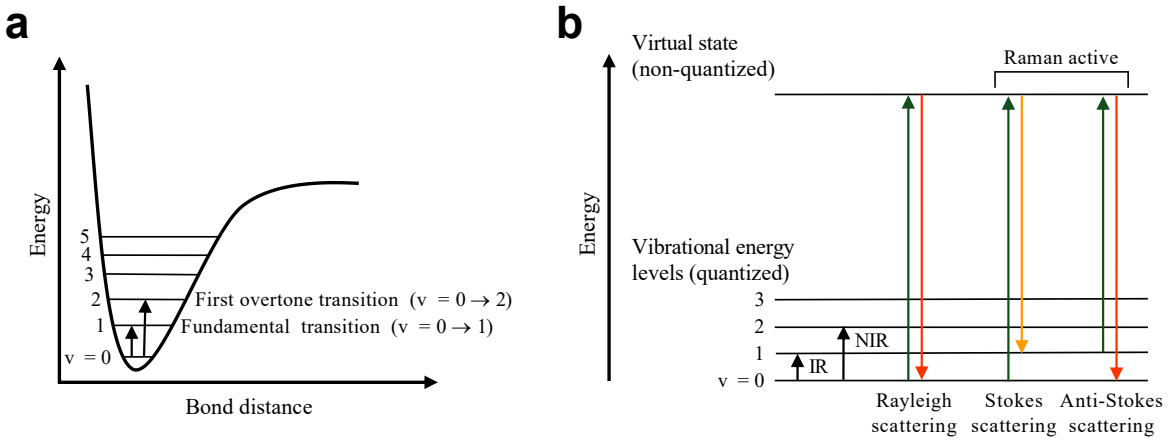

Figure 6. Vibrational transitions probed by IR, NIR, and Raman spectroscopy. (a) IR probes the fundamental vibrational transition, while the anharmonic nature of molecular vibrations gives rise to unequally spaced energy levels and allows NIR to probe overtone transitions[86]. (b) Raman scattering involves excitation to a virtual, non-quantized state. Rayleigh scattering is elastic, with the molecule returning to its original vibrational state (v=0) and is therefore not Raman active. Stokes scattering occurs when a molecule relaxes to a higher vibrational level than its initial state, whereas Anti-Stokes scattering originates from a thermally populated excited state and relaxes to a lower energy state; both are Raman-active[85].

Raman spectroscopy

In contrast to IR and NIR spectroscopy, Raman spectroscopy is based on inelastic scattering of light rather than direct absorption[87]. Upon irradiation, the oscillating electric field of the incident light induces a temporary distortion of the molecular electron cloud, transiently promoting the molecule to a non-quantized virtual state[87] (Figure 6b). The molecule then relaxes to a vibrational energy level. If the molecule returns to the same vibrational level from which it started, the scattered photon retains the same energy as the incident photon[87]. This process is known as Rayleigh scattering and does not involve a change in vibrational energy; therefore, it does not constitute the Raman effect[87]. Raman scattering arises from inelastic processes in which the molecule relaxes to a different vibrational level than its initial state. If the molecule relaxes to a higher vibrational level (e.g., $v = 0 \rightarrow 1$), the scattered photon has lower energy, producing a Stokes shift[87]. Conversely, if the molecule relaxes to a lower vibrational level (e.g., $v = 1 \rightarrow 0$), the scattered photon gains energy, resulting in an anti-Stokes shift[87]. Under ambient conditions, most molecules reside in the vibrational ground state, and

Stokes scattering is therefore more intense. In practical Raman measurements, only the Stokes region is typically recorded. Raman activity requires a change in molecular polarizability during vibration, corresponding to deformation of the electron density[87]. Vibrations involving distortion of easily polarizable electron clouds, such as stretching of non-polar double bonds (e.g., C=C), therefore typically produce strong Raman signals[88]. Thus, Raman spectroscopy is especially sensitive to symmetric and non-polar bonds.

Complementarity of vibrational techniques in complex matrices

Because IR, NIR, and Raman spectroscopy probe molecular vibrations through different physical mechanisms, and spectral regions, some vibrational modes may be prominent in one technique but weak or absent in another. The three methods therefore provide complementary structural information[80].

In chemically complex matrices such as propolis, vibrational spectra exhibit extensive band overlap arising from numerous structurally diverse constituents[89]. Rather than yielding isolated signals from individual compounds, the spectral response reflects the collective vibrational contributions of multiple molecular species. This is particularly evident in the NIR region, where overtone and combination bands produce broad, overlapping features that are difficult to interpret through direct peak assignment. Consequently, interpretation often relies on multivariate analysis rather than peak-based identification[90].

Vibrational spectroscopy is therefore well suited for non-targeted chemical profiling, where the complete spectral pattern is treated as a compositional fingerprint rather than a source of detailed structural elucidation. NIR measurements, in particular, capture global compositional variation and matrix level characteristics[91], while IR and Raman provide complementary information on specific functional groups and bond types. The minimal sample preparation and rapid acquisition make vibrational spectroscopy particularly advantageous for profiling chemically heterogeneous materials such as propolis[23]. However, while vibrational methods provide global compositional fingerprints, more detailed structural information at the molecular level often requires complementary techniques such as NMR spectroscopy.

2.3.1.3 Proton nuclear magnetic resonance spectroscopy

^{1}H NMR spectroscopy exploits the magnetic properties of ^{1}H nuclei, which possess a nuclear spin quantum number of ½[92]. This intrinsic spin generates a magnetic moment that enables interaction

with an external magnetic field[92]. When placed in a strong static magnetic field, the nuclei adopt discrete energy states aligned either parallel (with) or anti-parallel (against) to the field, the latter being higher in energy (Figure 7). Transitions between these states occur upon absorption of radiofrequency radiation at the characteristic Larmor frequency, which corresponds to the energy difference between the two levels[93]. After the radiofrequency pulse is removed, the nuclei relax back toward equilibrium within the static magnetic field, generating a measurable signal that is detected as the NMR spectrum[93].

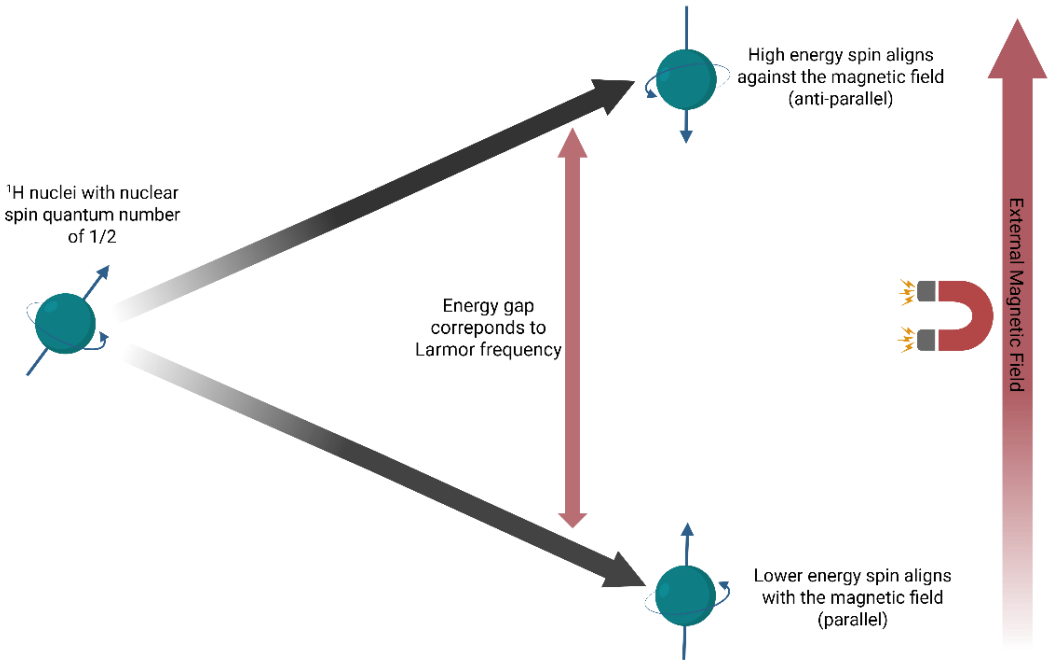

Figure 7. Energy level splitting of ^{1}H nuclei (spin ½) in a strong static magnetic field. The external field separates the nuclei into parallel (lower energy) and anti-parallel (higher energy) states. The energy difference between these states corresponds to the Larmor frequency at which radiofrequency absorption occurs. Created with BioRender.com.

The exact resonance frequency of a proton depends on its electronic environment. Electrons surrounding the nucleus partially shield it from the external magnetic field, resulting in chemical shift differences that reflect molecular structure[93]. In addition, spin-spin coupling between nearby nuclei generates characteristic splitting patterns that provide insight into local structural relationships within the molecule[94].

In contrast to vibrational spectroscopy, ^{1}H NMR provides detailed structural information while simultaneously enabling detection of a broad range of compounds without prior separation[23].

Because signal intensity is directly proportional to molar concentration and does not depend on chromophores or ionization efficiency, NMR is inherently quantitative and well suited for non-targeted metabolic profiling[23].

2.3.2 Chromatography

Chromatography is a separation technique based on the distribution of compounds between a stationary phase and a mobile phase[95]. As components of a mixture migrate through the stationary phase, differences in physicochemical properties such as polarity, hydrophobicity, charge, or molecular size result in varying retention times[95]. This enables separation of complex mixtures into individual constituents prior to detection and quantification. Chromatographic techniques are widely applied in analytical chemistry due to their high resolving power, reproducibility, and compatibility with various detection systems[96].

2.3.2.1 Chromatographic separation of complex natural products

Propolis represents a chemically heterogeneous matrix composed of structurally diverse constituents[50], necessitating efficient chromatographic separation prior to targeted detection and quantification. Reversed-phase HPLC is commonly employed for this purpose[16, 17]. Here, separation is often achieved using a non-polar C18 (octadecylsilane) stationary phase combined with a relatively polar mobile phase[95]. Analytes are retained based on hydrophobic interactions, with more polar compounds eluting earlier and more hydrophobic compounds exhibiting longer retention times due to stronger interactions with the stationary phase[95].

Following separation, detection is frequently performed using ultraviolet-visible (UV-Vis) spectroscopy, which is well suited for polyphenolic compounds due to their conjugated aromatic systems[17]. For enhanced selectivity and structural confirmation, chromatographic systems may also be coupled to mass spectrometry[17].

2.3.3 Complementarity of analytical techniques

Due to the chemical heterogeneity of propolis, no single analytical technique provides a complete characterization of its composition. Vibrational spectroscopy enables rapid, non-targeted profiling based on global spectral fingerprints, capturing matrix-level compositional variation but offering limited direct structural resolution.

In contrast, ^{1}H NMR spectroscopy provides detailed structural and quantitative information without prior separation, allowing simultaneous detection of multiple compound classes within complex

mixtures. Chromatographic techniques such as HPLC facilitate separation of individual constituents prior to targeted detection and quantification, thereby increasing sensitivity and specificity for selected bioactive compounds.

The combination of these analytical platforms therefore allows integration of holistic compositional profiling with molecular-level specificity and quantitative precision. In the context of this thesis, this multi-platform approach enables both exploratory, non-targeted characterization and targeted validation of specific bioactive constituents, providing a more comprehensive understanding of propolis composition and its biological effects (Table 1).

Table 1. Overview of the analytical techniques applied in this thesis, summarizing their fundamental principles, main strengths, and key limitations when applied to chemically complex matrices.

Technique	Principle	Main Strengths	Main Limitations
Vibrational spectroscopy	Transitions between quantized vibrational energy levels	Rapid analysis with minimal sample preparation; Suitable for chemically complex matrices; Provides spectral fingerprints	Extensive band overlap; Limited structural specificity and sensitivity
^{1}H NMR spectroscopy	Transitions between nuclear spin states in a magnetic field	Detailed structural information; Inherently quantitative; Broad compound detection without prior separation	Extensive spectral overlap; Requires extraction
Chromatography	Separation based on stationary and mobile phases	Efficient separation of complex mixtures prior to detection and quantification;	Longer analysis time; Requires extraction and separation before detection

Together, these analytical platforms form the foundation of this thesis, and their outputs constitute the high-dimensional datasets that necessitate the multivariate modeling approaches described in the following section.

2.4 Multivariate modeling of high-dimensional chemical data

The analytical techniques described above generate complex datasets in which each sample is represented by a large number of correlated variables (e.g., spectral intensities at different

wavelengths or chemical shifts). Such data can be represented as a data matrix $X \in R^{nxp}$, where R^{nxp} denotes the set of all real-valued matrices with n samples, and p measured variables per sample. In other words, each row corresponds to one sample and each column to one measured variable. When functional or biological measurements are included, these can be expressed as a response matrix $Y \in R^{nxm}$, where m denotes the number of response variables. Multivariate modeling aims to extract systematic variation from X, reduce dimensionality, and, where relevant, model relationships between chemical features (X) and functional outcomes (Y).

However, the reliability and interpretability of such models depend critically on how well the data matrix reflects genuine chemical variation. Because raw analytical data often contains experimental artifacts such as baseline shifts, intensity differences, and noise, preprocessing constitutes a fundamental step prior to dimensionality reduction or regression modeling. Common approaches include baseline correction, scaling, and derivative filtering, each directly influencing the variance structure of the data[97]. A detailed treatment of individual preprocessing methods is beyond the scope of this section; however, as the present work relies heavily on multivariate modeling of spectroscopic data, it is important to acknowledge that appropriate preprocessing is central to ensuring that observed compositional patterns reflect genuine chemical differences rather than analytical artifacts.

2.4.1 Exploratory modeling: Principal component analysis

Principal component analysis (PCA) is an unsupervised technique used to reduce dimensionality while preserving the dominant sources of systematic variation[98]. It is particularly useful for exploring similarities and differences between samples in high-dimensional datasets, as PCA transforms the original variables into a smaller number of orthogonal components, termed principal components[98].

Each principal component is a linear combination of the original variables and is constructed to capture the maximum remaining variance under the constraint of orthogonality to preceding components[98]. Accordingly, the first component explains the largest proportion of variance, the second explains the largest remaining variance, and so forth.

Mathematically, the data matrix X is decomposed as[98]:

$$X = TP^{\top} + E$$

where T contains the scores describing relationships between samples, P contains the loadings describing the contribution of each variable to the components, P^T denotes the transpose of P, and E represents residual variation not captured by the model.

Score plots visualize similarities, clustering patterns, and potential outliers among samples, whereas loadings indicate which variables drive these patterns. Because PCA does not incorporate response variables, it is primarily used for exploratory analysis and for identifying dominant trends in high-dimensional datasets.

2.4.2 Supervised modeling: Linking chemical profiles to functional outcomes

While PCA explores structure within X, partial least squares (PLS) regression is a supervised method that models the relationship between predictor variables (X) and response variables (Y)[99]. In this context, X may represent spectral or chromatographic data, whereas Y may represent functional measurements such as antioxidative activity or cytokine levels.

PLS extracts latent variables that maximize the covariance between X and Y, thereby identifying patterns in the chemical data that are directly associated with functional outcomes[99]. By projecting both matrices into a lower-dimensional latent space, PLS addresses multicollinearity and is well suited for situations where the number of variables exceeds the number of samples.

The decomposition can be expressed as[99]:

$$X = TP^T + E$$
$$Y = UQ^T + F$$

where T and U are score matrices, P and Q are loading matrices, and E and F are residual matrices. The resulting regression relationship may be summarized as[99]:

$$Y = XB + E_Y$$

where B contains the regression coefficients and E_Y represents the residual prediction error. Model performance is typically assessed using cross-validation to estimate predictive ability and reduce the risk of overfitting.

To enhance interpretability and reduce the influence of irrelevant variables, several extensions of PLS have been developed, such as recursive weighted PLS (rPLS)[100], which iteratively refines variable selection based on model performance. Such an approach facilitates identification of chemically

meaningful spectral features contributing to functional activity and supports exploration of structure-activity relationships in complex natural product matrices.

2.4.2.1 Interpretation and limitations of multivariate models

Multivariate models provide a structured approach for analyzing high-dimensional chemical data and linking them to functional outcomes. However, interpretation requires caution. In spectroscopic datasets, the number of variables often greatly exceeds the number of samples, increasing susceptibility to overfitting. Robust validation strategies, such as cross-validation, are therefore essential.

Model outcomes are also influenced by preprocessing and scaling choices, as these directly shape the variance structure of the data. Moreover, regression methods such as PLS identify statistical associations rather than causal relationships. Correlations between chemical features and biological endpoints do not alone establish mechanistic relevance, particularly in complex matrices where multiple constituents may covary.

When properly validated and interpreted within a chemically and biologically informed framework, multivariate modeling provides a powerful approach for investigating structure-activity relationships in heterogeneous natural products. In this thesis, these analytical and chemometric tools were applied in conjunction with functional assays to link compositional variation to biological activity.

2.5 Functional and biological activity assessment

While analytical and chemometric approaches enable detailed characterization of chemical composition, functional models are required to evaluate biological relevance. In the present work, antioxidative capacity and immunomodulatory effects were assessed using complementary *in vitro* and *in vivo* systems to investigate the biological significance of chemical variation in propolis.

2.5.1 Functional assessment of antioxidative activity

Radical scavenging activity (RSA) provides a functional measure of antioxidative capacity by assessing the ability of a sample to neutralize reactive radical species[101]. The unpaired electron of radicals renders them highly reactive and capable of initiating oxidative chain reactions[102].

In RSA assays, 2,2-diphenyl-1-picrylhydrazyl (DPPH), a stable nitrogen-centered radical, is commonly employed as a probe molecule (Figure 8)[103, 104]. DPPH exhibits a strong absorbance in

the visible region, which decreases upon reduction by antioxidative compounds as the radical is converted to its non-radical form[101]. This change in absorbance provides a quantitative measure of radical scavenging capacity.

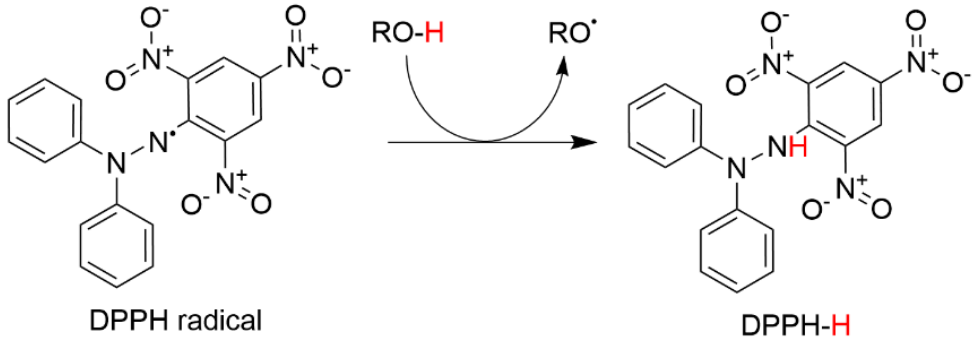

Figure 8. Schematic representation of the DPPH radical scavenging reaction. The DPPH radical accepts a hydrogen atom from a polyphenolic antioxidant (RO-H), resulting in formation of the reduced DPPH-H species and a corresponding polyphenol-derived radical (RO•)[103, 104].

Antioxidative properties are particularly relevant for polyphenol-rich natural products, as these compounds can donate electrons or hydrogen atoms to stabilize radical species[64, 65].

RSA assays therefore provide a rapid and reproducible estimate of the cumulative antioxidative potential of complex mixtures. Although such assays do not necessarily replicate physiological oxidative processes, they serve as a practical proxy for comparing samples and for linking chemical fingerprints to functional antioxidative capacity.

2.5.2 Functional assessment of immunomodulatory activity

The functional immunomodulatory effects of propolis were evaluated using complementary experimental models representing both *in vitro* immune responses and *in vivo* autoimmune disease development. Together, these systems provide mechanistic insight at the cellular level and allow assessment of integrated physiological effects in a preclinical model of autoimmune diabetes.

2.5.2.1 Human peripheral blood mononuclear cells

PBMCs comprise circulating mononuclear immune cells, including T cells, B cells, natural killer cells, monocytes and dendritic cells[105]. PBMCs are characterized by a single round nucleus and represent key adaptive and innate immune populations in peripheral blood[106]. Monocytes within this population can differentiate into macrophage- or dendritic-like cells under appropriate *in vitro* conditions[107].

Upon stimulation, PBMCs produce cytokines that reflect activation of specific immune pathways, enabling assessment of pro- and anti-inflammatory responses[108]. These responses may be mediated through propolis-relevant signaling pathways such as TLR4-dependent activation of NF-κB and MAPK (Figure 4). A principal strength of the PBMC model lies in its heterogeneous cellular composition, which preserves physiologically relevant cell-cell interactions and allows evaluation of coordinated immune signaling in a human-derived system.

Although *in vitro* systems cannot fully reproduce the complexity of systemic immune regulation, PBMCs provide a controlled and translationally relevant platform for investigating immune-modulatory effects of complex natural products.

2.5.2.2 Non-obese diabetic mice

The NOD mouse is a widely used and well-characterized preclinical model of spontaneous autoimmune T1D, characterized by immune-mediated destruction of pancreatic β-cells[24]. In this model, insulitis is a prominent feature, manifesting as extensive infiltration of immune cells into the pancreatic islets[109]. Female NOD mice develop disease with immunological and pathological features that parallel certain aspects of human T1D, whereas males display partial resistance[24]. Disease progression is marked by early lymphocytic infiltration of the pancreatic islets, followed by progressive β-cell loss and the onset of hyperglycemia[24].

The NOD model reproduces several important immunopathological features of autoimmune diabetes and enables evaluation of functional effects within a physiologically integrated system, capturing interactions between immune regulation, metabolic control, and systemic inflammation[110]. Although no animal model fully replicates human disease, the NOD mouse provides a robust experimental platform for investigating disease mechanisms and assessing therapeutic potential beyond *in vitro* systems.

Together, these complementary functional systems enabled assessment of propolis' biological activity across increasing levels of complexity, from radical scavenging capacity and cellular immune responses to integrated disease evaluation in a preclinical autoimmune model.

3 Brief methodological overview

This thesis integrates analytical and biological approaches to investigate relationships between propolis composition, factors influencing this composition, and functional activity. Spectroscopic, chromatographic, chemometric, and functional methodologies were combined to capture both holistic compositional patterns and specific bioactive constituents, with biological activity assessed across complementary *in vitro* and *in vivo* systems. Detailed experimental procedures are provided in the appended manuscripts; the present section outlines the overarching methodological strategy and its integration across studies.

Spectroscopic techniques, including IR, Raman, NIR, and ^{1}H NMR spectroscopy, were applied for comprehensive non-targeted chemical characterization. Vibrational spectroscopies enabled rapid, non-destructive comparative profiling, whereas ^{1}H NMR provided quantitative and structurally informative metabolomic data. For detailed ^{1}H NMR analysis, a two-phase extraction procedure was employed to separate hydrophilic and hydrophobic fractions, resolving compositional ambiguities that could not be addressed through single-phase extraction and improving discrimination of compound classes within the chemically complex propolis matrix. HPLC provided higher-resolution analysis of polyphenolic constituents and enabled targeted association of individual compounds with immunomodulatory effects, thereby complementing the holistic spectroscopic approaches.

Multivariate and chemometric analyses were used to manage high-dimensional datasets and to identify chemical features associated with geographical origin, bee species, antioxidative capacity, and immunomodulatory activity. These approaches enabled systematic integration of chemical and functional data across the included studies.

Functional activity was evaluated using radical scavenging assays, PBMCs, and the NOD mouse model. This tiered strategy enabled assessment of propolis effects across increasing levels of biological complexity.

Overall, the methodological framework integrates complementary analytical techniques with multivariate modeling and biologically relevant functional systems, providing a coherent strategy for investigating chemical variability and structure-activity relationships in propolis and evaluating its potential to modulate immune responses and influence the development of T1D.

4 Summary of manuscripts

The four manuscripts included in this thesis collectively address the central hypothesis that dietary propolis can modulate immune and inflammatory processes relevant to the development of T1D. The work is structured as a hierarchical investigation progressing from chemical characterization to functional immune validation and to evaluation in a preclinical disease model.

Manuscripts I and II characterize the chemical diversity of propolis and relate compositional fingerprints to antioxidative capacity. Manuscript III integrates chromatographic profiling with functional immune assays to identify candidate contributors to anti-inflammatory activity in PBMCs. Manuscript IV extends these findings to an *in vivo* autoimmune model, assessing whether dietary propolis influences immune regulation and disease kinetics. Together, the manuscripts establish a framework linking propolis composition to biological function across analytical, cellular, and organismal levels.

Each manuscript summary is structured around the study aim and key findings. Detailed methodologies and complete results are presented in the appended manuscripts, while the brief methodological overview in Section 3 outlines the overarching analytical strategy applied across studies. Where relevant, key figures and tables from the appended manuscripts are referenced using the notation (MI, Fig./Tbl. X), (MII, Fig./Tbl. X), (MIII, Fig./Tbl. X), and (MIV, Fig./Tbl. X) for Manuscripts I-IV, respectively.

4.1 Manuscript I

Comparative Spectroscopic Analysis of Bee Propolis: NIR, FT-IR, FT-Raman and ^{1}H NMR. Focus on Provenance and Antioxidative Correlation

Aim: The aim of this study was to compare the chemical composition and antioxidative capacity, expressed as RSA, of propolis from Australia, Denmark, and Norway using IR, Raman, NIR, and ^{1}H NMR spectroscopy combined with multivariate data analysis. A further aim was to evaluate the ability of these techniques to discriminate geographical chemotypes and predict RSA.

Results: PCA revealed clear geographical clustering, with Danish and Norwegian propolis characterized by higher relative aromatic content, while Australian samples exhibited enrichment in carbohydrates and terpenoids (MI, Fig. 3). Consistent with these compositional differences, Scandinavian samples demonstrated significantly higher RSA compared to Australian propolis, whereas Danish and Norwegian samples did not differ significantly from each other (MI, Fig. 4).

Spectral correlation analysis identified strong associations between RSA and signals corresponding to conjugated aromatic structures, particularly at 1631 cm^{-1} in Raman spectra and 1666 nm in NIR spectra (MI, Tbl. 2). These regions are attributed to conjugated C=C stretching vibrations and overtone vibrations associated with aromatic systems, respectively. Among the applied techniques, NIR spectroscopy provided the most accurate predictive models of RSA, demonstrating robust cross-validated performance (MI, Fig. 6). The findings highlight the suitability of NIR as a rapid and non-destructive method for assessing antioxidative potential in propolis.

Overall, the study demonstrates that geographical origin determines propolis chemotype and antioxidative capacity, and that combining complementary spectroscopic approaches provides both holistic compositional insights and reliable functional screening, with NIR spectroscopy emerging as the most accurate tool for RSA prediction in propolis.

4.2 Manuscript II

Comparative ^{1}H NMR Metabolomics Between Scandinavian Propolis and Australian Propolis: The Quest to Identify Radical Scavenging Compounds

Aim: The aim of this study was to characterize and compare the metabolite composition of *A. mellifera* propolis from Scandinavia and Australia, and cerumen from *Tetragonula carbonaria* (*T. carbonaria*), using untargeted quantitative ^{1}H NMR metabolomics, to evaluate how geographical origin and bee species influence hydrophilic and hydrophobic metabolite profiles and antioxidative capacity.

Results: PCA of the ^{1}H NMR spectra demonstrated clear separation between Scandinavian and Australian *A. mellifera* propolis, indicating strong geographical structuring of chemotypes (MII, Fig. 4). Hydrophilic extracts revealed higher levels of aromatic compounds in Scandinavian propolis, whereas Australian propolis was enriched in carbohydrates. Cerumen from *T. carbonaria* showed a distinct profile characterized by higher terpenoid content. Analysis of hydrophobic extracts revealed pronounced differences in wax composition. Australian propolis exhibited the highest wax content, characterized by shorter chain lengths and increased free fatty acids, while Scandinavian samples displayed more uniform wax structures and higher aromatic content (MII, Fig. 3). rPLS modeling identified signals attributable to ferulic acid and *p*-coumaric acid as important descriptors of antioxidative activity, supported by statistical total correlation spectroscopy (MII, Fig. 6).

Overall, the findings demonstrate that geographical origin and bee species are primary determinants of propolis metabolite composition, and that quantitative ^{1}H NMR metabolomics provides a reproducible framework for chemotype discrimination and identification of functionally relevant constituents.

4.3 Manuscript III

Linking Propolis Chemical Composition and Geographical Origin to Immunomodulatory Effects in Human Immune Cells

Aim: The aim of this study was to evaluate the relationship between chromatographic fingerprints of propolis from Australia, Denmark, and Norway and suppression of LPS-induced interleukin (IL)-1β secretion in PBMCs, and subsequently to identify specific chemical contributors to this anti-inflammatory effect.

Results: Chromatographic profiling showed higher levels of aromatic compounds in Danish and Norwegian samples compared to Australian propolis (MIII, Fig. 1). Functionally, this compositional difference was reflected in immune activity, as propolis suppressed LPS-induced IL-1β secretion in PBMCs, with the strongest inhibition observed for Scandinavian samples (MIII, Fig. 3).

Correlation analysis revealed that total chromatographic area explained a substantial proportion of the variation in IL-1β suppression, indicating that overall extract abundance is an important contributor to anti-inflammatory activity (MIII, Fig. 4a). Log_{10} transformation of the chromatographic area reduced this dominance, and subsequent PLS modeling with forward stepwise selection and variable inclusion frequency analysis identified chrysin as an independent contributor to IL-1β suppression (MIII, Fig. 4b, Fig. 5, Tbl. 1). Testing of individual compounds further confirmed chrysin as the most potent inhibitor of IL-1β release among the selected polyphenols tested (MIII, Tbl. 2), supporting its role as a candidate contributor to the anti-inflammatory activity of propolis alongside broader matrix-level polyphenolic enrichment.

Multiplex cytokine profiling further demonstrated selective rather than generalized immune modulation, with propolis decreasing IL-1β, IL-10, and interferon (IFN)-γ while increasing IL-4, IL-6, and tumor necrosis factor (TNF)-α, indicating that propolis alters defined inflammatory pathways rather than inducing broad immunosuppression (MIII, Fig. 6).

Overall, the study demonstrates that the anti-inflammatory activity of propolis is compositionally driven, with chrysin identified as an independent candidate contributor, and reveals that propolis modulates specific inflammatory pathways rather than acting as a broad immunosuppressant.

Ethical considerations: The use of human immune cells in this study was approved by the Danish Committee on Health Research Ethics (H-25003840).

4.4 Manuscript IV

Immunomodulatory Effects of Dietary Propolis in Autoimmune Diabetes: A Preclinical Study in NOD Mice

Aim: The aim of this study was to investigate whether long-term dietary supplementation with propolis modulates autoimmune diabetes development in the NOD mouse model. Specifically, the study evaluated effects on disease incidence, pancreatic immune infiltration, T cell distribution, systemic cytokine profiles, and gut microbiota composition to assess whether propolis influences immune regulation and disease kinetics.

Results: Dietary propolis delayed the onset of autoimmune diabetes, with a significant reduction in diabetes incidence during early disease development, although cumulative incidence converged at later time points, indicating modulation of early disease kinetics rather than complete disease prevention (MIV, Fig. 2).

High-dose dietary propolis (3.6% w/w) reduced pancreatic immune infiltration (MIV, Fig. 3) and altered T cell distribution, decreasing $CD4^+$ T helper (Th) cells in pancreatic lymph nodes while increasing total splenic T cell numbers, suggesting redistribution of immune activity rather than generalized immunosuppression (MIV, Fig. 4). Consistently, systemic cytokine analysis demonstrated reduced IL-4 levels alongside increased IL-10 and IFN-γ, while classical pro-inflammatory cytokines remained unchanged, further supporting selective modulation of immune signaling rather than broad suppression (MIV, Fig. 5). Dietary propolis also altered gut microbiota composition, notably increasing the abundance of *Akkermansia muciniphila* (*A. muciniphila*), a bacterium associated with a protective role in T1D, supporting a potential interaction between immune modulation and the gut microbiota axis (MIV, Fig. 6).

Overall, these findings demonstrate that long-term dietary propolis transiently delays autoimmune diabetes onset and modulates immune responses and gut microbial composition in NOD mice, supporting its evaluation as a dietary immunomodulatory strategy in autoimmune disease contexts.

Ethical considerations: Animal experiments were approved by the Danish Animal Experiments Inspectorate and conducted in accordance with Directive 2010/63/EU (license no. 2021-15-0201-00847).

5 Discussion

The following sections provide an integrative discussion of the collective findings and their contributions to natural product characterization, immunomodulation and dietary modulation of autoimmune disease, with particular emphasis on T1D. Detailed methodological considerations and study-specific interpretations are presented in the respective manuscripts.

5.1 Chemical heterogeneity and functional implications of propolis

The findings confirm that propolis composition is strongly influenced by both geographical origin and bee species, with distinct chemotypes identified across Scandinavian, Australian, and cerumen samples.

The observed compositional patterns reflect regional botanical availability in combination with species-specific resin collection and material utilization strategies. In temperate regions, *A. mellifera* preferentially collects poplar-derived resins rich in polyphenols. In contrast, the absence of native poplar species in Australian ecosystems likely necessitates alternative resin sources. However, the clear distinction between Australian propolis and cerumen demonstrates that regional flora alone cannot explain compositional variability, as species-dependent factors also modulate the balance between resin-derived and structural components.

As polyphenols are primarily responsible for the bioactive properties of propolis, the observed geographical variation in polyphenolic abundance underscores the importance of considering botanical and geographical origin when selecting propolis for therapeutic or research purposes. Chemical heterogeneity should therefore not be regarded as analytical noise, but as a biologically structured determinant of functional potential.

5.1.1 Spectroscopic fingerprinting and chemometric discrimination

A central methodological strength of this work lies in the integration of vibrational spectroscopy, two-phase ^{1}H NMR, and multivariate analysis to resolve structured compositional variability. Rather than relying exclusively on targeted compound identification, this strategy enabled holistic chemotype discrimination across analytical platforms. PCA consistently separated Australian and Scandinavian samples, demonstrating robust compositional clustering.

Vibrational spectroscopy provided rapid, non-destructive chemical fingerprinting and enabled discrimination between regional chemotypes; however, its resolution was limited when structurally similar compound classes contributed overlapping spectral features. In Manuscript I, Australian samples exhibited increased C-O and C-O-C vibrations, but these signals could not distinguish carbohydrate-derived versus terpenoid-derived contributions. Furthermore, one-phase chloroform extraction proved incompatible with Australian samples, precluding molecular clarification by NMR at that stage.

The implementation of a two-phase extraction strategy in Manuscript II was therefore decisive. Separation of hydrophilic and hydrophobic fractions prior to ^{1}H NMR analysis enabled clear differentiation between carbohydrate-associated resonances and terpenoid signals. This demonstrated that carbohydrate enrichment was a general feature of Australian samples, whereas elevated terpenoid content was specifically associated with *T. carbonaria* cerumen. In addition, ^{1}H NMR revealed that Australian *A. mellifera* propolis contained higher relative wax content compared to Scandinavian samples, while cerumen exhibited the lowest wax proportion overall. Thus, the two-phase NMR approach resolved compositional ambiguities that could not be addressed through vibrational spectroscopy alone.

The functional predictive capacity of the applied techniques reflected their intrinsic physical principles. NIR demonstrated the strongest predictive performance for RSA, due to its broader sampling depth and ability to capture bulk polyphenolic enrichment across heterogeneous matrices. Raman also showed strong correlations with RSA, consistent with its sensitivity to C=C polarization within aromatic systems. Complementing this fingerprint-level prediction, rPLS modeling of hydrophilic ^{1}H NMR extracts identified signals arising from ferulic acid and *p*-coumaric acid as important descriptors of RSA, illustrating the strength of integrating molecular-level spectroscopy with chemometric variable selection to extract functionally relevant descriptors from complex natural product matrices.

The applied analytical strategy therefore combines complementary strengths and inherent limitations. Vibrational spectroscopy enables rapid and reproducible profiling but lacks compound-level specificity. ^{1}H NMR provides greater structural resolution yet requires extraction and remains susceptible to spectral overlaps in chemically dense matrices. In addition, the restricted geographical and species representation limits broader generalizability. The findings should therefore be interpreted as structured compositional and functional fingerprints rather than exhaustive chemical

characterizations. From a translational perspective, however, such fingerprint-based frameworks are highly relevant for assessing batch variability and functional potential in complex natural products. Collectively, Manuscripts I and II demonstrate that propolis heterogeneity is structured and functionally meaningful, providing a chemical foundation for subsequent immunological investigations and future efforts toward functionally informed standardization.

5.2 Chemical drivers of immunomodulatory function

Having established chemical heterogeneity across propolis chemotypes and demonstrated its relationship to antioxidative capacity, the next question was whether defined compositional features also explain differences in immunomodulatory activity.

5.2.1 Linking polyphenolic composition to IL-1β suppression

Geographical variation in chromatographic fingerprints translated directly into functional differences, with Scandinavian propolis more effectively suppressing LPS-induced IL-1β release in PBMCs compared to Australian samples.

Disentangling compound-specific contributions from the bulk effect through $\log_{10}$ transformation and multivariate modeling identified chrysin as an independent contributor to this activity. However, attributing the anti-inflammatory activity of propolis to a single compound remains inherently reductive. Propolis is a chemically complex matrix in which bioactive constituents likely act additively or synergistically, and the analytical approach relied on detection at 280 nm, overlooking potential contributions from non-UV-absorbing constituents. The data therefore support a dual model in which both matrix-level polyphenolic enrichment and compound-specific potency shape immunomodulatory responses, with chrysin serving as a plausible marker rather than an isolated driver of activity.

5.2.2 Selective immunomodulation of cytokines

While the primary anti-inflammatory focus was IL-1β suppression, general cytokine profiling revealed broader selective immunomodulation. In contrast to dexamethasone, which reduced all measured cytokines, propolis differentially regulated pro- and anti-inflammatory mediators, reducing IL-1β and IFN-γ while increasing TNF-α, IL-6, and IL-4.

The reduction in IL-1β suggests modulation of inflammasome-dependent signaling pathways, consistent with the two-step mechanism governing IL-1β production. At the same time, the absence of global cytokine suppression and the increase in other NF-κB-associated mediators suggest that upstream priming pathways remain active. Although TNF-α is often reported to decrease following propolis exposure[69], increased TLR4 expression and NF-κB activation have also been described, underscoring the importance of compositional context and experimental conditions[68]. The consistent reduction in IFN-γ further suggests modulation of pro-inflammatory T cell responses.

Collectively, these findings support the interpretation that propolis affects inflammatory balance rather than acting as a broad immunosuppressive agent.

5.3 Dietary propolis in autoimmune diabetes

Having demonstrated selective immunomodulatory effects in vitro, the translational relevance of these findings was evaluated *in vivo* using the NOD mouse model.

5.3.1 Modulation of disease onset

Dietary propolis delayed the onset of autoimmune diabetes in the NOD mouse model, particularly at the higher dose, without altering final cumulative incidence. This temporal delay indicates modulation of early immunological events before clinical onset. However, although complete protection was not achieved under the conditions tested, early immune regulation may still influence the trajectory of subsequent disease progression. The observed reduction in insulitis and redistribution of T cells between pancreatic lymph nodes and spleen suggest altered local immune dynamics within pancreatic tissue without evidence of systemic immunosuppression. Rather than simply suppressing inflammation, this pattern may reflect qualitative changes in immune activation, potentially shifting from destructive autoimmune responses toward a more regulated or non-cytotoxic inflammatory state. Such modulation aligns with the selective immunological effects observed *in vitro* and supports the interpretation that propolis modulates immune activity rather than broadly suppressing it.

5.3.2 Selective immune regulation and microbiota modulation

Systemic cytokine profiling in propolis-treated NOD mice revealed significantly increased IFN-γ and IL-10 compared to the control group, suggesting a rebalancing of immune activity toward a more regulated state. Notably, the increase in IFN-γ contrasts with the *in vitro* findings where it was reduced, and surprisingly, IL-1β was not reduced *in vivo* despite being the primary target of anti-

inflammatory activity *in vitro*. These discordances underscore the importance of evaluating immunomodulatory candidates across multiple experimental systems. The elevation of IFN-γ may appear counterintuitive as it is a classical pro-inflammatory cytokine; however, for a detailed mechanistic discussion, the reader is referred to Manuscript IV.

The concurrent enrichment of *A. muciniphila* suggests involvement of gut immune interactions, although causality cannot be established. *A. muciniphila* has been associated with favorable metabolic and immunological profiles, including reports of milder disease progression in human T1D[111], raising the possibility that microbiota shifts may contribute to altered immune regulation.

Importantly, this study represents the first evaluation of dietary propolis in the NOD model. The transient nature of protection likely reflects the strong genetic susceptibility inherent to this model, within which propolis modulates disease dynamics rather than overcoming underlying predisposition. However, as the NOD model does not fully recapitulate human T1D, the findings should be interpreted as proof of concept rather than direct evidence of clinical efficacy.

5.4 Integrated interpretation: From composition to disease evaluation

Taken together, this work demonstrates that chemical heterogeneity in propolis is not incidental variability but structured compositional diversity with functional consequence. By systematically linking chemical fingerprinting, chemometric modeling, cellular immune assays, and *in vivo* disease evaluation, this thesis establishes a coherent framework for examining complex natural product matrices across analytical and biological systems.

The original hypothesis proposed that dietary propolis can modulate immune and inflammatory responses and thereby influence the development of T1D. Rather than addressing this question at a single experimental level, the present work approached it hierarchically. First, chemical fingerprinting defined structured chemotypes and clarified the compositional axes along which variability occurs. Second, integration of molecular scale spectroscopy with multivariate modeling enabled identification of functionally relevant compound descriptors within chemically dense matrices. Third, cellular and *in vivo* systems demonstrated that these compositional differences translate into selective immunomodulation and altered disease kinetics.

More broadly, the thesis highlights that meaningful evaluation of complex natural products requires integration of complementary spectroscopic techniques, chemometric resolution, and biological

validation. No single analytical approach proved sufficient. Instead, layered characterization was necessary to distinguish structurally similar constituents, resolve matrix effects, and relate chemical fingerprints to functional outcomes. Importantly, the demonstrated ability of NIR spectroscopy and chemometric fingerprinting to predict and describe functional outcomes such as RSA and IL-1β suppression suggests a practical path toward functionally anchored standardization, moving beyond crude extract identity toward quality benchmarks grounded in measurable biological activity.

By establishing a structured pipeline from compositional fingerprints to immunological consequence and disease evaluation, this thesis provides a methodological blueprint for systematic assessment of complex dietary bioactives in immune-mediated disease contexts.

6 Conclusions

This thesis provides a systematic demonstration that the biological activity of propolis is directly determined by its chemical composition, and that this relationship can be resolved, predicted, and functionally validated across analytical and biological systems. Geographical and species-dependent variability was shown to be structured, reproducible, and functionally consequential, linking compositional fingerprints to measurable differences in antioxidative capacity, anti-inflammatory effect, and autoimmune disease kinetics. Through integration of chemical profiling, chemometric modeling, cellular immune assays, and *in vivo* disease evaluation, propolis emerges not as an undefined natural mixture, but as a structured immunomodulatory matrix.

Across experimental systems, propolis modulated inflammatory responses without inducing generalized immunosuppression. At the molecular level, chrysin was identified as an independent contributor to anti-inflammatory activity alongside broader matrix-level polyphenolic enrichment, illustrating that both specific constituents and bulk compositional features shape immunomodulatory responses. In the NOD model, this translated into altered disease kinetics rather than complete disease prevention, underscoring both the promise and the inherent constraints of dietary immunomodulation in genetically driven autoimmune contexts.

The findings therefore support the hypothesis that dietary propolis can modulate immune and inflammatory processes relevant to T1D development. Beyond the specific case of propolis, this work also establishes an integrative and hierarchical framework in which compositional fingerprinting, molecular resolution, and functional validation converge to enable systematic evaluation of chemically complex bioactive materials. Such an approach defines the analytical and biological depth required for meaningful standardization and rational translational development of heterogeneous natural products in immune-mediated disease settings.

7 Future perspectives

The findings of this thesis establish a framework that not only advances understanding of propolis but also defines the analytical and biological standards necessary to responsibly transition complex natural products from experimental models into clinical integration. However, if findings never reach the patient, even the strongest frameworks are rendered moot. Progression toward clinical investigation is therefore imperative, requiring standardization to move toward functionally anchored quality benchmarks, with defined compositional fingerprints linked to reproducible biological outcomes as prerequisites for regulatory credibility. Although propolis has a long history of safe use in traditional medicine, a chemically diverse matrix represents multiple potential sources of adverse reactions and drug-constituent interactions, and rigorous safety and tolerability assessment will be essential in any clinical program.

Finally, it is worth reflecting that bees have produced propolis for millions of years to defend their colonies against pathogens, and the resinous plant materials from which it derives represent evolutionary defense systems refined through millennia of symbiosis. Nature has therefore spent incomparably longer developing complex biological defense strategies than human science has existed to study them. Thus, while this is no guarantee that a natural product is safe for humans, and propolis must rightly undergo rigorous clinical testing prior to integration into evidence-based treatment, the pharmacological potential of naturally derived substances merits serious attention rather than dismissal on the grounds of complexity, natural variation, or lack of patentability alone. After all, some of the most transformative medicines in history began as natural products long before science had the tools to understand why they worked.

8 References

1. Roep BO, Thomaidou S, van Tienhoven R, Zaldumbide A. Type 1 diabetes mellitus as a disease of the β-cell (do not blame the immune system?). Nature Reviews Endocrinology. 2021;17(3):150-61. DOI: 10.1038/s41574-020-00443-4
2. Burrack AL, Martinov T, Fife BT. T Cell-Mediated Beta Cell Destruction: Autoimmunity and Alloimmunity in the Context of Type 1 Diabetes. Frontiers in Endocrinology. 2017;Volume 8 - 2017. DOI: 10.3389/fendo.2017.00343
3. Bell KJ, Lain SJ. The Changing Epidemiology of Type 1 Diabetes: A Global Perspective. Diabetes, Obesity and Metabolism. 2025;27(S6):3-14. DOI: 10.1111/dom.16501
4. Ogle GD, Wang F, Haynes A, Gregory GA, King TW, Deng K, et al. Global type 1 diabetes prevalence, incidence, and mortality estimates 2025: Results from the International diabetes Federation Atlas, 11th Edition, and the T1D Index Version 3.0. Diabetes Research and Clinical Practice. 2025;225:112277. DOI: 10.1016/j.diabres.2025.112277
5. Tack CJ, Lancee GJ, Heeren B, Engelen LJ, Hendriks S, Zimmerman L, et al. Glucose Control, Disease Burden, and Educational Gaps in People With Type 1 Diabetes: Exploratory Study of an Integrated Mobile Diabetes App. JMIR Diabetes. 2018;3(4):e17. DOI: 10.2196/diabetes.9531
6. Ezzatvar Y, López-Gil JF, Yáñez-Sepúlveda R, Hurtado-Almonacid J, García-Hermoso A. Life expectancy in individuals with type 1, type 2 diabetes and without diabetes: a systematic review and meta-analysis. Frontiers in Endocrinology. 2025;Volume 16 - 2025. DOI: 10.3389/fendo.2025.1704277
7. Insel RA, Dunne JL, Atkinson MA, Chiang JL, Dabelea D, Gottlieb PA, et al. Staging presymptomatic type 1 diabetes: a scientific statement of JDRF, the Endocrine Society, and the American Diabetes Association. Diabetes Care. 2015;38(10):1964-74. DOI: 10.2337/dc15-1419
8. Herold KC, Bundy BN, Long SA, Bluestone JA, DiMeglio LA, Dufort MJ, et al. An Anti-CD3 Antibody, Teplizumab, in Relatives at Risk for Type 1 Diabetes. The New England Journal of Medicine. 2019;381(7):603-13. DOI: 10.1056/NEJMoa1902226
9. Herold KC, Gitelman SE, Gottlieb PA, Knecht LA, Raymond R, Ramos EL. Teplizumab: A Disease-Modifying Therapy for Type 1 Diabetes That Preserves β-Cell Function. Diabetes Care. 2023;46(10):1848-56. DOI: 10.2337/dc23-0675

10. Hossain R, Quispe C, Khan RA, Saikat ASM, Ray P, Ongalbek D, et al. Propolis: An update on its chemistry and pharmacological applications. Chinese Medicine. 2022;17(1):100. DOI: 10.1186/s13020-022-00651-2
11. Balasubramaniam AK, Elangovan A, Rahman MA, Nayak S, Swain D, Babu HP, et al. Propolis: A comprehensive review on the nature's polyphenolic wonder. Fitoterapia. 2025;183:106526. DOI: 10.1016/j.fitote.2025.106526
12. Búfalo MC, Ferreira I, Costa G, Francisco V, Liberal J, Cruz MT, et al. Propolis and its constituent caffeic acid suppress LPS-stimulated pro-inflammatory response by blocking NF-κB and MAPK activation in macrophages. Journal of Ethnopharmacology. 2013;149(1):84-92. DOI: 10.1016/j.jep.2013.06.004
13. Nichitoi MM, Josceanu AM, Isopescu RD, Isopencu GO, Geana E-I, Ciucure CT, et al. Polyphenolics profile effects upon the antioxidant and antimicrobial activity of propolis extracts. Scientific Reports. 2021;11(1):20113. DOI: 10.1038/s41598-021-97130-9
14. Wieczorek PP, Hudz N, Yezerska O, Horčinová-Sedláčková V, Shanaida M, Korytniuk O, et al. Chemical Variability and Pharmacological Potential of Propolis as a Source for the Development of New Pharmaceutical Products. Molecules. 2022;27(5). DOI: 10.3390/molecules27051600
15. Osés SM, Marcos P, Azofra P, de Pablo A, Fernández-Muíño M, Sancho MT. Phenolic Profile, Antioxidant Capacities and Enzymatic Inhibitory Activities of Propolis from Different Geographical Areas: Needs for Analytical Harmonization. Antioxidants (Basel). 2020;9(1). DOI: 10.3390/antiox9010075
16. Barrientos L, Herrera CL, Montenegro G, Ortega X, Veloz J, Alvear M, et al. Chemical and botanical characterization of Chilean propolis and biological activity on cariogenic bacteria Streptococcus mutans and Streptococcus sobrinus. Brazilian Journal of Microbiology. 2013;44(2):577-85. DOI: 10.1590/s1517-83822013000200038
17. Zhang Y, Cao C, Yang Z, Jia G, Liu X, Li X, et al. Simultaneous determination of 20 phenolic compounds in propolis by HPLC-UV and HPLC-MS/MS. Journal of Food Composition and Analysis. 2023;115:104877. DOI: 10.1016/j.jfca.2022.104877
18. Xiao X, Liu F, Sun M, Tang Z, Wu Y, Lyu J, et al. Development of a high-performance liquid chromatography method for simultaneous quantification of sixteen polyphenols and application to tomato. Journal of Chromatography A. 2024;1733:465254. DOI: 10.1016/j.chroma.2024.465254

19. Surek M, Cobre AdF, Fachi MM, Santos TG, Pontarolo R, Crisma AR, et al. Propolis authentication of stingless bees by mid-infrared spectroscopy and chemometric analysis. LWT – Food Science and Technology. 2022;161:113370. DOI: 10.1016/j.lwt.2022.113370
20. Revilla I, Vivar-Quintana AM, González-Martín I, Escuredo O, Seijo C. The potential of near infrared spectroscopy for determining the phenolic, antioxidant, color and bactericide characteristics of raw propolis. Microchemical Journal. 2017;134:211-7. DOI: 10.1016/j.microc.2017.06.006
21. Stavropoulou MI, Stathopoulou K, Cheilari A, Benaki D, Gardikis K, Chinou I, et al. NMR metabolic profiling of Greek propolis samples: Comparative evaluation of their phytochemical compositions and investigation of their anti-ageing and antioxidant properties. Journal of Pharmaceutical and Biomedical Analysis. 2021;194:113814. DOI: 10.1016/j.jpba.2020.113814
22. Kumazawa S, Hayashi K, Kajiya K, Ishii T, Hamasaka T, Nakayama T. Studies of the Constituents of Uruguayan Propolis. Journal of Agricultural and Food Chemistry. 2002;50(17):4777-82. DOI: 10.1021/jf020279y
23. Khakimov B, Gürdeniz G, Engelsen S. Trends in the application of chemometrics to foodomics studies. Acta Alimentaria. 2015;44:4-31. DOI: 10.1556/AAlim.44.2015.1.1
24. Chen YG, Mathews CE, Driver JP. The Role of NOD Mice in Type 1 Diabetes Research: Lessons from the Past and Recommendations for the Future. Frontiers in Endocrinology. 2018;9:51. DOI: 10.3389/fendo.2018.00051
25. Maahs DM, West NA, Lawrence JM, Mayer-Davis EJ. Epidemiology of Type 1 Diabetes. Endocrinology and Metabolism Clinics of North America. 2010;39(3):481-97. DOI: 10.1016/j.ecl.2010.05.011
26. Redondo MJ, Steck AK, Pugliese A. Genetics of type 1 diabetes. Pediatric Diabetes. 2018;19(3):346-53. DOI: 10.1111/pedi.12597
27. Elding Larsson H, Vehik K, Gesualdo P, Akolkar B, Hagopian W, Krischer J, et al. Children followed in the TEDDY study are diagnosed with type 1 diabetes at an early stage of disease. Pediatric Diabetes. 2014;15(2):118-26. DOI: 10.1111/pedi.12066
28. Zajec A, Trebušak Podkrajšek K, Tesovnik T, Šket R, Čugalj Kern B, Jenko Bizjan B, et al. Pathogenesis of Type 1 Diabetes: Established Facts and New Insights. Genes (Basel). 2022;13(4). DOI: 10.3390/genes13040706

29. Leung PS. Physiology of the Pancreas. In: Leung PS, editor. The Renin-Angiotensin System: Current Research Progress in The Pancreas: The RAS in the Pancreas. Dordrecht: Springer Netherlands; 2010. p. 13-27.
30. Ullsten S, Espes D, Quach M, Fex M, Sandberg M, Carlsson PO. Highly blood perfused, highly metabolically active pancreatic islets may be more susceptible for immune attack. Physiological Reports. 2020;8(13):e14444. DOI: 10.14814/phy2.14444
31. Bender RHF, O'Donnell BT, Shergill B, Pham BQ, Tahmouresie S, Sanchez CN, et al. A vascularized 3D model of the human pancreatic islet forex vivostudy of immune cell-islet interaction. Biofabrication. 2024;16(2). DOI: 10.1088/1758-5090/ad17d0
32. Jeker LT, Bour-Jordan H, Bluestone JA. Breakdown in peripheral tolerance in type 1 diabetes in mice and humans. Cold Spring Harbor Perspectives in Medicine. 2012;2(3):a007807. DOI: 10.1101/cshperspect.a007807
33. Sims EK, Besser REJ, Dayan C, Geno Rasmussen C, Greenbaum C, Griffin KJ, et al. Screening for Type 1 Diabetes in the General Population: A Status Report and Perspective. Diabetes. 2022;71(4):610-23. DOI: 10.2337/dbi20-0054
34. In't Veld P. Insulitis in human type 1 diabetes: a comparison between patients and animal models. Seminars in Immunopathology. 2014;36(5):569-79. DOI: 10.1007/s00281-014-0438-4
35. Bulek AM, Cole DK, Skowera A, Dolton G, Gras S, Madura F, et al. Structural basis for the killing of human beta cells by CD8(+) T cells in type 1 diabetes. Nat Immunol. 2012;13(3):283-9. DOI: 10.1038/ni.2206
36. Pinkse GGM, Tysma OHM, Bergen CAM, Kester MGD, Ossendorp F, van Veelen PA, et al. Autoreactive CD8 T cells associated with β cell destruction in type 1 diabetes. Proceedings of the National Academy of Sciences. 2005;102(51):18425-30. DOI: 10.1073/pnas.0508621102
37. Li C, Gao Q, Jiang H, Liu C, Du Y, Li L. Changes of macrophage and CD4+ T cell in inflammatory response in type 1 diabetic mice. Scientific Reports. 2022;12(1):14929. DOI: 10.1038/s41598-022-19031-9
38. Staeva TP, Chatenoud L, Insel R, Atkinson MA. Recent lessons learned from prevention and recent-onset type 1 diabetes immunotherapy trials. Diabetes. 2013;62(1):9-17. DOI: 10.2337/db12-0562

39. Martin S, Schernthaner G, Nerup J, Gries FA, Koivisto VA, Dupré J, et al. Follow-up of cyclosporin A treatment in type 1 (insulin-dependent) diabetes mellitus: lack of long-term effects. Diabetologia. 1991;34(6):429-34. DOI: 10.1007/bf00403182
40. Skyler JS, Rabinovitch A. Cyclosporine in recent onset type I diabetes mellitus. Effects on islet beta cell function. Miami Cyclosporine Diabetes Study Group. Journal of Diabetes and Its Complications. 1992;6(2):77-88. DOI: 10.1016/1056-8727(92)90016-e
41. Feutren G, Papoz L, Assan R, Vialettes B, Karsenty G, Vexiau P, et al. Cyclosporin increases the rate and length of remissions in insulin-dependent diabetes of recent onset. Results of a multicentre double-blind trial. Lancet. 1986;2(8499):119-24. DOI: 10.1016/s0140-6736(86)91943-4
42. Menon AP, Moreno B, Meraviglia-Crivelli D, Nonatelli F, Villanueva H, Barainka M, et al. Modulating T Cell Responses by Targeting CD3. Cancers (Basel). 2023;15(4). DOI: 10.3390/cancers15041189
43. Lledó-Delgado A, Preston-Hurlburt P, Currie S, Clark P, Linsley PS, Long SA, et al. Teplizumab induces persistent changes in the antigen-specific repertoire in individuals at risk for type 1 diabetes. The Journal of Clinical Investigation. 2024;134(18). DOI: 10.1172/jci177492
44. Haller MJ, Rotthaeuser B, Cherkas A, Coudert M, Labard P, Baccara-Dinet M, et al. 2021-LB: FABULINUS - A Randomized, Controlled Trial with FrexalimAB, to Assess Endogenous Insulin Secretion in New-Onset Stage 3 Type 1 Diabetes Adults and Adolescents. Diabetes. 2024;73(Supplement_1):2021-LB. DOI: 10.2337/db24-2021-LB
45. Blair PJ, Riley JL, Harlan DM, Abe R, Tadaki DK, Hoffmann SC, et al. CD40 ligand (CD154) triggers a short-term CD4(+) T cell activation response that results in secretion of immunomodulatory cytokines and apoptosis. The Journal of Experimental Medicine. 2000;191(4):651-60. DOI: 10.1084/jem.191.4.651
46. Wagh VD. Propolis: a wonder bees product and its pharmacological potentials. Adv Pharmacol Sci. 2013;2013:308249. DOI: 10.1155/2013/308249
47. Kasote D, Bankova V, Viljoen AM. Propolis: chemical diversity and challenges in quality control. Phytochemistry Reviews. 2022;21(6):1887-911. DOI: 10.1007/s11101-022-09816-1
48. Bankova V. Chemical diversity of propolis and the problem of standardization. Journal of Ethnopharmacology. 2005;100(1):114-7. DOI: 10.1016/j.jep.2005.05.004

49. Ristivojević P, Trifković J, Andrić F, Milojković-Opsenica D. Poplar-type Propolis: Chemical Composition, Botanical Origin and Biological Activity. Natural Product Communications. 2015;10(11):1869-76.
50. Anjum SI, Ullah A, Khan KA, Attaullah M, Khan H, Ali H, et al. Composition and functional properties of propolis (bee glue): A review. Saudi Journal of Biological Sciences. 2019;26(7):1695-703. DOI: 10.1016/j.sjbs.2018.08.013
51. Svečnjak L, Chesson LA, Gallina A, Maia M, Martinello M, Mutinelli F, et al. Standard methods for Apis mellifera beeswax research. Journal of Apicultural Research. 2019;58(2):1-108. DOI: 10.1080/00218839.2019.1571556
52. Drescher N, Klein AM, Schmitt T, Leonhardt SD. A clue on bee glue: New insight into the sources and factors driving resin intake in honeybees (Apis mellifera). PLoS One. 2019;14(2):e0210594. DOI: 10.1371/journal.pone.0210594
53. Dobrosielska M, Dobrucka R, Kozera P, Brząkalski D, Gabriel E, Głowacka J, et al. Beeswax as a natural alternative to synthetic waxes for fabrication of PLA/diatomaceous earth composites. Sci Rep. 2023;13(1):1161. DOI: 10.1038/s41598-023-28435-0
54. Cuní J, Cuni P, Eisen B, Savizky R, Bové J. Characterization of the binding medium used in Roman encaustic paintings on wall and wood. Anal Methods. 2012;4:659-69. DOI: 10.1039/C2AY05635F
55. Szwajkowska-Michałek L, Przybylska-Balcerek A, Rogoziński T, Stuper-Szablewska K. Phenolic Compounds in Trees and Shrubs of Central Europe. Applied Sciences. 2020;10(19). DOI: 10.3390/app10196907
56. Baştürk A, Yavaş B. Antioxidant Activity, Total Phenolic Content, and Volatile Component Profiles of Propolis From Eight Turkish Regions. Chemistry & Biodiversity. 2025;22(4):e202402269. DOI: 10.1002/cbdv.202402269
57. Miłek M, Franke G, Tomczyk M, Górecki M, Cwiková O, Jarošová A, et al. The Influence of Geographical Origin on Poplar Propolis Composition and the Impact of Human Microbiota. Pharmaceuticals (Basel). 2024;17(6). DOI: 10.3390/ph17060768
58. El Menyiy N, Bakour M, El Ghouizi A, El Guendouz S, Lyoussi B. Influence of Geographic Origin and Plant Source on Physicochemical Properties, Mineral Content, and Antioxidant and Antibacterial Activities of Moroccan Propolis. International Journal of Food Science. 2021;2021(1):5570224. DOI: 10.1155/2021/5570224

59. Herrera-López MG, Richomme P, Peña-Rodríguez LM, Calvo-Irabien LM. Bee Species, Botanical Sources and the Chemical Composition of Propolis from Yucatan, Mexico. Journal of Chemical Ecology. 2023;49(7-8):408-17. DOI: 10.1007/s10886-023-01429-y
60. Grassi G, Capasso G, Gambacorta E, Perna AM. Chemical and Functional Characterization of Propolis Collected from Different Areas of South Italy. Foods. 2023;12(18):3481. DOI: 10.3390/foods12183481
61. Bonvehí JS, Gutiérrez AL. The antimicrobial effects of propolis collected in different regions in the Basque Country (Northern Spain). World Journal of Microbiology and Biotechnology. 2012;28(4):1351-8. DOI: 10.1007/s11274-011-0932-y
62. Mony TJ, Elahi F, Choi JW, Park SJ. Neuropharmacological Effects of Terpenoids on Preclinical Animal Models of Psychiatric Disorders: A Review. Antioxidants (Basel). 2022;11(9). DOI: 10.3390/antiox11091834
63. Pahlavani N, Malekahmadi M, Firouzi S, Rostami D, Sedaghat A, Moghaddam AB, et al. Molecular and cellular mechanisms of the effects of Propolis in inflammation, oxidative stress and glycemic control in chronic diseases. Nutrition & Metabolism. 2020;17(1):65. DOI: 10.1186/s12986-020-00485-5
64. Kurek-Górecka A, Rzepecka-Stojko A, Górecki M, Stojko J, Sosada M, Swierczek-Zieba G. Structure and antioxidant activity of polyphenols derived from propolis. Molecules. 2013;19(1):78-101. DOI: 10.3390/molecules19010078
65. Ahmed R, Tanvir EM, Hossen MS, Afroz R, Ahmmed I, Rumpa NE, et al. Antioxidant Properties and Cardioprotective Mechanism of Malaysian Propolis in Rats. Evidence-Based Complementary and Alternative Medicine. 2017;2017:5370545. DOI: 10.1155/2017/5370545
66. Neshchadin D, Batchelor SN, Bilkis I, Gescheidt G. Short-lived phenoxyl radicals formed from green-tea polyphenols and highly reactive oxygen species: an investigation by time-resolved EPR spectroscopy. Angew Chem Int Ed Engl. 2014;53(48):13288-92. DOI: 10.1002/anie.201407995
67. Liu T, Zhang L, Joo D, Sun S-C. NF-κB signaling in inflammation. Signal Transduction and Targeted Therapy. 2017;2(1):17023. DOI: 10.1038/sigtrans.2017.23
68. Zhu H, Li C, Jia L, Qiao J, El-Seedi HR, Zhang Y, et al. Supercritical CO2 extracts of propolis inhibits tumor proliferation and Enhances the immunomodulatory activity via activating the TLR4-MAPK/NF-κB signaling pathway. Food Research International. 2024;196:115137. DOI: 10.1016/j.foodres.2024.115137

69. Yu C, Wang D, Yang Z, Wang T. Pharmacological Effects of Polyphenol Phytochemicals on the Intestinal Inflammation via Targeting TLR4/NF-κB Signaling Pathway. Int J Mol Sci. 2022;23(13). DOI: 10.3390/ijms23136939
70. Hori JI, Zamboni DS, Carrão DB, Goldman GH, Berretta AA. The Inhibition of Inflammasome by Brazilian Propolis (EPP-AF). Evidence-Based Complementary and Alternative Medicine. 2013;2013(1):418508. DOI: 10.1155/2013/418508
71. Contieri LS, de Souza Mesquita LM, Sanches VL, Viganó J, Martinez J, da Cunha DT, et al. Standardization proposal to quality control of propolis extracts commercialized in Brazil : A fingerprinting methodology using a UHPLC-PDA-MS/MS approach. Food Research International. 2022;161:111846. DOI: 10.1016/j.foodres.2022.111846
72. Vujić M, Pollak L. Composition, labelling, and safety of food supplements based on bee products in the legislative framework of the European Union - Croatian experiences. Arh Hig Rada Toksikol. 2015;66(4):243-9. DOI: 10.1515/aiht-2015-66-2654
73. Vettorazzi A, López de Cerain A, Sanz-Serrano J, Gil AG, Azqueta A. European Regulatory Framework and Safety Assessment of Food-Related Bioactive Compounds. Nutrients. 2020;12(3). DOI: 10.3390/nu12030613
74. Kasote D, Bankova V, Viljoen AM. Propolis: chemical diversity and challenges in quality control. Phytochem Rev. 2022;21(6):1887-911. DOI: 10.1007/s11101-022-09816-1
75. Prasad RD, Sarvalkar PD, Prasad N, Prasad SR, Prasad RS, Prasad Â RB, et al. A Review on Spectroscopic Techniques for Analysis of Nanomaterials and Biomaterials. ES Energy and Environment. 2025;27:1264. DOI: 10.30919/esee1264
76. Xu J-L, Riccioli C, Sun D-W. An Overview on Nondestructive Spectroscopic Techniques for Lipid and Lipid Oxidation Analysis in Fish and Fish Products. Comprehensive Reviews in Food Science and Food Safety. 2015;14(4):466-77. DOI: 10.1111/1541-4337.12138
77. Krull UJ, Thompson M. Analytical Chemistry. In: Meyers RA, editor. Encyclopedia of Physical Science and Technology (Third Edition). New York: Academic Press; 2003. p. 543-79.
78. Burgess C. Chapter 2 - The basis for good spectrophotometric UV–visible measurements. In: Thomas O, Burgess C, editors. UV-Visible Spectrophotometry of Waters and Soils (Third Edition): Elsevier; 2022. p. 25-58.
79. Chapter 1 Electromagnetic radiation and the electromagnetic spectrum. Comprehensive Analytical Chemistry. 35: Elsevier; 2001. p. 1-9.

80. Hashimoto K, Badarla VR, Kawai A, Ideguchi T. Complementary vibrational spectroscopy. Nature Communications. 2019;10(1):4411. DOI: 10.1038/s41467-019-12442-9
81. Marion D. An introduction to biological NMR spectroscopy. Mol Cell Proteomics. 2013;12(11):3006-25. DOI: 10.1074/mcp.O113.030239
82. Introduction. Infrared Spectroscopy: Fundamentals and Applications. Analytical Techniques in the Sciences2004. p. 1-13.
83. Mobaraki N, Hemmateenejad B. Structural characterization of carbonyl compounds by IR spectroscopy and chemometrics data analysis. Chemometrics and Intelligent Laboratory Systems. 2011;109(2):171-7. DOI: 10.1016/j.chemolab.2011.08.011
84. Roggo Y, Chalus P, Maurer L, Lema-Martinez C, Edmond A, Jent N. A review of near infrared spectroscopy and chemometrics in pharmaceutical technologies. Journal of Pharmaceutical and Biomedical Analysis. 2007;44(3):683-700. DOI: 10.1016/j.jpba.2007.03.023
85. Singh R. Harmonic and Anharmonic Oscillator Models for Pure Vibrational Infrared Spectroscopy of Diatomic Molecules. International Journal of Advanced Science and Engineering. 2021;8. DOI: 10.29294/IJASE.8.1.2021.2016-2024
86. Osborne BG, Fearn T, Hindle PH, Hindle PT. Practical NIR Spectroscopy with Applications in Food and Beverage Analysis: Longman Scientific & Technical; 1993.
87. Pandey DK, Kagdada HL, Sanchora P, Singh DK. Overview of Raman Spectroscopy: Fundamental to Applications. In: Singh DK, Pradhan M, Materny A, editors. Modern Techniques of Spectroscopy: Basics, Instrumentation, and Applications. Singapore: Springer Singapore; 2021. p. 145-84.
88. Berger E, Komsa H-P. Polarizability models for simulations of finite temperature Raman spectra from machine learning molecular dynamics. Physical Review Materials. 2024;8(4):043802. DOI: 10.1103/PhysRevMaterials.8.043802
89. Lima ABSd, Batista AS, Santos MRC, Rocha RdSd, Silva MVd, Ferrão SPB, et al. Spectroscopy NIR and MIR toward predicting simultaneous phenolic contents and antioxidant in red propolis by multivariate analysis. Food Chemistry. 2022;367:130744. DOI: 10.1016/j.foodchem.2021.130744
90. Rinnan Å, Berg Fvd, Engelsen SB. Review of the most common pre-processing techniques for near-infrared spectra. TrAC Trends in Analytical Chemistry. 2009;28(10):1201-22. DOI: 10.1016/j.trac.2009.07.007

91. Ma L, Peng Y, Pei Y, Zeng J, Shen H, Cao J, et al. Systematic discovery about NIR spectral assignment from chemical structural property to natural chemical compounds. Scientific Reports. 2019;9(1):9503. DOI: 10.1038/s41598-019-45945-y
92. Pohmann R. Physical Basics of NMR. In: Schröder L, Faber C, editors. In vivo NMR Imaging: Methods and Protocols. Totowa, NJ: Humana Press; 2011. p. 3-21.
93. Tognarelli JM, Dawood M, Shariff MI, Grover VP, Crossey MM, Cox IJ, et al. Magnetic Resonance Spectroscopy: Principles and Techniques: Lessons for Clinicians. J Clin Exp Hepatol. 2015;5(4):320-8. DOI: 10.1016/j.jceh.2015.10.006
94. Autschbach J, Le Guennic B. Analyzing and Interpreting NMR Spin–Spin Coupling Constants Using Molecular Orbital Calculations. Journal of Chemical Education. 2007;84(1):156. DOI: 10.1021/ed084p156
95. Bachhav R, Bachhav MP, Sonawane V, Sonawane G, Bhamare M. A Brief Review on Different Chromatographic Techniques. Open Access Journal of Pharmaceutical Research. 2024;Volume 8:000294.
96. Debnath S, Das M, Mondal S, Sarkar BK, Babu G. Advances in chromatography: contemporary techniques and applications. Essential Chem. 2025;2(1):1-27. DOI: 10.1080/28378083.2025.2466624
97. van den Berg RA, Hoefsloot HC, Westerhuis JA, Smilde AK, van der Werf MJ. Centering, scaling, and transformations: improving the biological information content of metabolomics data. BMC Genomics. 2006;7:142. DOI: 10.1186/1471-2164-7-142
98. Eriksson L, Byrne T, Johansson E, Trygg J, Vikström C. Multi- and Megavariata Data Analysis Basic Principles and Applications. 3 ed: MKS Umetrics AB; 2013. p. 33-53.
99. Eriksson L, Byrne T, Johansson E, Trygg J, Vikström C. Multi- and Megavariata Data Analysis Basic Principles and Applications. 3 ed: MKS Umetrics AB; 2013. p. 55-88.
100. Rinnan Å, Andersson M, Ridder C, Engelsen SB. Recursive weighted partial least squares (rPLS): an efficient variable selection method using PLS. Journal of Chemometrics. 2014;28(5):439-47. DOI: 10.1002/cem.2582
101. Blois MS. Antioxidant Determinations by the Use of a Stable Free Radical. Nature. 1958;181(4617):1199-200. DOI: 10.1038/1811199a0
102. Chandimali N, Bak SG, Park EH, Lim H-J, Won Y-S, Kim E-K, et al. Free radicals and their impact on health and antioxidant defenses: a review. Cell Death Discovery. 2025;11(1):19. DOI: 10.1038/s41420-024-02278-8

103. Mărghitaş LA, Dezmirean D, Moise A, Mihai CM, Laslo L. DPPH Method for evaluation of propolis antioxidant activity. Bull USAMV. 2009;66:253-8.
104. Moţ AC, Silaghi-Dumitrescu R, Sârbu C. Rapid and effective evaluation of the antioxidant capacity of propolis extracts using DPPH bleaching kinetic profiles, FT-IR and UV–vis spectroscopic data. Journal of Food Composition and Analysis. 2011;24(4):516-22. DOI: 10.1016/j.jfca.2010.11.006
105. Kleiveland CR. Peripheral Blood Mononuclear Cells. In: Verhoeckx K, Cotter P, López-Expósito I, Kleiveland C, Lea T, Mackie A, et al., editors. The Impact of Food Bioactives on Health: in vitro and ex vivo models. Cham (CH): Springer. Copyright 2015, The Author(s). 2015. p. 161-7.
106. Ding T, Du Y, Yang B, Tian W, Li J, Xie J. Comprehensive review of macrophage models: primary cells and immortalized lines across species. Front Immunol. 2025;Volume 16 - 2025. DOI: 10.3389/fimmu.2025.1640935
107. Chapuis F, Rosenzwajg M, Yagello M, Ekman M, Biberfeld P, Gluckman JC. Differentiation of human dendritic cells from monocytes in vitro. Eur J Immunol. 1997;27(2):431-41. DOI: 10.1002/eji.1830270213
108. Henderson DC, Rippin JJ. Stimulus-dependent production of cytokines and pterins by peripheral blood mononuclear cells. Immunol Lett. 1995;45(1-2):29-34. DOI: 10.1016/0165-2478(94)00222-d
109. Pugliese A. Insulitis in the pathogenesis of type 1 diabetes. Pediatric Diabetes. 2016;17 Suppl 22(Suppl Suppl 22):31-6. DOI: 10.1111/pedi.12388
110. Shoda LKM, Young DL, Ramanujan S, Whiting CC, Atkinson MA, Bluestone JA, et al. A Comprehensive Review of Interventions in the NOD Mouse and Implications for Translation. Immunity. 2005;23(2):115-26. DOI: 10.1016/j.immuni.2005.08.002
111. Hansen CHF, Krych L, Nielsen DS, Vogensen FK, Hansen LH, Sørensen SJ, et al. Early life treatment with vancomycin propagates Akkermansia muciniphila and reduces diabetes incidence in the NOD mouse. Diabetologia. 2012;55(8):2285-94. DOI: 10.1007/s00125-012-2564-7

9 Full manuscripts

The following manuscripts constitute the primary scientific contributions of this thesis. Each manuscript is presented in its published or submitted form and should be read in conjunction with the synopsis, which provides an integrative discussion of the collective findings.

Manuscript I

Pharmacological Research - Natural Products 10 (2026) 100578

Contents lists available at ScienceDirect

Pharmacological Research - Natural Products

journal homepage: www.sciencedirect.com/journal/prenap

Comparative spectroscopic analysis of bee propolis: NIR, FT-IR, FT-Raman and ^{1}H NMR. Focus on provenance and antioxidative correlation

Jonas Pordel Vind [a,*], Violetta Aru [b], Henrik Munch Jørgensen [a], Julie Christine Antvorskov [c], Hasim Tekin [a], Knud Josefsen [a], Søren Balling Engelsen [b]

[a] Department of Pathology, The Bartholin Institute, Copenhagen University Hospital, Copenhagen, Denmark
[b] Department of Food Science, University of Copenhagen, Rolighedsvej 26, Frederiksberg, 1958, Denmark
[c] Department of Clinical Research, Steno Diabetes Center Copenhagen, Translational Type 1 Diabetes Research, Herlev, Denmark

ARTICLE INFO

Keywords:
Propolis
Polyphenols
Antioxidative
IR
Raman
NIR
^{1}H NMR

ABSTRACT

Propolis is a polyphenol-rich resinous substance well known for its antioxidative properties. This study describes and compares the chemical composition and radical scavenging activity (RSA) of propolis from Australia (N = 8), Denmark (N = 38), and Norway (N = 7) using infrared (IR), Raman, near-infrared (NIR), and proton nuclear magnetic resonance (^{1}H NMR) spectroscopy through multivariate data analysis. Principal Component Analysis (PCA) showed that Danish and Norwegian propolis samples had a higher content of aromatic compounds, whereas Australian samples were richer in carbohydrates and terpenoids. The RSA of Danish and Norwegian propolis samples was found to be similar ($p \geq 0.05$), while the Australian samples exhibited significantly lower RSA. The strongest spectral correlation ($R^2 = 0.64$) to RSA was found at 1631 cm^{-1} (Raman) and 1666 nm (NIR), attributed to conjugated C=C stretching vibrations and first overtones of C-H stretching vibrations from aromatic/conjugated structures, respectively. NIR spectroscopy provided the most accurate predictions of RSA ($R^2 = 0.75$, RMSECV = 6.66%), highlighting its potential as a rapid, non-destructive quality assessment tool for propolis. Overall, this study demonstrates that the combined use of multiple non-targeted spectroscopic techniques provides complementary insights into complex matrices, enabling a robust characterisation of propolis and its antioxidant activity.

Introduction

Propolis is a natural resinous substance produced by the western honey bee (*Apis mellifera* L.; abbr. *A. mellifera*) to seal and protect the hive from intruders, pathogenic bacteria, fungi, and viruses [1]. Propolis is a mixture of beeswax, plant resins, and glucosidase-containing bee secretions [1–4]. Beeswax is primarily comprised of hydrocarbons and their ester and acid derivatives [5,6]. In contrast, resins are complex mixtures, typically containing terpenoids, and aromatic compounds such as polyphenols [4]. Propolis is well-established to exert an antioxidative effect, and it is widely used in natural medicinal products [7,8]. In literature, the antioxidative properties of propolis are credited to its high concentrations of polyphenols and consequently, most research on the composition of propolis has focused on identifying specific polyphenolic compounds, often employing high-performance liquid chromatography (HPLC) and colorimetric assays [9–11]. Although a targeted identification method provides information about the presence and concentration of selected bioactive compounds, this approach may introduce bias and overlook other potentially important compounds. A more untargeted and unbiased approach to analyzing propolis can be performed using spectroscopic methods such as infrared (IR), Raman, and near-infrared (NIR) spectroscopy, that allow for non-invasive exploratory analysis with minimal or no sample preparation [12]. Proton nuclear magnetic resonance (^{1}H NMR) requires more extensive sample preparation including extraction, but it also delivers inherently quantitative, non-targeted chemical analysis, providing information about the detailed metabolite composition in complex biological mixtures [12]. Overall, the spectroscopic techniques have proven effective not only for assessing polyphenolic content, but also for examining general chemical profiles in propolis, serving as valuable tools for propolis quality control [13–16].

The aim of the present study was to establish an unbiased spectroscopic method to screen propolis, determining its overall chemical composition and predicting its antioxidative activity, expressed as

* Corresponding author.
E-mail address: Jonas.Pordel.Vind@regionh.dk (J.P. Vind).

https://doi.org/10.1016/j.prenap.2026.100578
Received 19 June 2025; Received in revised form 4 February 2026; Accepted 25 February 2026
Available online 27 February 2026

radical scavenging activity (RSA). The study employed several non-targeted spectroscopic methods, including IR, Raman, NIR, and ^{1}H NMR to examine and compare the chemical composition and antioxidative activity in a set of propolis samples (N = 53) from Australia (N = 8), Denmark (N = 38), and Norway (N = 7). ^{1}H NMR data were combined with the data from the vibrational spectroscopic techniques in 2D correlation spectra to aid in signal assignment. Correlation between spectral signals and antioxidative activity was performed. Finally, Partial Least Squares (PLS) regression models [17] were developed to predict the antioxidative activity of propolis from different origins based on the spectroscopic data. To our knowledge, this is the first study to compare and integrate multiple spectroscopic techniques through 2D correlation spectra and multivariate analysis for propolis characterization. The study brings new insights into structure-bioactivity relationships and demonstrates that RSA can be predicted directly from spectral data.

Experimental section

Chemicals

Analytical grade chloroform ($CHCl_3$, ≥99.8%), analytical grade deuterated chloroform ($CDCl_3$, 99%), deuterated dimethyl sulfoxide-d_6 (DMSO-d_6), ferulic acid (99%), HPLC grade caffeic acid (≥98.0%), HPLC grade p-coumaric acid (≥98.0%), NMR grade tetramethylsilane (TMS, ≥99.9%), and 2,2-Diphenyl-1-picrylhydrazyl (DPPH) were purchased from Sigma-Aldrich (Copenhagen, Denmark).

Collection and storage of raw propolis

A total of 53 raw propolis samples were collected from local beekeepers in Australia (N = 8), Denmark (N = 38), and Norway (N = 7). All Danish and Norwegian samples, as well as five of the Australian samples, were obtained from *A. mellifera*. The remaining three Australian samples originated from *Tetragonula carbonaria* (*T. carbonaria*). The differences in bee species for the Australian samples are addressed for each of the relevant analyses described below. Upon arrival, the samples were stored at 4 °C in nitrogen-filled, food-grade ziplock bags placed inside airtight glass containers, also filled with nitrogen. Prior to extraction, liquid nitrogen was applied to the raw propolis, which was then ground into a fine powder using a pestle and mortar.

Propolis extract preparations

Propolis extract preparation for ^{1}H NMR spectroscopy

For each extraction, 100 mg of crushed propolis was mixed with 5 mL of chloroform in round-bottom glass tubes and homogenized for 30 s using a T10 Basic ULTRA-TURRAX ® (IKA-Werke, Germany). After storing in the dark at room temperature for 1 h, the mixture was centrifuged at 3600 RPM for 15 min at 4 °C. After centrifugation, the supernatant (1 mL) was transferred into HPLC vials and left to evaporate overnight in a fume hood. The resulting precipitate was redissolved in 720 μL $CDCl_3$ + TMS (5 mM) and 80 μL DMSO-d_6. Following dissolution, 600 μL of redissolved extract was transferred to an NMR SampleJet tube (Bruker Biospin, Ettlingen, Germany, L = 103.5 mm, D = 5.0 mm) for analysis. Unexpectedly, the Australian samples proved incompatible with the extraction protocol due to high levels of non-dissolvable dispersed solids, which hindered clear and reproducible acquisition of ^{1}H NMR spectra. Several extraction approaches were initially evaluated, including varying concentrations of ethanol and methanol, but none yielded satisfactory reproducibility for the Australian samples (data not shown). However, chloroform provided the best spectral quality and repeatability for the Danish and Norwegian samples (data not shown). It was therefore selected as the standard solvent to ensure consistency across the dataset. Given the distinct chemical profiles of the Australian samples observed from the vibrational spectroscopic analyses and their markedly lower RSA, optimising a separate extraction protocol solely for these samples was considered beyond the scope of this study, particularly as 2D correlations and PLS regression were not feasible for the Australian samples due to their distinct vibrational spectra.

Propolis extract preparation for DPPH RSA assay

Ethanol extracts were prepared following the same approach as described for the extracts prepared for ^{1}H NMR spectroscopy, using ethanol (70%) instead of chloroform, as this approach has proven effective in earlier DPPH RSA studies on propolis [18,19]. After centrifugation, the supernatant (4 mL) was transferred into 15 mL Falcon™ conical centrifuge tubes and stored in a dark cooling room (4 °C) until analysis.

Sample measurements

IR and Raman spectroscopy

IR spectra were obtained using a Bruker Vertex 80 spectrometer equipped with a deuterated triglycine sulfate (DTGS) detector, a potassium bromide (KBr) beam splitter, and a single reflection Platinum Attenuated Total Reflection (ATR) diamond accessory. For Raman measurements, the same instrument was used with a Raman accessory featuring an InGaAs detector and a Nd laser (1065 nm, 200 mW). Both types of spectra were recorded in the range of 500 cm^{-1} to 4000 cm^{-1} with 128 scans per sample. The IR spectra were recorded with a resolution of 4 cm^{-1}, while the Raman spectra were recorded with a resolution of 8 cm^{-1}. IR and Raman spectra were measured in three replicates on raw grounded propolis samples.

NIR spectroscopy

The NIR spectra were measured using the DS2500 analyser (FOSS Analytical A/S, Hillerød, Denmark). The instrument is equipped with a silicon detector (400–1100 nm) and a lead sulfide (PbS) detector (1100–2500 nm). The measurements were collected in the reflectance mode, where the propolis samples were added to a ring cup equipped with a quartz window. The scans were conducted within a wavelength range of 400–2500 nm, with a spectroscopic resolution of 0.5 nm with an average of 8 scans for each sample. NIR spectra were measured in three replicates on raw grounded propolis samples.

^{1}H NMR spectroscopy

Samples included in the study were measured using a Bruker Avance III operating at a proton Larmor's frequency of 600.13 MHz and equipped with a 5-mm broadband inverse (BBI) probe (Bruker Biospin, Rheinstetten, Germany). The magnet was equipped with an automated sample changer (SampleJet™, Bruker Biospin, Rheinstetten, Germany) with a refrigerated storage station (278 K) and heating/drying station (306 K). Cooling of the probe and SampleJet system were controlled by the BCU (Bruker Cooling Unit). Data acquisition and processing were carried out in the TopSpin software (version 3.6, Bruker, Rheinstetten, Germany). Automation of the overall measurement procedure was controlled by the iconNMR™ software (Bruker Biospin, Rheinstetten, Germany). Icon NMR (Bruker Biospin, Germany) was used to control measurement automation. The following parameter setup was employed: 128 scans, a 90° pulse, a 20-ppm sweep width (sw), an acquisition time (aq) of 2.73 s, and a relaxation delay (D1) of 4 s. The ^{1}H NMR spectra were collected into 65 K data points. The receiver gain (RG) value was determined experimentally for each sample. Phase and baseline correction were performed in TopSpin 4.3.0 (Bruker Biospin, Rheinstetten, Germany).

DPPH RSA

The DPPH RSA of propolis ethanol extracts was determined using the DPPH free radical assay [20]. The propolis ethanol extracts were diluted in ethanol to a concentration of 0.5 mg/mL. In a Thermo Scientific™ 96-well conical bottom plate (non-treated surface), 20 μL of each diluted

solution was mixed with 180 μL of a DPPH in ethanol solution (0.1 mM). Positive and negative controls were prepared by mixing 20 μL of ascorbic acid in ethanol (0.5 mg/mL) and 20 μL of ethanol with 180 μL of the DPPH in ethanol solution (0.1 mM), respectively. The 96-well plate was kept in darkness at room temperature for 20 min, after which the absorbance of each well was measured at 517 nm using the CLARIOstar® Plus plate reader (BMG Labtech, Ortenberg, Germany). The DPPH RSA of the propolis samples, relative to the negative control, was used for analysis. RSA values for each sample were calculated as the average of triplicate measurements.

Data analysis

Initial pre-processing of ^{1}H NMR data

The ^{1}H NMR spectra were imported into MATLAB ver. R2023b (MathWorks Inc., Massachusetts, United States) where they were referenced to the TMS singlet at 0.00 ppm. and aligned using *i*coshift [21]. Noisy regions, including the chloroform signal at 7.26 ppm and TMS signal were removed prior to data analysis. The spectra were normalized relative to the RG and mass (mg) of the respective propolis sample.

2D correlation analysis

In this study, 2D correlation spectroscopy plots between vibrational versus ^{1}H NMR spectroscopy and Raman versus NIR spectroscopy [22,23] were generated using covariance calculations in MATLAB (version R2023b). The covariance was calculated using the *cov* function, where XSPEC1 represented the data from one spectroscopic method and XSPEC2 represented the data from another spectroscopic method. In these matrices, rows corresponded to samples and columns represented spectral variables. The vibrational spectroscopy regions for 2D correlation analysis were selected to capture distinct spectral variations relevant to the chemical diversity and the antioxidative activity of the samples. For IR and Raman spectroscopy, this analysis focused on the informative fingerprint region in the 1800–1000 cm^{-1} range which contains all relevant chemical information including carbonyl, ether, ester, acid and aromatic signals. The pure C-H, N-H and O-H stretching (2800–3600 cm^{-1}) proved too unspecific for discriminating between our propolis samples, while the region below 1000 cm^{-1} did not provide useful information, as covariance values were very low and no interpretable features were observed. For NIR spectroscopy, the entire 1100–2500 nm range (PbS detector) was selected for exploring covariations with ^{1}H NMR. IR and Raman spectroscopy data were preprocessed using the Standard Normal Variate (SNV) method [24] to correct for scatter-related intensity variation, followed by Pareto scaling to reduce the dominance of higher intensity signals. NIR data were preprocessed with SNV followed by mean centering. The ^{1}H NMR data were autoscaled prior to analysis to account for the large dynamic range of signal intensities, particularly the highly abundant wax-associated signals. To further improve sensitivity and capture more subtle covariations, the vibrational spectroscopy data were divided into two regions for 2D correlation analysis.

Correlation of spectroscopy data to RSA

For vibrational spectroscopy, the R^2 value was calculated between the maxima of signals attributed to aromatic compounds, as identified in the 2D correlation analysis, and the RSA. For ^{1}H NMR, the average intensity of the aromatic region ($\Delta\delta$ = 6.0–8.5 ppm) was used for correlation analysis. This approach was adopted because the aromatic region of the ^{1}H NMR spectra is densely populated with overlapping signals due to propolis' complex chemical composition, rendering correlations to specific signals unfeasible. Prior to correlation analysis, the IR and Raman data were pre-processed using SNV, while the second derivative was applied to the NIR data. The ^{1}H NMR data were not further pre-processed than beyond the initial processing.

Statistical analysis of DPPH RSA data

For the statistical analysis of DPPH RSA in propolis from different origins, a one-way ANOVA followed by Tukey's HSD test was performed to compare the means among the three groups (Australia, Denmark, and Norway). Although three of the Australian propolis samples were derived from *T. carbonaria* rather than *A. mellifera*, they exhibited no significant difference in RSA and were therefore pooled with the other Australian samples for simplicity.

Multivariate data analysis

Multivariate data analysis was performed with LatentiX 2.13 (LatentiX ApS, Gilleleje, Denmark). For Principal Component Analysis (PCA) [25] the spectral regions analysed were 3600–700 cm^{-1} for IR, 3100–800 cm^{-1} for Raman, 2500–1100 nm for NIR, and the entire recorded spectral range for ^{1}H NMR. The IR, Raman, and NIR data were pre-processed using SNV, to correct for scatter-related intensity variation, followed by mean centering. In contrast, the ^{1}H NMR data were Pareto scaled to reduce the dominance of high-intensity signals while preserving relative metabolite variation. The maximum number of components for PCA was determined using scree plots, resulting in the use of 3 components for the IR and 2 components for the Raman, NIR and ^{1}H NMR data. Higher-order components were also briefly evaluated for all spectroscopic techniques, but they did not improve class discrimination. The Australian samples were again pooled for PCA for simplicity, as the three derived from *T. carbonaria* showed little to no distinction from those of *A. mellifera*. For Partial Least Squares (PLS) regression [26] of the spectral data to the DPPH RSA, the same spectral regions were used for the vibrational spectroscopic techniques as in the PCA. For the ^{1}H NMR data, only the aromatic region ($\Delta\delta$ = 6.0–8.5 ppm) was used, as this provided highest prediction power. The same pre-processing was applied to IR, Raman, and ^{1}H NMR data as in the PCA. NIR data was pre-processed with the second derivative Savitzky-Golay filter and Pareto scaling. The number of latent variables (LVs) for PLS regression was identified based on a plot of Root Mean Square Error of Cross-Validation (RMSECV) versus the number of LVs. This approach led to the selection of one LV for the IR data, two LVs for the Raman and ^{1}H NMR data, and four LVs for the NIR data. Cross-validation was performed using a ten-segment repeated random approach with 25 repetitions, allowing for better representation of the heterogeneity of the propolis samples and reducing the risk of overfitting.

Results and discussion

Introduction to spectroscopic data

The average IR, Raman and NIR spectra for the Australian, Danish and Norwegian propolis samples are presented in Fig. 1A-C. The average ^{1}H NMR spectra for the Danish and Norwegian propolis samples are presented in Fig. 1D. The IR spectra for Danish and Norwegian samples display similar spectroscopic patterns (Fig. 1A), indicating comparable chemical compositions. In contrast, the Australian sample exhibits distinct signals, most notably a broad band around 1040 cm^{-1}. This feature may suggest a higher content of carbohydrates and terpenoids, as it likely arises from overlapping aliphatic C-O and C-O-C stretching vibrations common to both compound classes [27,28]. The propolis samples generally exhibit characteristic IR peaks associated with compounds commonly found in beeswax and resin. Notably, the peaks at 2916 cm^{-1} and 2849 cm^{-1} correspond to the asymmetric and symmetric C-H stretching of aliphatic methylene groups, respectively, which are omni-present in propolis due to the hydrocarbons and its ester and acid derivatives [5]. The carbonyl stretches of the hydrocarbon ester derivatives are observed at 1736 cm^{-1}[5]. Other less pronounced signals include symmetric C-H stretching of aliphatic methyl groups at 2958 cm^{-1}[5] and carbonyl stretching of free fatty acids at 1710 cm^{-1}[29]. The presence of aromatic compounds is suggested by

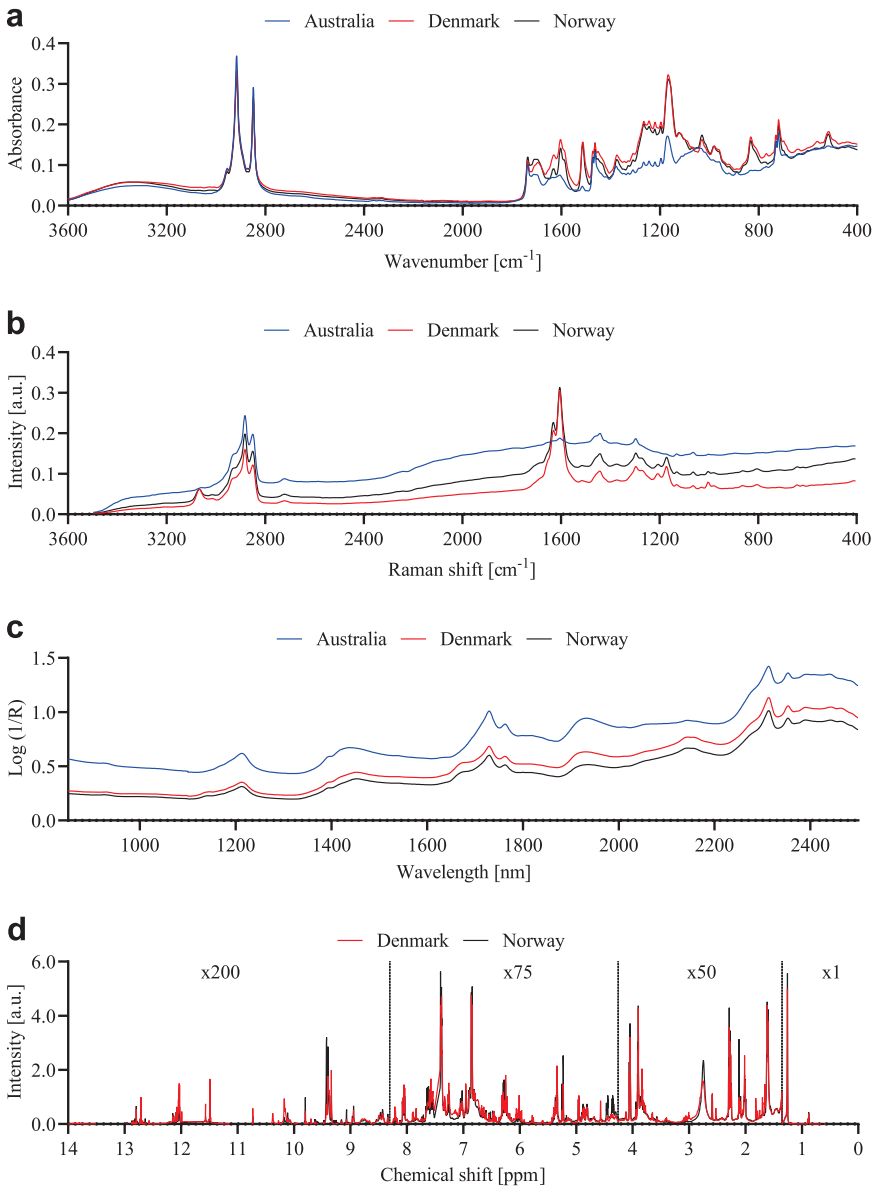

Fig. 1. Average (a) IR, (b) Raman, and (c) NIR spectra for the Australian (N = 8), Danish (N = 38), and Norwegian (N = 7) propolis samples; (d) Average ^{1}H NMR spectra for the Danish and Norwegian propolis samples.

the C═C stretching vibrations appearing in the spectroscopic range of 1610–1510 cm^{-1} [30].

The average Raman spectra (Fig. 1B) also show high similarities between Danish and Norwegian propolis samples, whereas the Australian sample exhibits a distinctly different and more amorphous spectroscopic pattern. Significant fluorescent interference, particularly in the Australian samples, complicates the identification of spectroscopic differences. Nonetheless, in the Raman spectra, the asymmetric and symmetric aliphatic methylene C-H stretches manifest as peaks at 2882 cm^{-1} and 2850 cm^{-1}, respectively [31]. Furthermore, the symmetric C-H stretching of aliphatic methyl groups is observed at 2935 cm^{-1} [31], while the C═C stretches of aromatic compounds are identified at around 1602 cm^{-1} [32].

This brief visual inspection of the IR and Raman spectra already suggests a distinctive chemical profile of the Australian propolis samples compared to the Danish and Norwegian samples. These dissimilarities in chemical composition may reflect differences in the botanical sources and environmental conditions influencing the chemical composition of propolis of different origins.

Fig. 1C presents the average NIR spectra for Danish, Norwegian and Australian propolis samples. While accurate spectroscopic assignment of the NIR spectra is not feasible without supplementary information, the NIR spectra contain substantial information about the chemical composition of the propolis samples through the vibrational combination bands and overtones. In order to elucidate the origins of these, 2D correlation analysis with the ^{1}H NMR data was performed and will be discussed later (Fig. 2).

The ^{1}H NMR spectra (Fig. 1D) of propolis show numerous signals across the spectrum, indicating successful extraction of a wide range of chemically diverse compounds. The most intense signal is observed at $\Delta\delta$ = 1.21 ppm and arises from aliphatic methylene (-CH_2-) protons found primarily in beeswax. The signal appears as a broad singlet, due to the intensity of the prominent protons in hydrocarbons and their ester and acid derivatives [33,34]. Despite the poor baseline resolution due to numerous overlapping signals from the complex chemical composition of propolis, the ^{1}H NMR spectra still provide valuable insights into the proton environments of the compounds present. These spectra not only facilitate the assessment of the types and quantities of compounds

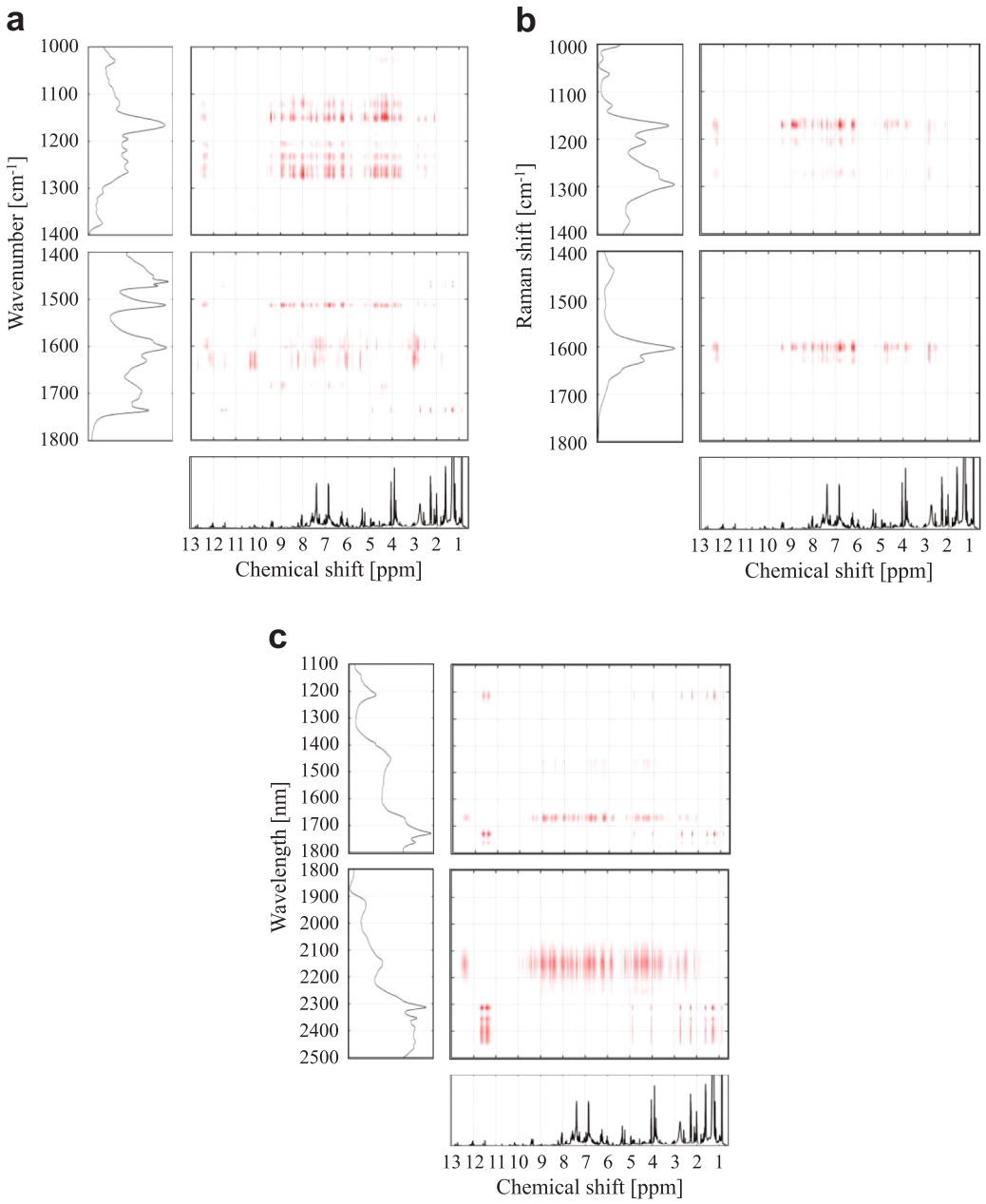

Fig. 2. 2D covariation spectra of (a) IR, (b) Raman, and (c) NIR spectra versus ^{1}H NMR spectra from Danish (N = 38) and Norwegian (N = 8) propolis samples. Preprocessing included Pareto scaling and Standard Normal Variate (SNV) for IR and Raman, mean centering and SNV for NIR, and autoscaling for ^{1}H NMR. The graphics show averaged raw spectra, with the most intense ^{1}H NMR signals truncated for clarity.

within the propolis samples but may also be used to enhance the interpretation of the vibrational spectroscopy data, e.g., IR, Raman, and NIR, by performing 2D correlation spectroscopy [35].

2D correlation spectroscopy and assignment of vibrational spectroscopy signals

To trace the origin of less prominent vibrational spectroscopy signals, potentially linked to antioxidative components, 2D correlation analysis was performed with ^{1}H NMR data. Fig. 2 shows the 2D correlation spectra between IR, Raman, and NIR with ^{1}H NMR. Table 1 summarizes the wavenumber, Raman shift, and wavelength ranges of selected IR, Raman, and NIR signals from raw propolis samples, along with their corresponding vibration modes and putative compounds.

The 2D correlation analysis of IR (Fig. 2A), Raman (Fig. 2B), and NIR (Fig. 2C) with ^{1}H NMR revealed distinct patterns of covariation. Vibrational spectroscopy signals associated with the aromatic region of the ^{1}H NMR spectrum ($\Delta\delta$ = 6.0–8.5 ppm) covary with a wide range of other ^{1}H NMR signals, suggesting co-occurrence of diverse resin-derived non-aromatic compounds. In contrast, vibrational signals linked to the aliphatic methylene signal at $\Delta\delta$ = 1.21 ppm in the ^{1}H NMR spectrum show no covariation with aromatic protons, indicating a clear separation between beeswax and resin components. Several IR signals covary with the aromatic region of the ^{1}H NMR spectrum (Fig. 2A). These signals may be attributed to aromatic C═O stretches (1695–1688 cm^{-1}) [39], aromatic/conjugated C═C stretches (1655–1510 cm^{-1}) [30], and aromatic C-O and C-O-C stretches (1374–1160 cm^{-1}) [30,39]. Signals ranging between 1124 and 1100 cm^{-1} seemingly also correlates strongly with the aromatic region, however, this region is often attributed to aliphatic C-O and C-O-C stretches and likely arise from carbohydrates and terpenoids found in resin. Signals at 1736–1710 cm^{-1} have

Table 1
Spectral regions from IR, Raman, and NIR analyses of raw propolis, along with corresponding vibrational modes and suspected compounds.

IR, Raman, and NIR spectroscopy of crude propolis			
IR			
Wavenumber (cm^{-1})	**Vibration Mode**	**Suspected compounds**	**Ref.**
3500–3100	ν(O-H)	Polyphenols, carbohydrates	[36]
3065	ν(C-H) (aromatic)	Polyphenols	[37]
3020	ν(C-H) (olefinic)	Terpenoids	[37]
2958–2849	$\nu_s(CH_3)$, $\nu_{as/s}(CH_2)$ (aliphatic)	Wax	[5]
1736	ν(C═O) (ester)	Wax	[38]
1710	ν(C═O) (carboxylic acid)	Wax	[38]
1695–1688	ν(C═O) (conjugated)	Polyphenols	[39]
1655–1620	ν(C═C) (conjugated)	Polyphenols	[30]
1610–1510	ν(C═C) (aromatic)	Polyphenols	[30]
1471–1450	$\delta_{ip}(CH_2)$ (aliphatic)	Wax	[5]
1374–1160	ν(C-O), ν(C-O-C) (aromatic)	Polyphenols	[30, 39]
1124–1000	ν(C-O), ν(C-O-C)	Carbohydrates, terpenoids	[27]
Raman			
Raman shift (cm^{-1})	**Vibration Mode**	**Suspected compounds**	**Ref.**
3068	ν(C-H) (aromatic)	Polyphenols	[30]
3018	ν(C-H) (olefinic)	Terpenoids	[31]
2935–2850	$\nu_s(CH_3)$, $\nu_{as/s}(CH_2)$ (aliphatic)	Wax	[31]
1655–1630	ν(C═C) (conjugated)	Polyphenols	[30]
1600–1605	ν(C═C) (aromatic)	Polyphenols	[30]
1445	δ_{ip}(C-H) (aliphatic)	Wax	[31]
1294–1170	δ_{ip}(C-H) (aromatic)	Polyphenols	[32]
NIR			
Wavelength (nm)	**Vibration mode**	**Suspected compounds**	**Ref**
2445–2310, 1416–1390	Combination bands (aliphatic)	Wax	[40]
2170–2130	Combination bands (aromatic)	Polyphenols	[41]
1940–1900	Combination bands (O-H)	Carbohydrates, terpenoids, polyphenols	[42]
1765–1730	2ν(C-H) (aliphatic)	Wax	[40]
1680–1665	2ν(C-H) (aromatic/ conjugated)	Polyphenols	[41]
1450	2ν(O-H)	Carbohydrates, terpenoids, polyphenols	[42]
1215	3ν(C-H) (aliphatic)	Wax	[43]

Keys: $\nu_{as/s}$, asymmetric/symmetric stretching; δ_{ip}, in-plane bending; 2ν, first overtone; 3ν, second overtone

been previously assigned to carbonyls of hydrocarbons derivatives of beeswax and they also covary with characteristic wax signals observed in the ^{1}H NMR spectra (e.g., at $\Delta\delta = 1.21$ ppm). The same is observed for IR signals at 1471–1462 cm^{-1} , arising due to in-plane bending of aliphatic C-H groups [5,44]. In contrast to IR, no covariation was observed between the Raman and ^{1}H NMR signals originating from beeswax in the selected spectral region (Fig. 2B). However, several Raman signals exhibited covariation with the aromatic region of the ^{1}H NMR spectra. These signals include those at 1655–1600 cm^{-1} (aromatic/conjugated C═C stretches) and 1294–1170 cm^{-1} (in-plane bending of aromatic C-H).

The 2D correlation analysis of the NIR and ^{1}H NMR spectra reveal the origin of several of the observed NIR signals (Fig. 2C). The covariation with ^{1}H NMR signals originating from beeswax suggests that the signals at wavelengths 2314–2443 nm and 1390–1416 nm may correspond to combination bands arising from the vibrations of aliphatic compounds in beeswax [40]. The first and second overtones of these compounds are likely observed at 1730–1765 nm and 1215 nm, respectively [43]. NIR signals exhibiting covariation with the aromatic region include signals at 2130–2170 nm (combination bands) [40] and 1665–1680 nm (first overtones) [41], although the latter range cannot be definitively attributed to aromatic or conjugated C-H and is discussed in detail later (Fig. 5). Signals observed at 1900–1940 nm and 1450 nm also weakly exhibit covariation with the aromatic region, however, these are more likely to originate from the combination bands and first overtones of hydroxyl groups found primarily on carbohydrates, terpenoids, and polyphenols [42], and will be discussed further later (Fig. 3C). The separation of resin- and beeswax-derived features in the IR and NIR 2D correlations indicates that the analysis primarily reflects differences in the overall resin-to-wax ratio. As a result, resin signals tend to covary with other resin-associated signals, while beeswax features covary within a narrower aliphatic domain. Although such covariance does not imply that a single compound gives rise to all correlated signals, it is valuable for distinguishing the chemical origin of bands. Notably, this differentiation is also biologically relevant, as the resin fraction contains the aromatic and polyphenolic constituents responsible for antioxidant activity, whereas beeswax would be expected to contribute minimally.

Principal component analysis of the propolis samples

To further investigate the chemical differences among the propolis samples, PCA was employed to analyse spectral patterns and sample variability. Fig. 3 presents the scores and loadings plots from the PCA of IR, Raman, NIR, and ^{1}H NMR spectroscopy data for the propolis samples. For IR, Raman, and NIR all replicate measurements are shown in the PCA, while there were no technical replicates for ^{1}H NMR. Two Danish samples were excluded from the ^{1}H NMR PCA analysis because their spectra indicated faulty extraction process. For all vibrational spectroscopic methods, the scores plot shows substantial inter-sample variability with a clustering of the Australian samples, distinct from the Danish and Norwegian samples (Fig. 3A-C). However, no clear differentiation between the Danish and Norwegian samples is observed in any of the four spectroscopic methods (Fig. 3A-D). Notably, the IR and Raman scores plots also demonstrate considerable intrasample (replicate) variability, whereas the NIR scores plot shows comparatively lower variability.

In the IR scores plot (Fig. 3A), no apparent discrimination based on sample origin is seen along PC#1. The loadings plot for PC#1 shows that this component primarily distinguishes the samples based on signals from wax (negative loadings at 2916 and 2849 cm^{-1}) and, to a lesser extent, aromatic compounds (positive loadings at 1603 and 1512 cm^{-1}). However, the clustering of Australian samples relative to Danish and Norwegian samples is explained along PC#2. For PC#2, negative loadings are primarily attributed to signals in the region of 1265–1160 cm^{-1} (C-O and C-O-C stretches of polyphenols) and the signal at 1512 cm^{-1} (aromatic C═C stretches). In contrast, positive loadings are dominated by signals in the region of 1105–880 cm^{-1}, attributed to C-O and C-O-C stretches of carbohydrates and terpenoids. Furthermore, the broad signal with a maximum around 3300 cm^{-1}, attributed to O-H stretching vibrations (Table 1), also contributes to the positive loadings, suggesting that these O-H stretches predominantly originate from carbohydrates and terpenoids rather than polyphenols. The IR data, therefore, suggests no differentiation in wax content based on the origin of the propolis samples. However, Danish and Norwegian propolis appear to contain higher amounts of polyphenols, while Australian propolis has a higher carbohydrate and terpenoid content.

The Raman scores plot (Fig. 3B) shows no clear clustering of the Australian and Danish/Norwegian samples based on any single principal component. However, when considering both PC#1 and PC#2 together, the Australian samples appear to cluster in the upper left quadrant (negative PC#1 and positive PC#2). PC#1 is primarily influenced by signals from polyphenols (positive loadings at 1631 and 1602 cm^{-1}) and wax (negative loadings at 2882 and 2848 cm^{-1}). Similarly, these signals also drive the loadings for PC#2, where both contribute negatively. The clustering of Australian samples in the upper left quadrant thus aligns with the findings from IR spectroscopy (Fig. 3A), supporting the conclusion that Danish and Norwegian propolis samples contain higher

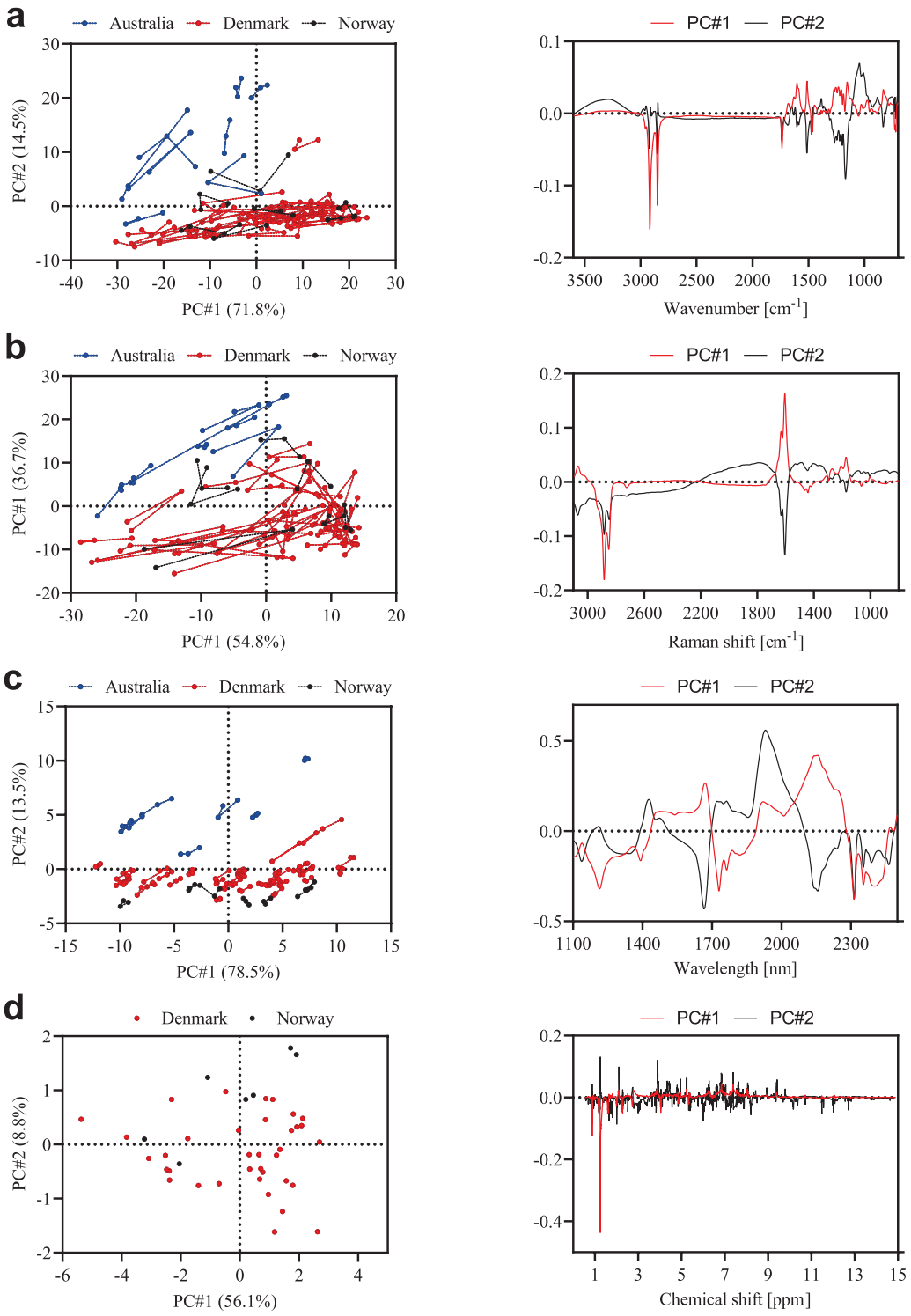

Fig. 3. PCA scores plots (left) and corresponding loadings plots (right) for (a) IR, (b) Raman shift, and (c) NIR measurements of Australian (N = 8), Danish (N = 38), and Norwegian (N = 7) propolis samples, and (d) ^{1}H NMR measurements of Danish and Norwegian propolis samples. Replicates for IR, Raman, and NIR (n = 3) are connected by stippled line.

amounts of aromatic compounds.

The NIR scores plot reveals a similar sample differentiation pattern to the IR scores plot, with the clustering of Australian samples driven by PC#2 rather than PC#1. PC#1 is primarily influenced by signals attributed to beeswax, including combination bands (2310–2445 nm) and overtones (1730–1765 nm, 1215 nm), which contribute to the negative loadings. In contrast, positive loadings are associated with signals from aromatic/conjugated compounds (2130–2170 nm, 1665–1680 nm). Signals ascribed to combination bands of hydroxyl-containing compounds (1900–1940 nm) also contribute positively to PC#1, albeit to a lesser extent. In contrast, these hydroxyl-related signals strongly drive the positive loadings for PC#2. The negative loadings for PC#2 are primarily driven by signals attributed to combination bands of either wax (2310–2445 nm) or aromatic compounds (2130–2170 nm), as well as the first overtones of aromatic/conjugated compounds (1665–1680 nm). The differentiation between signals

associated with aromatic and hydroxyl-containing compounds is particularly noteworthy. Although some aromatic compounds, such as polyphenols, include hydroxyl moieties, carbohydrates and terpenoids also contribute significantly to this functional group. The differentiation observed in PC#2, further supported by the PCA of IR data, suggest that these hydroxyl-related signals primarily originate from carbohydrates and terpenoids rather than polyphenols. This interpretation indicates that the PCA of NIR data highlights not only the lower concentration of aromatic compounds in Australian samples (as corroborated by IR and Raman data) but also their higher carbohydrate and terpenoid content, which drives their distinct clustering. Furthermore, the aforementioned comparatively larger intra-sample variability observed in the IR and Raman scores plots, relative to NIR, may be explained by NIR's superior ability to sample heterogeneous materials. Its larger sampling area and volume allow for more representative analysis, resulting in more robust chemical information [45]. The larger intra-sample variation observed for the IR and Raman data is primarily due to the small sample size measured, which, combined with the heterogeneous samples, contribute to replicate variability. In Raman spectroscopy, sample presentation can be influenced by varying sample fluorescence, whereas in IR spectroscopy it can be influenced by sample contact to the ATR crystal. To minimise these effects, measurements including replicates were performed in randomised runs under standardised acquisition settings.

Like for the vibrational spectroscopy, the ^{1}H NMR scores plot (Fig. 3D) does not reveal any chemical differences between the Danish and Norwegian samples. The negative loadings for PC#1 are primarily driven by signals in the aliphatic region, such as the aliphatic methylene signal at $\Delta\delta = 1.21$ ppm arising from wax, while the positive loadings are driven, to a lesser extent, by signals from the aromatic region ($\Delta\delta =$ 6.0–8.5 ppm). Variation along PC#2 appears to be primarily influenced by signals associated with wax (negative loadings). However, contributions from other spectral regions are less distinct, indicating potential variability in the chemical composition that remains unexplained. In summary, all employed vibrational spectroscopy techniques demonstrated a clear distinction between the Australian propolis samples compared to the Danish and Norwegian samples, primarily based on their aromatic content. Additionally, IR and NIR spectroscopy suggested that the Australian samples contained higher levels of carbohydrates and terpenoids relative to the Danish and Norwegian samples. This strongly indicates that the chemical composition of propolis is highly dependent on geographical location and the available flora for resin collection.

DPPH radical scavenging activity of propolis

To validate the PCA findings on differences in aromatic content, the antioxidative activity of the propolis samples was assessed using the 2,2-Diphenyl-1-picrylhydrazyl (DPPH) Radical Scavenging Activity (RSA) assay [46]. Since aromatic compounds, such as polyphenols, are major contributors to the antioxidant activity of propolis, the RSA serves as a relevant metric for this analysis. Fig. 4 presents a country-grouped boxplot showing the RSA of propolis samples from Australia, Denmark, and Norway.

Based on a one-way ANOVA followed by Tukey's HSD test, the RSA of the Danish and Norwegian samples showed no significant difference ($p \geq 0.05$), whereas the Australian samples exhibited significantly lower RSA compared to both the Danish ($p < 0.0001$) and Norwegian ($p < 0.001$) samples. This similarity in RSA between the Danish and Norwegian samples aligns with the spectral PCA results, which revealed no clear chemical distinction between them. In contrast, the PCA indicated that the Australian samples differed chemically from the others, primarily due to their lower aromatic content. As RSA is largely influenced by the aromatic content of a sample, these PCA findings are consistent with the observed RSA differences. Notably, one Danish sample appeared as an outlier, exhibiting a comparatively lower RSA, which was not expected based on the PCA. This highlights that the antioxidant capacity of propolis may vary substantially even within a single geographic origin and could depend on factors not fully represented in the PCA.

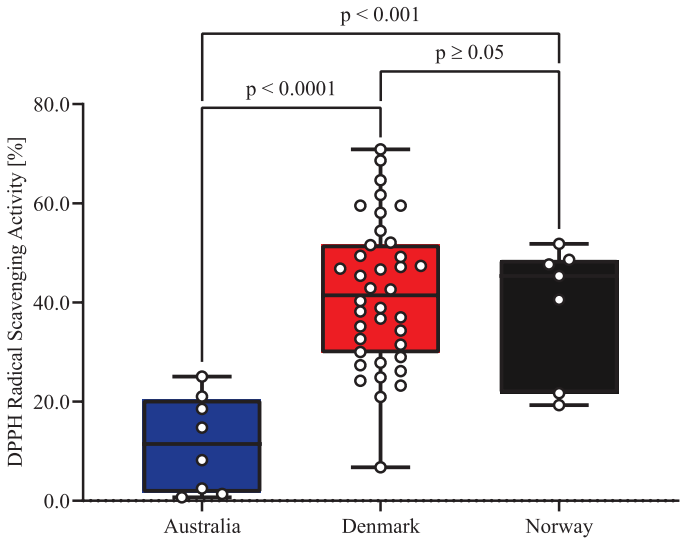

Fig. 4. Country-grouped boxplot displaying the 2,2-Diphenyl-1-picrylhydrazyl (DPPH) radical scavenging activity (RSA) of propolis samples from Australia (N = 8), Denmark (N = 38), and Norway (N = 7) relative to the negative control. White dots represent the average RSA of triplicates for each sample.

Correlation of spectroscopic signals to DPPH radical scavenging activity

To further explore the relationship between vibrational spectroscopy data and antioxidant activity, the correlation between spectral signals and the measured RSA was examined. The Australian samples were excluded due to their distinct spectral features compared to the Danish and Norwegian samples.

R^2 values were calculated between RSA and vibrational spectroscopic signals associated with aromatic compounds, specifically those covarying with the aromatic region shown in Fig. 2. For ^{1}H NMR, the average signal intensity in the aromatic region was used for correlation with RSA. The highest correlation (Table 2) was observed with similar magnitude ($R^2 = 0.64$) in both the Raman and NIR spectra at 1631 cm^{-1} and 1666 nm, respectively. The tentative assignment of these bands will be discussed later in Fig. 5. The aromatic region of ^{1}H NMR showed a

Table 2
Spectral variables, their respective vibration modes (as presented in Table 1) or signal origin, and Pearson's correlation coefficients to the 2,2-Diphenyl-1-picrylhydrazyl (DPPH) Radical Scavenging Activity (RSA) (Fig. 4). Preprocessing techniques included standard normal variate (SNV) for IR and Raman data, and the second derivative for NIR data, while no preprocessing was applied to the ^{1}H NMR data. For ^{1}H NMR, the average signal intensity of the aromatic region (6.0–8.5 ppm) was used for correlation analysis.

Technique	Identified Variable	Vibration mode/origin of signal	R^2 to RSA
IR	1232 cm^{-1}	ν(C-O), ν(C-O-C) (aromatic) [30, 39]	0.55
	1273 cm^{-1}	ν(C-O), ν(C-O-C) (aromatic) [30, 39]	0.52
Raman	1602 cm^{-1}	ν(C═C) (aromatic) [30], Fig. 5	0.58
	1631 cm^{-1}	ν(C═C) (conjugated) [30], Fig. 5	0.64
NIR	1666 nm	2ν(C-H) (aromatic/conjugated) [41], Fig.5	0.64
	1678 nm	2ν(C-H) (aromatic/conjugated) [41], Fig. 5	0.62
^{1}H NMR	6.0–8.5 ppm	Aromatic protons	0.58

Keys: ν; stretching, 2ν, first overtone

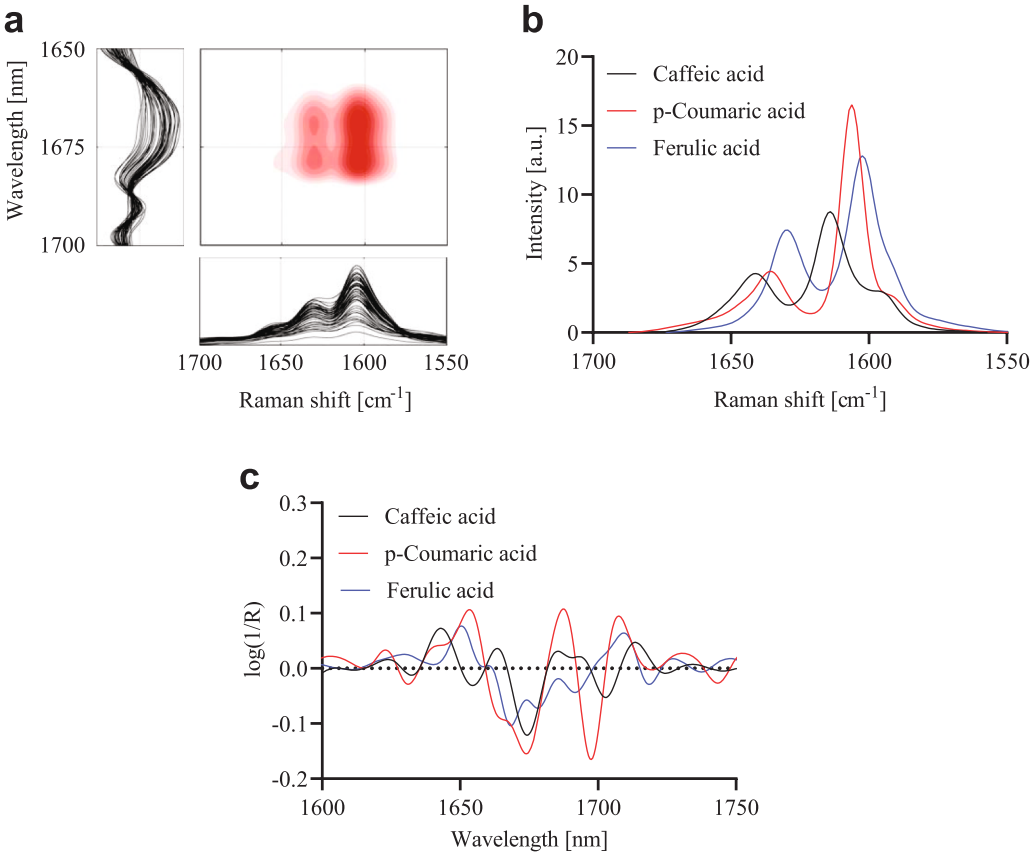

Fig. 5. (a) 2D covariation spectra of Raman (1700–1550 cm^{-1}) and NIR (1650–1700 nm) regions showing the highest correlations with RSA (Table 2). Raman data were pre-processed using standard normal variate (SNV) and Pareto scaling, while NIR data were treated with a second-derivative Savitzky-Golay filter and mean centering. Raw Raman and second-derivative NIR spectra are shown for Danish (N = 38) and Norwegian (N = 7) samples. (b) Raman and (c) second-derivative NIR spectra of selected regions for model compounds: caffeic acid, *p*-coumaric acid, and ferulic acid.

slightly lower correlation (R^2 = 0.58), while IR exhibited the weakest correlations among the four spectroscopic methods, with the signal at 1232 cm^{-1} yielding an R^2 value of 0.55.

The observed differences in correlation may be attributed to the principles underlying each technique. Raman spectroscopy, which is sensitive to changes in polarizability [47], is particularly responsive to C═C stretches of non-conjugated, conjugated and aromatic compounds. Given that antioxidant activity in propolis is largely driven by aromatic systems with the ability to stabilise radicals through hydrogen or electron donation, this sensitivity likely contributes to the strong correlation with RSA. In contrast, NIR spectroscopy allows for optimal sampling of heterogeneous samples due to its larger sampling area and volume as mentioned earlier [45]. While unprocessed NIR signals are typically broader and less specific, applying a second derivative enhances spectral resolution by reducing baseline effects and sharpening overlapping peaks [48]. This may improve sensitivity to aromatic structures and increase the specificity of signals, making NIR data more reliable for correlation analysis. IR spectroscopy, which is sensitive to changes in dipole moments [49], is particularly effective for detecting the stretching of polar bonds such as C-O and C-O-C. The signal observed at 1232 cm^{-1} has previously been attributed to these bonds. The slightly lower correlation observed for IR may result from its sensitivity to functional groups that do not directly contribute to antioxidant activity. Although such polar bonds may be present in aromatic compounds, the antioxidant activity of propolis is more strongly linked to conjugated C═C systems, which are more effectively detected by Raman spectroscopy. ^{1}H NMR showed a moderate correlation with RSA, reflecting the contribution of aromatic protons. However, averaging the entire aromatic region may dilute specificity, as signals from non-antioxidative compounds could also be present.

To support the assignment of the Raman and NIR signals showing the highest R^2 values to RSA, additional analysis was performed using 2D correlation spectroscopy (Fig. 5A). Furthermore, Raman and NIR spectra were recorded for three model compounds commonly found in propolis [50]: caffeic acid, p-coumaric acid, and ferulic acid, all of which contain both aromatic and conjugated C═C bonds. These measurements were used to aid in final signal assignment, and the relevant spectral regions are shown in Fig. 5B-C.

The 2D correlation spectrum (Fig. 5A) reveals covariation between the Raman and NIR signals of interest, consistent with their shared correlation with RSA. In the Raman spectrum, two distinct signals at 1602 and 1631 cm^{-1} are observed. While relatively well-resolved, these signals remain broad, suggesting potential overlap from multiple contributing aromatic compounds. In contrast, the NIR signals are notably broader and less distinguishable, indicating a higher degree of spectral overlap in this region. Nevertheless, two signals at wavelengths 1666 and 1678 nm exhibit stronger covariation with the Raman signal at 1631 cm^{-1} than other wavelengths in the selected region, aiding in the identification of the variables of interest.

The Raman spectra of the model compounds (Fig. 5B) also display both signals observed in Fig. 5A, although their exact peak positions and intensities vary among the compounds. Since these compounds differ only in the substituents on the benzene ring, specifically the presence or absence of a methoxy group and the different positioning of hydroxyl groups, this variation likely reflects the influence of electronic effects, particularly resonance and conjugation, on the electron distribution within the aromatic system and the associated C═C vibrational modes. The presence of both the 1631 and 1602 cm^{-1} signals across all three

compounds supports their assignment to distinct vibrational origins. The 1602 cm^{-1} signal is likely associated with aromatic C=C stretches within the benzene ring, reflecting lower energy and delocalized π-electrons. In contrast, the 1631 cm^{-1} signal is more plausibly attributed to conjugated (non-aromatic) C=C stretches, which typically resonate at slightly higher energy due to their more localized electronic structure.

The NIR spectra of the model compounds (Fig. 5C), by comparison, are more ambiguous. Application of the second-derivative Savitzky-Golay filter reveals several overlapping bands, which likely originate from the first overtones of aromatic and/or conjugated C-H stretches. However, unlike the Raman spectra, it is not feasible to distinguish which signals arise from aromatic versus conjugated C-H overtones in the NIR spectra of the model compounds, and by extension, in those of the propolis samples. This limitation stems primarily from the overlapping nature of these overtones and is further compounded by the extensive spectral congestion in the NIR region of the propolis samples, reflecting their inherently complex, polyphenol-rich composition. Although exact determination of the origin of these signals is not realistic, the 2D correlation analysis (Fig. 5A) helps to lessen this ambiguity by highlighting the two NIR bands, at 1666 nm and 1678 nm, that covary with the Raman signal at 1631 cm^{-1}. These findings underscore the relevance of these NIR features despite the spectral complexity and support their association with vibrational modes of aromatic and/or conjugated structures. Notably, the NIR peaks of the model compounds appear at slightly higher wavelengths compared to those in the propolis spectra. This discrepancy may be attributed to matrix effects, as the resinous nature of propolis could influence how compounds interact with the light source, potentially shifting their absorbance features.

Together, these results highlight how the different spectroscopic methods complement one another in providing insight into the chemical composition of propolis. Each method offers distinct advantages and limitations, with varying sensitivity and specificity toward the antioxidant-relevant structures in propolis.

Prediction of radical scavenging activity based on spectroscopic data

In order to scrutinize the relation between the chemical spectra and the RSA, a PLS regression model was created to evaluate the ability of the applied spectroscopic techniques to predict the RSA of the propolis samples. Due to the large replicate variability of IR and Raman measurements, observed in the PCA (Fig. 2), an average of the triplicates was used for PLS regression. The Australian samples were excluded from the analysis due to their distinct chemical composition and lower aromatic

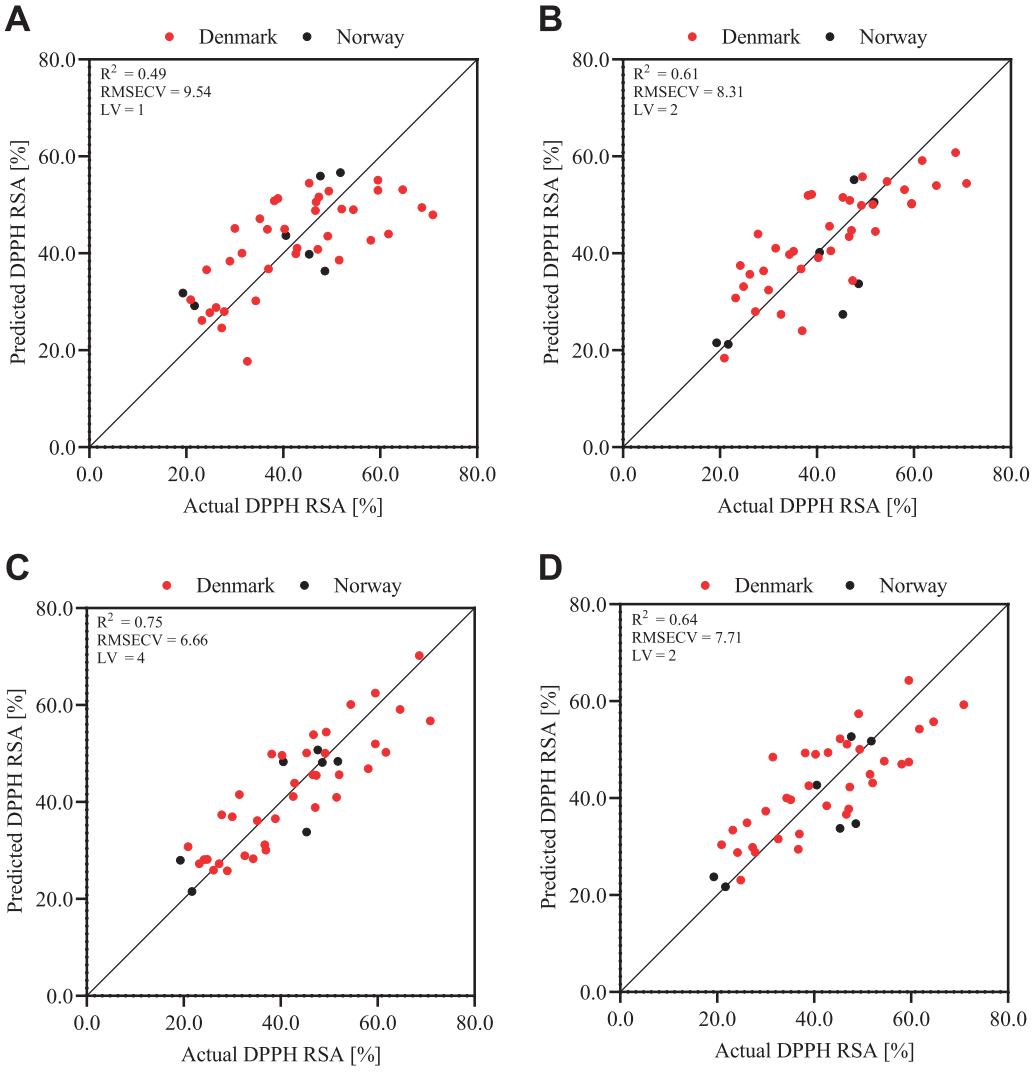

Fig. 6. Actual versus predicted plots for the (2,2-Diphenyl-1-picrylhydrazyl) DPPH Radical Scavenging Activity (RSA) of Danish (N = 37) and Norwegian (N = 7) propolis samples based on (a) IR, (b) Raman, (c) NIR, and (d) ^{1}H NMR data. The observed R^2 values for IR, Raman, NIR, and ^{1}H NMR data were 0.49, 0.61, 0.75, and 0.64, respectively, with corresponding respective Root Mean Square Error of Cross-Validation (RMSECV) values of 9.54%, 8.31%, 6.66%, and 7.71%. The latent variables (LV) for the IR, Raman, NIR, and ^{1}H NMR models were 1, 2, 4, and 2, respectively.

content, both of which are key determinants of RSA and could potentially obscure the relationship between chemical spectra and RSA in the Danish and Norwegian samples. In addition, the Danish sample previously identified as an RSA outlier was omitted from the spectroscopic models. For the ^{1}H NMR model, two additional samples previously associated with extraction errors were also excluded. These omissions were made to ensure a more robust and accurate evaluation of the PLS models. Fig. 6 shows the actual versus predicted plot of the RSA as predicted by the four spectroscopic-based PLS regression models.

The NIR-based model exhibited the best predictive power with R^2 and Root Mean Square Error of Cross-validation (RMSECV) values of 0.75 and 6.66%, respectively. The Raman-based model (R^2 = 0.61, RMSECV = 8.31%) and the ^{1}H NMR-based model (R^2 = 0.64, RMSECV = 7.71%) demonstrated similar predictive performance, while the IR-based model produced the worst predictive power (R^2 = 0.49, RMSECV = 9.54%). Thus, NIR proved to have the highest predictive power, likely explained by the much better sampling of heterogeneous samples by this method. The relatively high predictive power of Raman spectroscopy and ^{1}H NMR compared to IR for predicting RSA likely stems from their sensitivities to key molecular features, as discussed earlier. Raman spectroscopy is particularly effective at detecting aromatic/conjugated C=C stretching vibrations due to the changes in polarization, which are fundamental functional groups to antioxidative activity. Similarly, ^{1}H NMR provides detailed insights into proton environments, recording significant information about functional groups and molecular interactions that may influence RSA. In contrast, the lower performance of IR spectroscopy may result from its focus on dipole moment changes rather than polarization, as well as potential limitations associated with triple-bounce diamond ATR sampling.

However, a direct comparison between the vibrational spectroscopy-based models and the ^{1}H NMR-based model may not be entirely valid, as ^{1}H NMR analysis requires sample extraction prior to measurement, whereas vibrational spectroscopic methods can analyse the sample directly. The extraction step inherently increases the risk of biased errors, as evidenced by the two excluded outliers linked to issues during the extraction process. Furthermore, the analysis is also subsequently limited to the extracted components, potentially omitting compounds present in the crude sample. Consequently, the broader compositional overview offered by vibrational spectroscopy may be advantageous in certain contexts, with NIR being particularly well-suited for sampling of heterogeneous materials. Despite this fundamental limitation, liquid state ^{1}H NMR still offers the advantage of providing more detailed molecular information of complex biological samples compared to vibrational spectroscopic methods, allowing for more precise identification of specific chemical compounds. Therefore, when choosing a spectroscopic method, it is crucial to consider the strengths and limitations of each technique in relation to the analysis goals and recognize that they can all provide complementary information.

Limitations of this study include the small number of Australian samples and their exclusion from the ^{1}H NMR analysis, which weakens conclusions for this group and limits regional generalisability. Although repeated cross-validation ensured robust model performance, our limited sample set did not allow for an external validation set. Future studies should include independent datasets from other geographical regions to confirm the predictive performance and broader applicability of the models. A further limitation of the present study is that the applied spectroscopic approaches do not allow comprehensive chemical typing of propolis or unambiguous identification of individual compounds. While vibrational spectroscopic techniques provide rich information on overall chemical features and structural classes, they do not resolve the specific molecular constituents traditionally used to define propolis types. Although ^{1}H NMR has the potential to deliver more detailed molecular information, extensive signal overlap from aromatic protons within the chemically complex propolis matrix precluded confident compound-level identification in the present dataset. Consequently, the findings should be interpreted as functional and compositional fingerprints rather than exhaustive chemical characterizations. From a quality control perspective, this fingerprint-based strategy remains highly relevant, as it enables rapid, non-destructive assessment of antioxidant potential and batch-to-batch consistency and should be viewed as complementary to targeted analytical approaches used for propolis standardization.

Conclusion

This study presents an unbiased spectroscopic approach to screen the chemical composition of propolis from Australia, Denmark, and Norway using multiple spectroscopic techniques, and to predict antioxidative activity (expressed as DPPH RSA) in the Scandinavian samples based on Raman, NIR, and ^{1}H NMR spectroscopy. PCA showed no significant differences between Danish and Norwegian propolis, both of which had higher aromatic content than Australian samples, whereas the latter was richer in carbohydrates and terpenoids. Australian propolis also exhibited significantly lower RSA compared to Danish and Norwegian samples. Across all applied techniques, the strongest correlations with RSA were observed at 1631 cm^{-1} in Raman and 1666 nm in NIR, linked to conjugated C=C and first overtones of aromatic/conjugated C-H stretches, respectively. NIR spectroscopy yielded the most accurate RSA predictions (R^2 = 0.75, RMSECV = 6.66%), followed by ^{1}H NMR and Raman, while IR was less predictive. Thus, NIR, in particular, shows strong potential as a rapid, non-destructive tool for routine quality control of chemically complex natural products such as propolis. The results also clearly demonstrate the complementary nature of the applied spectroscopic techniques, as Raman exhibited sensitivity to aromatic features linked to RSA, IR provided broad functional-group information, and NIR captured both aromatic signatures and a more holistic chemical overview. In addition, 2D correlations with ^{1}H NMR spectroscopy enhanced the interpretation across the different techniques.

Finally, the clear compositional and functional differences between Australian and Scandinavian propolis highlight the strong influence of geographical and botanical variability on propolis chemistry and its associated bioactivity.

CRediT authorship contribution statement

Hasim Tekin: Writing – review & editing, Methodology, Funding acquisition, Conceptualization. **Julie Christine Antvorskov:** Writing – review & editing, Supervision, Project administration, Funding acquisition, Conceptualization. **Søren Balling Engelsen:** Writing – review & editing, Visualization, Supervision, Methodology, Data curation, Conceptualization. **Knud Josefsen:** Writing – review & editing, Supervision, Methodology, Funding acquisition, Data curation, Conceptualization. **Jonas Pordel Vind:** Writing – review & editing, Writing – original draft, Project administration, Data curation. **Henrik Munch Jørgensen:** Writing – review & editing, Supervision, Project administration, Funding acquisition. **Violetta Aru:** Writing – review & editing, Supervision, Methodology, Data curation.

Declaration of Competing Interest

The authors declare that they have no known competing financial interests or personal relationships that could have appeared to influence the work reported in this paper.

Funding/Acknowledgement

This work was funded by the European Union and the Danish Agricultural Agency under the national implementation of the Apiculture Support Scheme 2023–2026. Data was generated though accessing research infrastructure at the University of Copenhagen, including FOODHAY (Food and Health Open Innovation Laboratory, Danish

Roadmap for Research Infrastructure).

Appendix A. Supporting information

Supplementary data associated with this article can be found in the online version at doi:10.1016/j.prenap.2026.100578.

Data availability

Data will be made available on request.

References

[1] M. Simone-Finstrom, M. Spivak, Propolis and bee health: the natural history and significance of resin use by honey bees, Apidologie 41 (3) (2010) 295–311, https://doi.org/10.1051/apido/2010016.

[2] E.L. Ghisalberti, Propolis: A Review, Bee World 60 (2) (1979) 59–84, https://doi.org/10.1080/0005772X.1979.11097738.

[3] R. Hossain, C. Quispe, R.A. Khan, A.S.M. Saikat, P. Ray, D. Ongalbek, et al., Propolis: an update on its chemistry and pharmacological applications, Chin. Med. 17 (1) (2022) 100, https://doi.org/10.1186/s13020-022-00651-2.

[4] N. Drescher, A.M. Klein, T. Schmitt, S.D. Leonhardt, A clue on bee glue: new insight into the sources and factors driving resin intake in honeybees (Apis mellifera), PLoS One 14 (2) (2019) e0210594, https://doi.org/10.1371/journal.pone.0210594.

[5] M. Dobrosielska, R. Dobrucka, P. Kozera, D. Brząkalski, E. Gabriel, J. Głowacka, et al., Beeswax as a natural alternative to synthetic waxes for fabrication of PLA/diatomaceous earth composites, Sci. Rep. 13 (1) (2023) 1161, https://doi.org/10.1038/s41598-023-28435-0.

[6] J. Cuní, P. Cuni, B. Eisen, R. Savizky, J. Bové, Characterization of the binding medium used in Roman encaustic paintings on wall and wood, Anal. Methods 4 (2012) 659–669, https://doi.org/10.1039/C2AY05635F.

[7] A. Kurek-Górecka, Ş. Keskin, O. Bobis, R. Felitti, M. Górecki, M. Otręba, et al., Comparison of the Antioxidant Activity of Propolis Samples from Different Geographical Regions, Plants 11 (9) (2022), https://doi.org/10.3390/plants11091203.

[8] M.L.F. Bittencourt, P.R. Ribeiro, R.L.P. Franco, H.W.M. Hilhorst, R.D. de Castro, L. G. Fernandez, Metabolite profiling, antioxidant and antibacterial activities of Brazilian propolis: Use of correlation and multivariate analyses to identify potential bioactive compounds, Food Res. Int. 76 (2015) 449–457, https://doi.org/10.1016/j.foodres.2015.07.008.

[9] S.M. Osés, P. Marcos, P. Azofra, A. de Pablo, M. Fernández-Muíño, M.T. Sancho, Phenolic profile, antioxidant capacities and enzymatic inhibitory activities of propolis from different geographical areas: needs for analytical harmonization, Antioxidants 9 (1) (2020), https://doi.org/10.3390/antiox9010075.

[10] L. Barrientos, C.L. Herrera, G. Montenegro, X. Ortega, J. Veloz, M. Alvear, et al., Chemical and botanical characterization of Chilean propolis and biological activity on cariogenic bacteria Streptococcus mutans and Streptococcus sobrinus, Braz. J. Microbiol 44 (2) (2013) 577–585, https://doi.org/10.1590/s1517-83822013000200038.

[11] Y. Zhang, C. Cao, Z. Yang, G. Jia, X. Liu, X. Li, et al., Simultaneous determination of 20 phenolic compounds in propolis by HPLC-UV and HPLC-MS/MS, J. Food Compos. Anal. 115 (2023) 104877, https://doi.org/10.1016/j.jfca.2022.104877.

[12] B. Khakimov, G. Gürdeniz, S. Engelsen, Trends in the application of chemometrics to foodomics studies, Acta Aliment. 44 (2015) 4–31, https://doi.org/10.1556/AAlim.44.2015.1.1.

[13] M. Surek, Ad.F. Cobre, M.M. Fachi, T.G. Santos, R. Pontarolo, A.R. Crisma, et al., Propolis authentication of stingless bees by mid-infrared spectroscopy and chemometric analysis, LWT 161 (2022) 113370, https://doi.org/10.1016/j.lwt.2022.113370.

[14] I. Revilla, A.M. Vivar-Quintana, I. González-Martín, O. Escuredo, C. Seijo, The potential of near infrared spectroscopy for determining the phenolic, antioxidant, color and bactericide characteristics of raw propolis, Microchem. J. 134 (2017) 211–217, https://doi.org/10.1016/j.microc.2017.06.006.

[15] M.I. Stavropoulou, K. Stathopoulou, A. Cheilari, D. Benaki, K. Gardikis, I. Chinou, et al., NMR metabolic profiling of Greek propolis samples: Comparative evaluation of their phytochemical compositions and investigation of their anti-ageing and antioxidant properties, J. Pharm. Biomed. Anal. 194 (2021) 113814, https://doi.org/10.1016/j.jpba.2020.113814.

[16] S. Kumazawa, K. Hayashi, K. Kajiya, T. Ishii, T. Hamasaka, T. Nakayama, Studies of the constituents of uruguayan propolis, J. Agric. Food Chem. 50 (17) (2002) 4777–4782, https://doi.org/10.1021/jf020279y.

[17] Å. Rinnan, M. Andersson, C. Ridder, S.B. Engelsen, Recursive weighted partial least squares (rPLS): an efficient variable selection method using PLS, J. Chemom. 28 (5) (2014) 439–447, https://doi.org/10.1002/cem.2582.

[18] L.A. Mărghitaş, D. Dezmirean, A. Moise, C.M. Mihai, L. Laslo, DPPH method for evaluation of propolis antioxidant activity, Bull. USAMV 66 (2009) 253–258.

[19] M.M. Nichitoi, A.M. Josceanu, R.D. Isopescu, G.O. Isopencu, E.-I. Geana, C. T. Ciucure, et al., Polyphenolics profile effects upon the antioxidant and antimicrobial activity of propolis extracts, Sci. Rep. 11 (1) (2021) 20113, https://doi.org/10.1038/s41598-021-97130-9.

[20] S.B. Kedare, R.P. Singh, Genesis and development of DPPH method of antioxidant assay, J. Food Sci. Technol. 48 (4) (2011) 412–422, https://doi.org/10.1007/s13197-011-0251-1.

[21] F. Savorani, G. Tomasi, S.B. Engelsen, icoshift: A versatile tool for the rapid alignment of ^{1}D NMR spectra, J. Magn. Reson 202 (2) (2010) 190–202, https://doi.org/10.1016/j.jmr.2009.11.012.

[22] F.E. Barton, D.S. Himmelsbach, J.H. Duckworth, M.J. Smith, Two-dimensional vibration spectroscopy: correlation of mid- and near-infrared regions, Appl. Spectrosc. 46 (3) (1992) 420–429, https://doi.org/10.1366/0003702924125375.

[23] I. Noda, Generalized two-dimensional correlation method applicable to infrared, Raman, and other types of spectroscopy, Appl. Spectrosc. 47 (9) (1993) 1329–1336.

[24] R.J. Barnes, M.S. Dhanoa, S.J. Lister, Standard normal variate transformation and de-trending of near-infrared diffuse reflectance spectra, Appl. Spectrosc. 43 (5) (1989) 772–777, https://doi.org/10.1366/0003702894202201.

[25] S. Wold, K. Esbensen, P. Geladi, Principal component analysis, Chemom. Intell. Lab. Syst. 2 (1) (1987) 37–52, https://doi.org/10.1016/0169-7439(87)80084-9.

[26] The multivariate calibration problem in chemistry solved by the PLS method, in: S. Wold, H. Martens, H. Wold (Eds.), Matrix Pencils, Springer, Berlin, Heidelberg, 1983.

[27] E. Wiercigroch, E. Szafraniec, K. Czamara, M.Z. Pacia, K. Majzner, K. Kochan, et al., Raman and infrared spectroscopy of carbohydrates: a review, Spectrochim. Acta Part A Mol. Biomol. Spectrosc. 185 (2017) 317–335, https://doi.org/10.1016/j.saa.2017.05.045.

[28] B.M. Mitzner, V.J. Mancini, S. Lemberg, E.T. Theimer, Infrared spectra of monoterpenes and related compounds. II. Terpene alcohols, Appl. Spectrosc. 22 (1) (1968) 34–53.

[29] A. Hassabo, Saturated fatty acids derivatives as assistants materials for textile processes, J. Text. Sci. & Fash. Technol. 1 (2018), https://doi.org/10.33552/JTSFT.2018.01.000516.

[30] M. Krysa, M. Szymańska-Chargot, A. Zdunek, FT-IR and FT-Raman fingerprints of flavonoids - a review, Food Chem. 393 (2022) 133430, https://doi.org/10.1016/j.foodchem.2022.133430.

[31] H.G.M. Edwards, D.W. Farwell, L. Daffner, Fourier-transform Raman spectroscopic study of natural waxes and resins. I, Spectrochim. Acta Part A Mol. Biomol. Spectrosc. 52 (12) (1996) 1639–1648, https://doi.org/10.1016/0584-8539(96)01730-8.

[32] C. Corredor, T. Teslova, M.V. Cañamares, Z. Chen, J. Zhang, J.R. Lombardi, et al., Raman and surface-enhanced Raman spectra of chrysin, apigenin and luteolin, Vib. Spectrosc. 49 (2) (2009) 190–195, https://doi.org/10.1016/j.vibspec.2008.07.012.

[33] Majhi A. Himanshu, B. Behera, Prediction of wax content in crude oil and petroleum fraction by proton NMR, Pet. Sci. Technol. 37 (2018) 1–8, https://doi.org/10.1080/10916466.2018.1536713.

[34] A.G. Abdul Jameel, Identification and quantification of hydrocarbon functional groups in gasoline using (1)H NMR spectroscopy for property prediction, Molecules 26 (22) (2021), https://doi.org/10.3390/molecules26226989.

[35] I. Noda, A.E. Dowrey, C. Marcott, G.M. Story, Y. Ozaki, Generalized two-dimensional correlation spectroscopy, Appl. Spectrosc. 54 (7) (2000) 236A–248AA, https://doi.org/10.1366/0003702001950454.

[36] A.B. Brizuela, L.C. Bichara, E. Romano, A. Yurquina, S. Locatelli, S.A. Brandán, A complete characterization of the vibrational spectra of sucrose, Carbohydr. Res. 361 (2012) 212–218, https://doi.org/10.1016/j.carres.2012.07.009.

[37] G.E. McManis, L.E. Gast, IR spectra of long chain vinyl derivatives, J. Am. Oil Chem. Soc. 48 (11) (1971) 668–673, https://doi.org/10.1007/BF02638515.

[38] L. Svečnjak, G. Baranović, M. Vinceković, S. Prđun, D. Bubalo, I. Tlak Gajger, An approach for routine analytical detection of beeswax adulteration using FTIR-ATR spectroscopy, J. Apic. Sci. 59 (2015), https://doi.org/10.1515/JAS-2015-0018.

[39] O. Abbas, G. Compère, Y. Larondelle, D. Pompeu, H. Rogez, V. Baeten, Phenolic compound explorer: a mid-infrared spectroscopy database, Vib. Spectrosc. 92 (2017) 111–118, https://doi.org/10.1016/j.vibspec.2017.05.008.

[40] D. Wu, X. Chen, P. Shi, S. Wang, F. Feng, Y. He, Determination of α-linolenic acid and linoleic acid in edible oils using near-infrared spectroscopy improved by wavelet transform and uninformative variable elimination, Anal. Chim. Acta 634 (2) (2009) 166–171, https://doi.org/10.1016/j.aca.2008.12.024.

[41] M.V. Reboucas, B. de Barros Neto, Near infrared spectroscopic prediction of physical properties of aromatics-rich hydrocarbon mixtures, J. Infrared Spectrosc. 9 (4) (2001) 263–273, https://doi.org/10.1255/jnirs.312.

[42] L.G. Weyer, S.C. Lo, Spectra– structure correlations in the near-infrared, Handb. Vib. Spectrosc. (2006).

[43] M. Barea-Sepúlveda, J.L.P. Calle, M. Ferreiro-González, M. Palma, Rapid classification of petroleum waxes: a Vis-NIR spectroscopy and machine learning approach, Foods 12 (18) (2023), https://doi.org/10.3390/foods12183362.

[44] M. Baglioni, G. Poggi, G. Ciolli, E. Fratini, R. Giorgi, P. Baglioni, A triton X-100-based microemulsion for the removal of hydrophobic materials from works of art: SAXS characterization and application, Mater. (Basel) 11 (7) (2018), https://doi.org/10.3390/ma11071144.

[45] T.P. Czaja, S.B. Engelsen, Why nothing beats NIRS technology: the green analytical choice for the future sustainable food production, Spectrochim. Acta Part A Mol. Biomol. Spectrosc. 325 (2025) 125028, https://doi.org/10.1016/j.saa.2024.125028.

[46] S. Baliyan, R. Mukherjee, A. Priyadarshini, A. Vibhuti, A. Gupta, R.P. Pandey, et al., Determination of antioxidants by DPPH radical scavenging activity and quantitative phytochemical analysis of Ficus religiosa, Molecules 27 (4) (2022), https://doi.org/10.3390/molecules27041326.

[47] E. Berger, H.-P. Komsa, Polarizability models for simulations of finite temperature Raman spectra from machine learning molecular dynamics, Phys. Rev. Mater. 8 (4) (2024) 043802, https://doi.org/10.1103/PhysRevMaterials.8.043802.
[48] Å. Rinnan, F. Berg, S. Engelsen, Review of the most common pre-processing techniques for near-infrared spectra, TrAC Trends Anal. Chem. 28 (2009) 1201–1222, https://doi.org/10.1016/j.trac.2009.07.007.
[49] L.R. Bernal-Alvarez, P.E. Martinez-Munoz, A.M. Castillo-Paz, H.D. Garcia-Vazquez, B.M. Millán-Malo, M.E. Rodriguez-Garcia, Infrared spectroscopy as a tool to study the vibrational, mechanical, and structural changes in commercial plastic bags: physical principles, J. Mol. Struct. 1303 (2024) 137580, https://doi.org/10.1016/j.molstruc.2024.137580.
[50] L. Zhu, J. Zhang, H. Yang, G. Li, H. Li, Z. Deng, et al., Propolis polyphenols: a review on the composition and anti-obesity mechanism of different types of propolis polyphenols, Front. Nutr. 10 (2023), https://doi.org/10.3389/fnut.2023.1066789.

Supplementary Figures

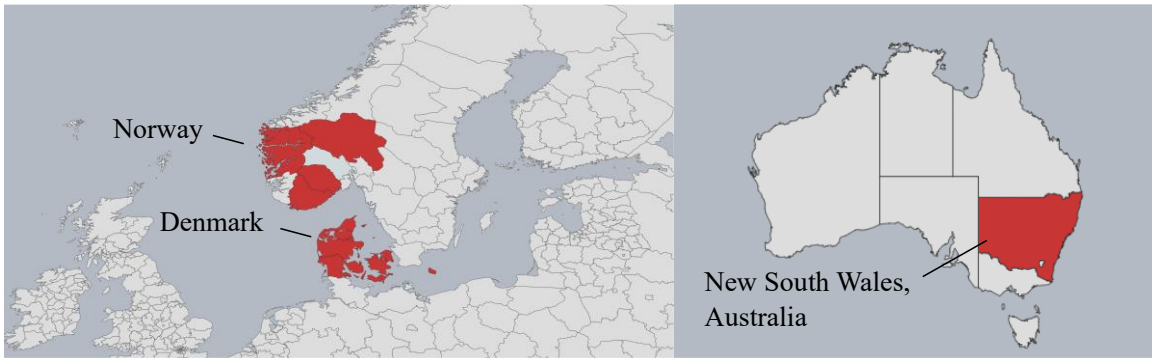

Supplementary Figure S1. Regions from which the propolis samples were harvested from.

Supplementary Figure S2. Representative pictures of the Danish (left), Norwegian (middle), and Australian (right) propolis samples used for the study.

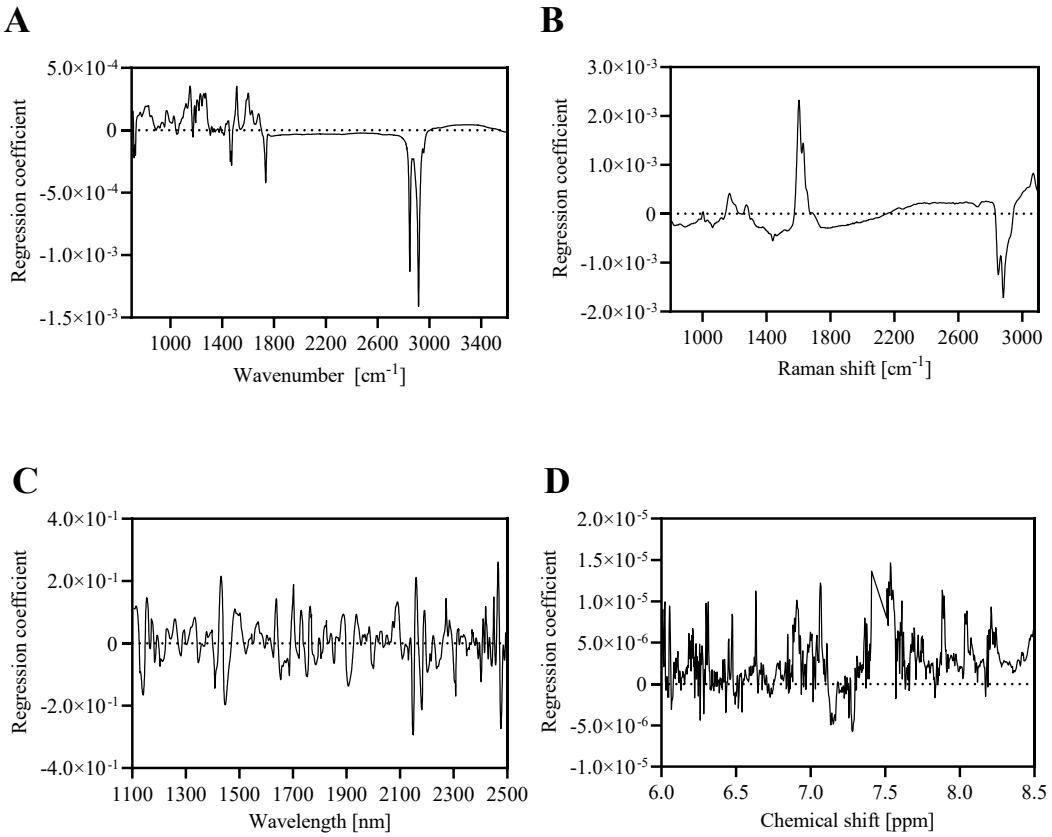

Supplementary Figure S3. Regression coefficients from PLS regression models used to predict radical scavenging activity (RSA) based on (A) IR, (B) Raman, (C) NIR, and (D) ^{1}H NMR spectra (Figure 6). The IR and Raman data were pre-processed using standard normal variate (SNV) followed by mean centering; NIR data were pre-processed using a second-derivative Savitzky-Golay filter followed by Pareto scaling; and ^{1}H NMR data (aromatic region, $\Delta\delta$ = 6.0–8.50 ppm) was Pareto scaled.

Manuscript II

Magnetic Resonance in Chemistry

WILEY

RESEARCH ARTICLE OPEN ACCESS

Comparative ^{1}H NMR Metabolomics Between Scandinavian Propolis and Australian Propolis: The Quest to Identify Radical Scavenging Compounds

Jonas Vind[1] | Søren Balling Engelsen[2] | Henrik Munch Jørgensen[1] | Julie Christine Antvorskov[3] | Knud Josefsen[1] | Violetta Aru[2]

[1]Department of Pathology, The Bartholin Institute, Copenhagen University Hospital, Copenhagen, Denmark | [2]Department of Food Science, University of Copenhagen, Frederiksberg, Denmark | [3]Department of Clinical Research, Steno Diabetes Center Copenhagen, Translational Type 1 Diabetes Research, Herlev, Denmark

Correspondence: Jonas Vind (jonas.pordel.vind@regionh.dk)

Received: 22 September 2025 | **Revised:** 25 December 2025 | **Accepted:** 5 January 2026

Keywords: ^{1}H NMR metabolomics | *A. mellifera* | cerumen | ferulic acid | *p*-coumaric acid | propolis | radical scavenging activity (RSA) | *r*PLS | STOCSY | *T. carbonaria*

ABSTRACT

Propolis from *Apis mellifera* and cerumen from *Tetragonula carbonaria* are complex mixtures of beeswax, plant resins, and bee secretions whose composition varies with geography and species. Understanding these differences is important for exploring their bioactive potential. This study employs untargeted quantitative ^{1}H NMR metabolomics to characterize *A. mellifera* propolis from Scandinavia (Denmark and Norway) and Australia, as well as cerumen from *T. carbonaria* in Australia. Hydrophilic and hydrophobic extracts were analyzed to assess compositional differences across geographical origin and bee species, and to link specific metabolites to radical scavenging activity (RSA). Principal component analysis (PCA) of the ^{1}H NMR spectra showed a marked separation between Scandinavian and Australian propolis. Hydrophilic extracts showed that Scandinavian propolis contains higher levels of aromatic compounds, whereas Australian propolis is richer in carbohydrates. In contrast, cerumen from *T. carbonaria* exhibits higher amounts of terpenoids. Hydrophobic extracts revealed that Australian propolis has the highest wax content, with shorter chains and more free fatty acids, while Scandinavian propolis samples display uniform wax structures and the highest aromatic content. Multivariate regression using recursive weighted partial least squares (*r*PLS) to RSA prediction highlighted signals attributable to ferulic acid and *p*-coumaric acid, which were confirmed by statistical total correlation spectroscopy (STOCSY). These findings demonstrate the utility of quantitative ^{1}H NMR metabolomics for distinguishing botanical and geographic chemotypes of propolis and cerumen. The findings further show that Scandinavian propolis is more consistent with respect to metabolite composition compared to Australian samples, presumably reflecting differences in resin sources for foraging.

1 | Introduction

Propolis is a wax-containing resinous material produced by honeybees (*Apis mellifera*) [1] and is used to fill crevices, reinforce hive structures, and protect against pathogens [2]. Due to its well-established antioxidative properties, propolis is used as a nutraceutical [3]. Clinical studies have reported that propolis supplementation can modulate endogenous redox-related biomarkers, including increasing reduced glutathione [4] and glutathione peroxidase [5] levels. Although the anti-oxidative properties are often linked to polyphenols [6], the specific origin of these antioxidative effects remains elusive [7].

[Correction added on 23 February 2026, after the first online publication: The copyright line was changed.]

Stingless bees also produce a similar substance known as cerumen, which plays a crucial role in constructing internal nest structures such as brood cells and honeypots, while also serving as a physical and chemical defense [8, 9]. Although *A. mellifera* has become globally widespread due to human domestication [10], stingless bees, such as *Tetragonula carbonaria*, remain naturally restricted to tropical and subtropical climates. Their limited ability to thermoregulate shapes both their nesting behavior and beekeeping potential [11]. As a result, despite the existence of over 500 stingless bee species [12], research on cerumen remains limited, and its chemical composition and bioactive potential are not yet fully understood to the extent of propolis.

Both propolis and cerumen are primarily composed of beeswax, foraged resins, and enzyme-rich bee secretions [13, 14]. While beeswax mainly consists of saturated hydrocarbons together with their ester and acid derivatives [15, 16], resins are chemically complex and contain a wide range of bioactive compounds, including flavonoids, phenolic acids, and terpenoids [17, 18]. The composition of foraged resins varies depending on geography, local flora, and bee species, reflecting hive- and nest-specific functional demands and contributing significantly to the chemical diversity of propolis and cerumen [19, 20].

Advances in analytical techniques have enabled detailed investigations of propolis, and in recent years increasing efforts have focused on comparative chemical characterization and bioactivity of both propolis and cerumen across geographic regions and bee species [21–23]. Studies consistently identify phenolic acids and flavonoids as dominant constituents of *A. mellifera* propolis, with regional differences shaping both composition and bioactivity [24, 25]. Egyptian propolis has even been shown to act synergistically with honey against multidrug-resistant uropathogens [26]. In contrast, cerumen from stingless bees contains polyphenols but is particularly enriched in terpenoids [9, 21]. Spectroscopic and chromatographic approaches have further identified unique chemical markers that distinguish different chemotypes and provide insight into the resin sources used by bees [27, 28]. Collectively, these findings highlight that propolis and cerumen are complex yet chemically traceable matrices.

Proton nuclear magnetic resonance (^{1}H NMR) spectroscopy provides a high-resolution, untargeted approach for profiling compounds in complex samples such as foods and natural products [29, 30]. ^{1}H NMR delivers a comprehensive and inherently quantitative view of chemical composition, making it particularly well-suited for exploratory comparative studies of propolis and cerumen [31]. When combined with multivariate data analysis techniques [30, 32], ^{1}H NMR offers a robust and widely adopted platform for untargeted metabolomics of low-molecular-weight compounds (< 1.5 kDa) in biological systems [30, 33]. In this context, metabolomics can translate complex spectral data into interpretable biochemical signatures, enabling robust classification, biomarker discovery, and quality control across diverse samples [34]. To date, however, ^{1}H NMR metabolomics studies of propolis and cerumen have largely focused on compositional profiling and geographical discrimination, with fewer studies investigating their biological activity or linking specific metabolites to functional effects [35].

In this study, ^{1}H NMR metabolomics was employed to investigate how bee species (*A. mellifera* and *T. carbonaria*) and geographical origin (Australia, Denmark, and Norway) influence the chemical composition of propolis and cerumen, considering both resin-derived constituents and beeswax. Propolis and cerumen extracts were measured by ^{1}H NMR spectroscopy. To identify candidate molecules contributing to the antioxidative capacity measured by the 2,2-diphenyl-1-picrylhydrazyl (DPPH) radical scavenging activity (RSA) assay [36], recursive weighted partial least squares regression (*r*PLS) [37] and statistical total correlation spectroscopy (STOCSY) were employed [38]. The combination of the two approaches enabled the identification of signals from compounds of interest and the detection of interrelated spectral features, thereby facilitating compound assignment of putative metabolite candidates responsible for the RSA activity.

2 | Experimental Section

2.1 | Chemicals

Analytical grade methanol (CH_3OH, P ≥ X%), chloroform ($CHCl_3$, P ≥ X%), deuterium oxide (D_2O, 99.9 atom % D), tetramethylsilane (TMS, ≥ 99.9%), 3-(trimethylsilyl)propionic-2,2,3,3-d4 acid sodium salt (TSP-d4, 98 atom % D, P ≥ 98.0%), potassium phosphate (KH_2PO_4, P ≥ 99.0%), dibasic potassium phosphate (K_2HPO_4, P ≥ 98.0%), and sodium azide (NaN_3, P ≥ 99.5%) and high-performance liquid chromatography (HPLC) grade *p*-coumaric acid (≥ 98.0%) and ferulic acid (99%) were purchased from Sigma-Aldrich (Merk KGaA, Darmstadt, Germany). MilliQ water was obtained using a Millipore lab water system (Merck KGaA) equipped with a 0.22-μm membrane filter.

2.2 | Sample Collection

Propolis (*A. mellifera*) and cerumen (*T. carbonaria*) samples were obtained from local beekeepers in New South Wales, Australia, across Denmark, and southern Norway (Table S1). Upon collection, the samples were stored at 4°C in food-grade ziplock bags filled with nitrogen, which were then placed inside airtight, nitrogen-filled glass containers. In total, 46 propolis samples were analyzed, including 5 from Australia, 35 from Denmark, and 6 from Norway. Three cerumen samples from New South Wales were also analyzed.

2.3 | Sample Extraction and Preparation for ^{1}H NMR Analysis

Raw propolis and cerumen samples were snap-frozen using liquid nitrogen and subsequently ground into a powder using a pestle and mortar. Extraction was performed according to a modified version of the Folch protocol [39]. Briefly, a 2:1 (v/v) solution containing $CHCl_3$ and CH_3OH was prepared. For each sample, an aliquot of 4 mL of the $CHCl_3$-CH_3OH solution was added to 100 ± 4 mg of powdered propolis/cerumen in round-bottom glass tubes and homogenized for 30 s using a T10 Basic ULTRA-TURRAX (IKA-Werke, Germany). After an hour of storage in the dark at room temperature, 1 mL of Milli-Q water

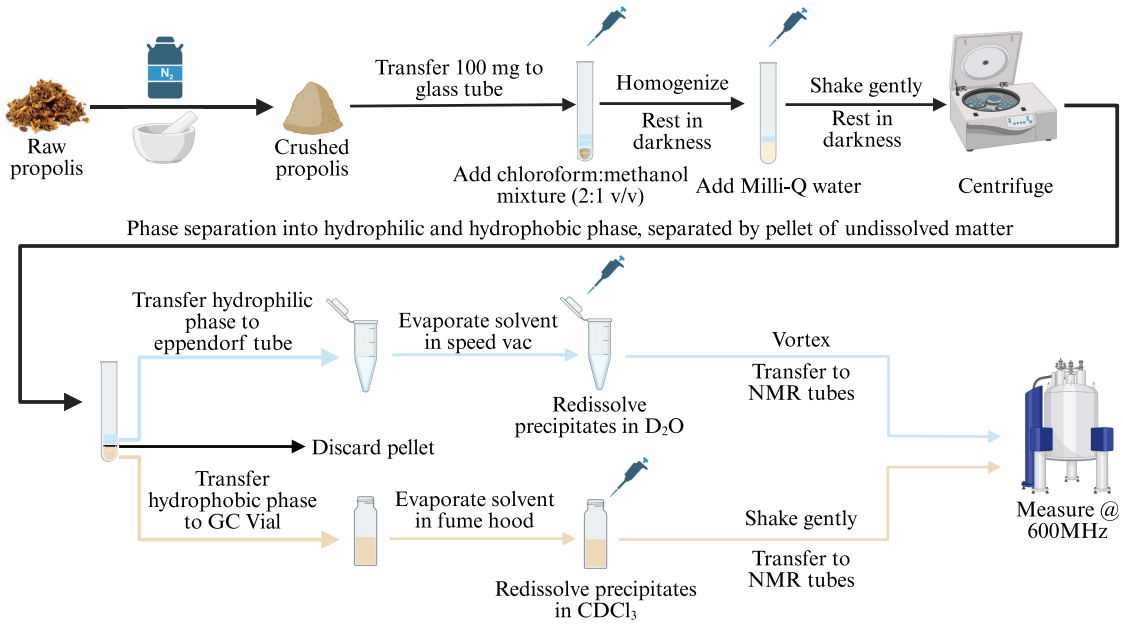

FIGURE 1 | Schematic of the analytical workflow applied to all propolis ($n = 46$) and cerumen ($n = 3$) samples. Each extraction yielded a hydrophilic phase and a hydrophobic phase. All samples were extracted in triplicates.

was added to each sample. The $CHCl_3$-CH_3OH-H_2O mixture was further mixed by gently tilting the tubes and stored at room temperature in the darkness for an additional hour. At the end of the extraction procedure, samples were centrifuged at 3600 rpm for 15 min at 4°C (Labogene Scanspeed 1580R, Allerød, Denmark). This resulted in the separation of the samples into two phases, a hydrophilic phase on top and a hydrophobic phase at the bottom, divided by a pellet of undissolved matter. For each sample, an aliquot of 1 mL of the top hydrophilic phase was transferred into an Eppendorf tube and dried overnight at 25°C and 1000 rpm using a Scanvac centrifugal vacuum concentrator (LaboGene ApS, Lillerød, Denmark). The dried hydrophilic samples were dissolved in 1 mL of phosphate buffer (pH = 7.6) containing 20% of D_2O and TSP (5 mM). The mixture was vortexed (Buch and Holm, Scientific Industries Vortex-Genie 2) at a medium speed to avoid foaming for 5 min. Subsequently, 600 µL of the mixture was transferred into SampleJet NMR tubes (Bruker BioSpin, Ettlingen, Germany) of L = 103.5 mm and O.D. = 5.0 mm and capped with a matching lid. For the bottom hydrophobic phase, 1 mL was transferred into a 1.5-mL glass vial. The chloroform mixture was dried overnight at room temperature under a fume hood, and the dried sample re-dissolved in 1.0 mL of $CDCl_3$. For each sample, an aliquot of 600 µL was transferred into a SampleJet NMR tube and capped with a matching lid. All samples were extracted in triplicates and stored inside the SampleJet at 4°C until analysis. An overview of the analytical workflow is given in Figure 1.

2.4 | Standard Addition

For the standard addition experiments, 10mM solutions of ferulic acid and *p*-coumaric acid were prepared in the beforementioned buffer (see Section 2.3). An aliquot of 20 µL was added directly to the NMR tube containing the hydrophilic extract from propolis.

2.5 | ^{1}H NMR Measurements

Samples were measured using a Bruker Avance III operating at a proton Larmor's frequency of 600.13 MHz and equipped with a 5-mm broadband inverse (BBI) probe (Bruker Biospin, Rheinstetten, Germany). The magnet was equipped with an automated sample changer (SampleJet, Bruker Biospin, Rheinstetten, Germany) with a refrigerated storage station (278 K) and heating/drying station (306 K). Cooling of the probe and SampleJet system were controlled by the BCU (Bruker Cooling Unit). Data acquisition and processing were carried out in the TopSpin software (version 3.6, Bruker, Rheinstetten, Germany). Automation of the overall measurement procedure was controlled by the iconNMR software (Bruker Biospin, Rheinstetten, Germany). The hydrophilic extracts and the samples spiked with standards were measured as described by Forsberg et al. [40]. Briefly, ^{1}HNMR spectra were acquired at 300 K using the *noesygppr1d* pulse sequence from the Bruker pulse program library. Each spectrum was collected with 32 scans following four dummy scans, with free induction decays (FIDs) recorded into 65,536 data points across a spectral width of 20 ppm. The acquisition time (AQ), relaxation delay (D1), and mixing time were set to 2.72, 4.0, and 0.01 s, respectively. The receiver gain (RG) was automatically set to of 90.5 for all samples, as described by Forsberg et al. [40]. Following Fourier transform (FT), automatic phasing and baseline correction were performed in the TopSpin software (version), with exponential line broadening applied (LB = 0.3 Hz) applied. An artificial signal at 12 ppm, corresponding to a known concentration of 10 mM protons, was used for data normalization [40]. ^{1}H NMR spectra of the hydrophobic extracts were recorded at 300 K, using the *zg* pulse sequence (Bruker pulse program library). A total of 128 scans were acquired following two dummy scans, with FIDs collected into 72,114 data points over a spectral width of 20 ppm. The AQ and D1 were set to 3.0 and 6.0 s, respectively. For each

sample, the RG value was automatically determined using the *rga* command (Bruker command nomenclature). As before, data processing, including FT, automatic phasing, and baseline correction, was conducted using TopSpin software.

2.6 | Data Analysis

2.6.1 | Principal Component Analysis (PCA)

The ^{1}H NMR spectra were imported into MATLAB R2024a (Mathworks Inc., Natick, MA, USA) where the spectra were referenced to the TMS or TSP singlet (hydrophobic or hydrophilic extract, respectively) at 0.00 ppm and aligned using *i*coshift [41]. Noisy regions, including signals from residual chloroform (hydrophobic extract) and water (hydrophilic extract) at 7.26 and 4.70 ppm, respectively, and the TMS/TSP singlet at 0.00 ppm were removed prior to data analysis. The ^{1}H NMR spectra of the hydrophilic extract were normalized to the area of the artificial signal at 12 ppm, while the ^{1}H NMR spectra of the hydrophobic extract were normalized to the RG. All spectra were also normalized relative to the mass (mg) of the sample. Principal component analysis (PCA) [42] was performed on the Pareto-scaled ^{1}H-NMR data from the hydrophilic and hydrophobic propolis extracts, respectively ($n = 3{\cdot}46$).

2.6.2 | Variable Selection by rPLS

An *r*PLS regression approach [37] was employed to identify spectral variables (metabolites) in the ^{1}H NMR spectra of the hydrophilic and hydrophobic extracts associated with RSA. Technical replicates were averaged after careful alignment and prior to data modelling, to obtain a single spectrum per sample. Before rPLS modelling, the ^{1}H NMR spectra were limited to include only the aromatic region (6.0–8.0 ppm), smoothed using a moving average filter (window size = 5), and Pareto-scaled. The response variable (RSA) was mean-centered. Recursive weighting was performed over 25 iterations without active variable pruning. In each iteration, PLS regression was applied with three latent variables (LVs); the absolute regression coefficients were normalized, and cumulative multiplication was used to update variable weights. The predictor matrix was then re-weighted for the next iteration. Model performance at each iteration was assessed by five-fold Venetian-blind cross-validation (CV), based on the root mean square error of cross-validation ($RMSE_{CV}$). For comparison, a standard PLS regression model was constructed on the same spectral region and evaluated using identical preprocessing and CV settings.

To assess the stability and predictive performance of the *r*PLS approach, Monte Carlo cross-validation (MCCV; 1000 repeats) was performed with random 80/20 splits into a training set and an external hold-out test set. Within each repeat, a five-fold Venetian-blind CV was applied to the training set, after which models were refitted on the complete training set to generate predictions for the hold-out test set. RMSE distributions were collected for both the internal CV and the external test predictions.

2.6.3 | Metabolites Assignment

Metabolite assignment was performed using literature data [43], ChemDraw software (Version 23; Revvity Signals Software Inc., Waltham, MA, USA), and previously recorded Infrared (IR) data [44]. Statistical total correlation spectroscopy (STOCSY) analysis [38] was subsequently used to identify signals originating from compounds corresponding to signals highlighted by *r*PLS. The coefficient of determination (r^2) was computed across the spectra to assess the strength of association. All analyses were conducted in MATLAB R2024a. Identification of ferulic acid and *p*-coumaric acid was additionally confirmed by standard addition (see Section 2.4). Furthermore, signals originating from beeswax were also identified using STOCSY. Here, the strong singlet at 1.22 ppm, arising from aliphatic methylene of the beeswax, was used as the driver signal. For these analyses, Danish and Norwegian propolis samples were clustered together due to their chemical similarity.

2.6.4 | Quantification of Ferulic Acid and *p*-Coumaric Acid

Quantification of ferulic acid and *p*-coumaric acid was based on the integral of the most shielded peak in the trans-olefinic doublet (coupling constant ~16 Hz) characteristic of hydroxycinnamic acids. This analysis was performed exclusively on the hydrophilic extracts, and concentrations were determined from the increase in peak intensity observed in spiking experiments. For these analyses, Danish and Norwegian propolis samples were clustered together due to their chemical similarity.

3 | Results

3.1 | ^{1}H NMR Spectra of Propolis and Cerumen

Figure 2 shows the averaged ^{1}H NMR profiles of hydrophilic (methanol/water) and hydrophobic (chloroform) fractions of *A. mellifera* propolis collected in Scandinavia and Australia ($n = 46$) and of *T. carbonaria* cerumen collected in Australia ($n = 3$).

In the spectra of the hydrophobic extract (Figure 2a), characteristic beeswax signals were detected across all groups, including a strong singlet at 1.22 ppm (aliphatic methylene, -CH_2-) and a triplet at 0.88 ppm (J = 7.16 Hz; aliphatic methyl, -CH_3). Beyond these common features, notable differences were apparent in the aromatic and aliphatic regions. Scandinavian propolis exhibited the strongest aromatic signals (6.0–8.0 ppm), followed by Australian propolis, which still displayed more pronounced aromatic peaks than cerumen. In contrast, cerumen was distinguished by a higher density of aliphatic signals (0.5–3.0 ppm) compared to Australian propolis, possibly reflecting terpenoid-like constituents. However, this interpretation remains tentative and will be discussed later.

The ^{1}H NMR spectra of the hydrophilic extract spectra also revealed clear differences between groups (Figure 2b). Propolis samples showed increased signal intensities in the 3.0–4.0 and 4.5–5.5 ppm regions, relative to cerumen. These regions are typically associated with protons adjacent to electronegative atoms,

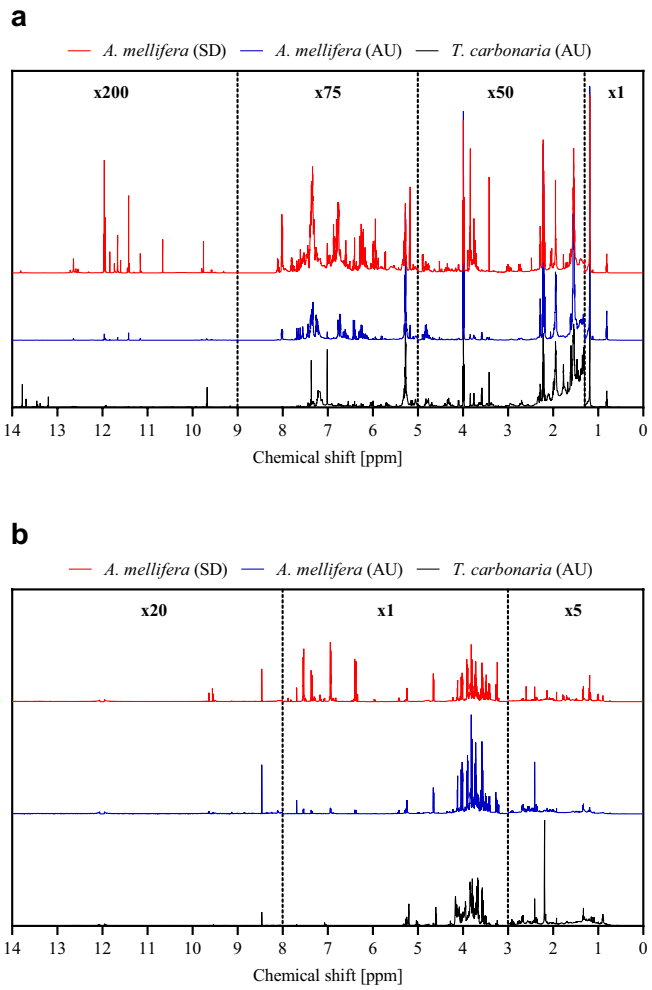

FIGURE 2 | Average ^{1}H NMR spectra of propolis extracts from *A. mellifera* in Scandinavia (SC, top spectrum) and Australia (AU, middle spectrum) and cerumen extracts from *T. carbonaria* in Australia (bottom spectrum). ^{1}H NMR spectra are shown for the (a) hydrophobic phase and (b) hydrophilic phase, obtained through a modified Folch extraction.

arising from carbohydrates, with the 4.5–5.5 ppm range specifically characteristic of anomeric protons from free sugars and glycosidic moieties. As in the hydrophobic extracts, Scandinavian propolis contained higher concentrations of aromatic compounds than Australian propolis. While Australian propolis displayed very low aromatic content in the hydrophilic extracts, cerumen spectra were virtually devoid of aromatic proton signals.

3.2 | Wax Analysis

As beeswax constitutes a major portion of propolis, quantifying wax-related signals and evaluating structural characteristics provides useful insight into species- and region-specific differences in chemical composition. To this end, STOCSY was applied to identify signals associated with beeswax (Figure 3a). Several signals were highlighted, including resonances at 1.22 ppm (s) and 0.88 ppm (t, J = 7.16 Hz), corresponding to methylene (-CH_2-) and methyl (-CH_3) groups, respectively. Additional signals were observed at 2.21 ppm (m) and 3.99 ppm (t, J = 6.68 Hz). The triplet at 3.99 ppm arises from methylene protons positioned alpha to an oxygen atom in esters ($COOCH_2$-), while the multiplet at 2.21 ppm likely originates from methylene protons positioned alpha to carbonyl groups in both esters and carboxylic acids (-CH_2COO-).

These signals were used to assess total beeswax content, average chain length (-CH_2-/-CH_3), and esterification (-CH_2-/-$COOCH_2$-). The ratio of -CH_2- to carbonyl-associated methylene protons (-CH_2-/-CH_2COO-) at 2.21 ppm, arising from both esters and carboxylic acids, was additionally used to evaluate differences potentially attributable to variations in free fatty acid content across origin and species (Figure 3b–e). Propolis from Australia contained higher beeswax levels compared to Scandinavian samples and cerumen. Furthermore, beeswax from Scandinavian and Australian *A. mellifera* showed similar average chain lengths of 10.7 and 10.2 -CH_2-/-CH_3, respectively, whereas *T. carbonaria* wax exhibited shorter chains, averaging 7.8 -CH_2-/-CH_3.

Differences in esterification were minor between *A. mellifera* samples from Scandinavia and Australia, with average -CH_2-/-$COOCH_2$- ratios of 44.7 and 47.9, respectively. In contrast, *T. carbonaria* wax displayed a higher ratio of 66.8, reflecting lower ester content relative to chain backbone. Analysis of the -CH_2-/-CH_2COO- ratio showed noticeably smaller differences across species, indicating a higher proportion of free fatty acids in *T. carbonaria* wax compared to *A. mellifera*, whose wax was more extensively esterified. No correlations were observed with highly deshielded proton signals (> 10 ppm) in the STOCSY analysis, consistent with the absence or broadening of carboxylic acid protons due to rapid exchange.

Interpretation of the 2.21 ppm multiplet is complicated by overlapping contributions from fatty esters and free fatty acids. To support the assignment of these components, the ^{1}H NMR observations were compared with infrared (IR) spectra of the same samples obtained in a separate study [44] (Figures S1 and S2). The IR data show distinct carbonyl absorptions for esters (1736 cm^{-1}) and carboxylic acids (1710 cm^{-1}) [44]. *A. mellifera* samples displayed a dominant ester band at 1736 cm^{-1}, consistent with an ester-driven 2.21 ppm multiplet in the NMR, likely reflecting high diester content. In contrast, *T. carbonaria* samples exhibited a stronger 1710 cm^{-1} band accompanied by a broader, more complex NMR multiplet, indicating a greater contribution from free fatty acids. Due to the limited number of *T. carbonaria* samples ($n = 3$), separate statistical correlation was not feasible, and the interpretation remains qualitative. Nonetheless, the combined IR-NMR evidence indicates a higher free acid content in *T. carbonaria* wax compared with the more esterified wax profile of *A. mellifera*. Supporting IR data are provided in Supporting Information (Figures S1 and S2).

3.3 | PCA

PCA was performed on the spectral ^{1}H NMR data to investigate the variation among samples based on geographical origin and bee species. A clear species- and region-specific separation can be observed in the scores plot of the hydrophobic extract (Figure 4a). Cerumen samples ($n = 3$) form a distinct cluster along PC2, driven by aliphatic signals tentatively attributed to terpenoids (Figure 4b). Nearly all Australian propolis samples

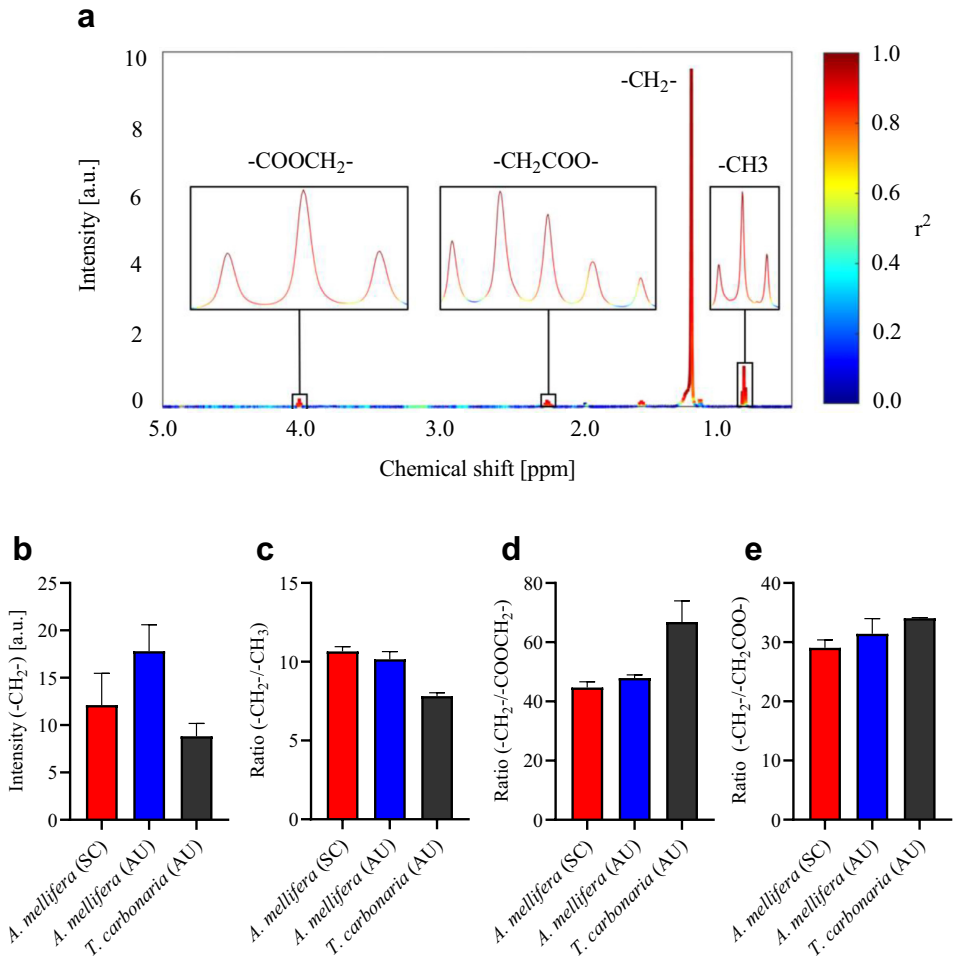

FIGURE 3 | Beeswax content and structural features in propolis from Scandinavia (SC, $n = 41$) and Australia (AU, $n = 5$) *A. mellifera* and cerumen ($n = 3$) from *T. carbonaria* across origin and species. (a) Signals associated with beeswax, highlighted by STOCSY, using the singlet at 1.22 ppm as driver. (b) Total beeswax content estimated from intensity of singlet at 1.22 ppm. (c) Average chain length calculated as the $-CH_2-/-CH_3$ ratio. (d) Degree of esterification derived from the $-CH_2-/-COOCH_2-$ ratio based on the ester-specific signal at 3.99 ppm. (e) $-CH_2-/-CH_2COO-$ ratio based on multiplet at 2.21 ppm. Bars and vertical lines indicate mean + standard deviation (SD).

(blue, $n = 5$) are clustered to the left along the PC1 axis, primarily due to a higher beeswax content (see loadings), consistent with the wax analysis. Scandinavian propolis, colored by country to emphasize similarity, span the whole PC1 axis, with negative scores associated with high beeswax content like the Australians and positive scores primarily associated with high aromatic signals.

In the scores plot of the hydrophilic extract (Figure 4c), most *A. mellifera* samples are grouped together in the middle of the scores plot, but with the majority of the Australian propolis samples diverging from Scandinavian samples along PC1. Notably, two Australian samples grouped with the Scandinavian cluster, whereas one Danish and one Norwegian sample deviated markedly from their main group. The cerumen samples of *T. carbonaria* ($n = 3$) form a separate group along PC2. According to the loadings plot (Figure 4d), PC1 separation was primarily influenced by signals at chemical shifts of 3.0–5.5 ppm, attributed to carbohydrates (negative loadings) and 6.0–8.0 ppm, attributed to aromatic compounds, constituted by mainly polyphenols (positive loadings). This suggests a general trend of higher carbohydrate content in Australian propolis and greater aromatic content in Scandinavian propolis. Additionally, cerumen separation along PC2 appeared linked to differences in carbohydrate composition, as indicated by loadings driven by specific carbohydrate signals. In the PC2 loadings plot, anomeric signals at 4.65 ppm (d, J = 7.9 Hz) and 4.60 ppm (d, J = 7.9 Hz) contribute to the positive and negative driving of the loadings, respectively, indicating a distinct carbohydrate profile for cerumen samples.

Overall, this PCA analysis underscores significant compositional differences in propolis and cerumen across both species and geographical regions. Scandinavian propolis generally contained higher levels of aromatic compounds, while Australian propolis was richer in carbohydrates. Cerumen samples, in turn, were characterized by a prominent aliphatic profile, tentatively attributed to terpenoid-like constituents, along with a distinct carbohydrate profile.

3.4 | Identification of Spectral Signals Important to RSA Using *r*PLS Regression

Following the analysis of overall chemical differences across extracts, the focus shifted toward identifying polar metabolites associated with RSA. To this end, previously reported RSA

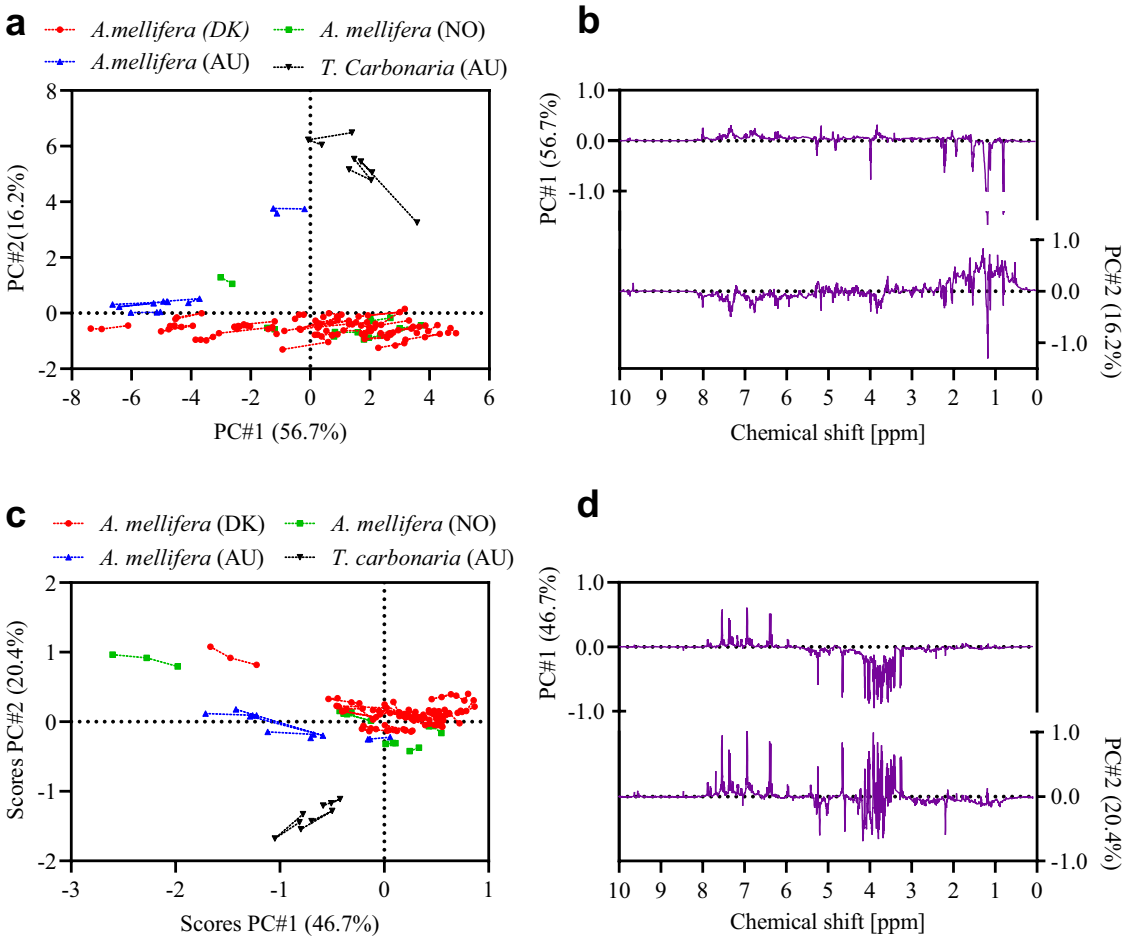

FIGURE 4 | PCA scores and loading plots of ^{1}H NMR data from propolis ($n = 3{\cdot}46$) and cerumen ($n = 3{\cdot}3$) extracts. (a) Scores and (b) loadings plot for the hydrophobic phase; (c) scores and (d) loadings plot for the hydrophilic phase. Scores are shown with connecting lines for triplicate samples.

TABLE 1 | DPPH RSA of propolis from *A. mellifera* in Australia ($n = 5$) and Scandinavia ($n = 41$) and cerumen from *T. carbonaria* in Australia ($n = 3$), expressed relative to the blank [44].

	***A. mellifera* (SC)**	***A. mellifera* (AU)**	***T. carbonaria* (AU)**
DPPH RSA (%) (mean ± SD)	42.6 ± 12.8	7.6 ± 10.2	18.1 ± 3.2

data [44] (Table 1) were combined with the present ^{1}H NMR data to construct an *r*PLS regression model. Australian samples were excluded from the dataset due to their distinct spectral profiles. Only the hydrophilic fraction was modeled, as extensive aromatic signal overlap in the hydrophobic spectra precluded reliable variable attribution and subsequent structure elucidation. For the sake of completeness and transparency, the development of variable weights in *r*PLS modelling of the hydrophobic data has been included in the Supporting Information (Figure S3).

Thus, *r*PLS was applied to Pareto-scaled ^{1}H NMR spectra against RSA data, with variable weights recursively reweighted across 25 iterations without enforced variable pruning. The evolution of variable weights and corresponding $RMSE_{CV}$ is shown in Figure 5.

Early iterations (1–8) exhibited unstable $RMSE_{CV}$ accompanied by gradual reduction in variable count. A pronounced reduction in both $RMSE_{CV}$ and variable count occurred between iterations 8 and 9, after which $RSME_{CV}$ gradually declined until iteration 16, where it reached its minimum at eight selected variables. Beyond this point, $RMSE_{CV}$ plateaued while the number of variables continued to drop until reaching three variables, consistent with the number of latent variables used. Iteration 16 was therefore selected as the final model, balancing predictive performance and retention of relevant signals.

Figure 6a displays the regression coefficients from a full PLS model (iteration 1), calculated using the same cross-validation strategy and number of latent variables as the *r*PLS model, with the *r*PLS-selected variables highlighted.

These variables, predominantly positively correlated with RSA, clustered into four distinct peaks at 6.390, 6.399, 6.945, and 6.960 ppm, pinpointing the spectral regions most relevant for activity. To test the robustness of these selected variables, MCCV (1000 repetitions) was performed. The predictive performance of the *r*PLS model is shown in Figure 6b as actual versus predicted

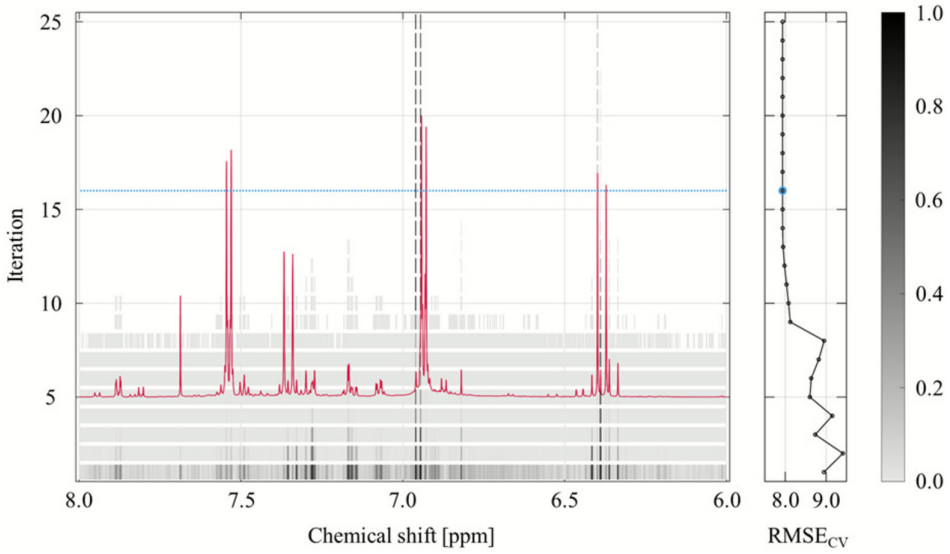

FIGURE 5 | Development of variable weights across recursive iterations in the three latent variable *r*PLS model. The grayscale lines in the main panel represent the evolution of normalized weights for each spectral variable over 25 iterations, illustrating how variable influence changes through recursive weighting. The red line overlays the average ^{1}H NMR spectrum (6.0–8.0 ppm) of the hydrophilic phase extracts for reference. The blue stippled horizontal line marks the iteration with the lowest RMSE$_{CV}$; as RMSE$_{CV}$ plateaued beyond this point, this iteration was employed as final *r*PLS model. The right-side plot shows the RMSE$_{CV}$ at each iteration, confirming model stability across the recursive process. The scale indicates normalized weights, where a value of 1 corresponds to high importance in the model.

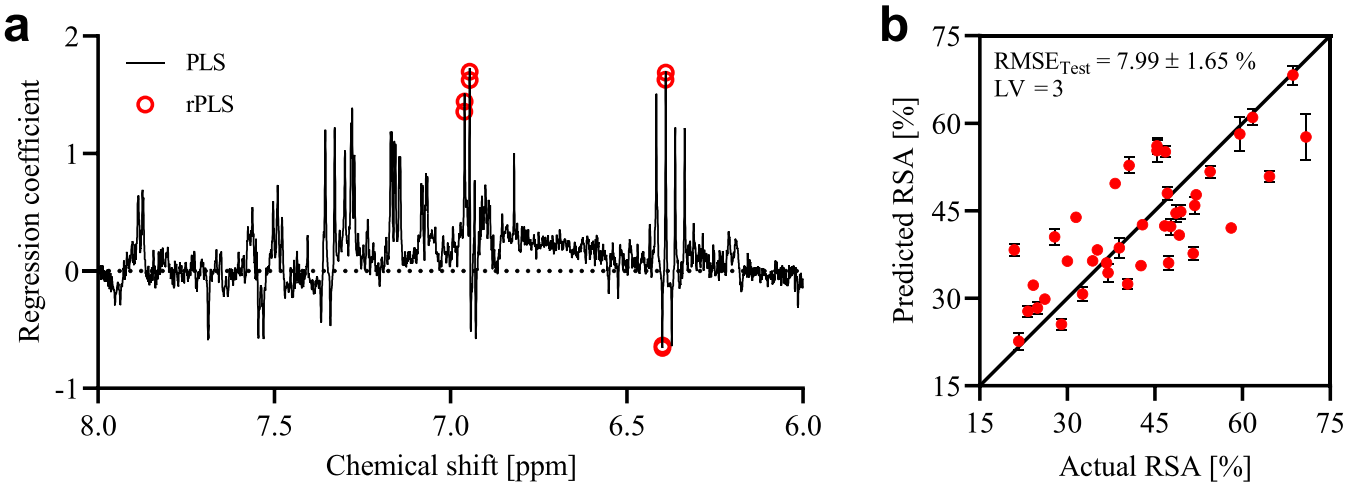

FIGURE 6 | (a) Regression coefficients from full PLS regression (three latent variables) based on Pareto-scaled ^{1}H NMR data. Variables selected by the *r*PLS model are highlighted as red circles. (b) Actual versus predicted RSA for the test sets of the MCCV, using the *r*PLS model (three latent variables). Data are shown as mean ± SD.

RSA plots, yielding an RMSE$_{test}$ of 7.99% ± 1.65%. Given the solid robustness of the *r*PLS model, structural elucidation of the selected signals was pursued using STOCSY.

3.5 | Identification of Compounds Correlated to RSA Using STOCSY

To identify the compounds corresponding to the *r*PLS-highlighted signals, STOCSY was applied using the selected variables as driver signals (Figure 7). Using the variable at 6.390 ppm as driver, several highly correlated signals were revealed, including signals at 6.960 ppm (d, J = 8.16 Hz), 7.152 ppm (dd, J = 8.16, 1.90 Hz), and 7.340 ppm (d, J = 15.94 Hz). The signal at 6.390 ppm appeared as a doublet with a coupling constant of 15.94 Hz, thus displaying coupling patterns characteristic of 3,4-substituted cinnamic acid derivatives such as caffeic and ferulic acid. However, it could not be ruled out that the signal-rich region between 3.0 and 4.0 ppm obscured a singlet at approximately 3.9 ppm, which is typical of the methoxy group in ferulic acid, and STOCSY was therefore unable to conclusively distinguish between the two compounds. Standard addition experiments confirmed that *r*PLS selected ferulic acid, revealing that the methoxy singlet was indeed masked by overlapping signals (Table 2).

Similarly, using the 6.399 ppm peak (d, J = 16.0 Hz) as driver revealed highly correlated signals at 6.934 ppm (d, J = 8.60 Hz),

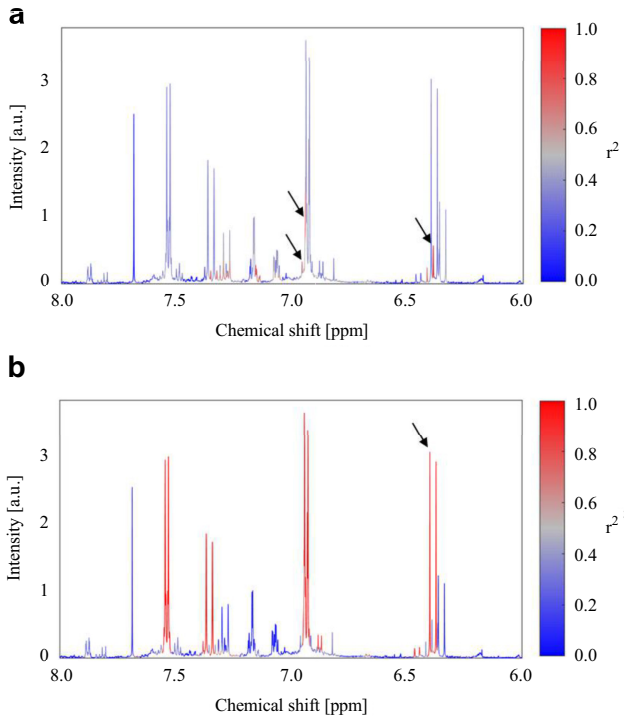

FIGURE 7 | STOCSY analysis leading to the identification of *p*-coumaric and ferulic acid using *r*PLS selected variables as driver signals. Black arrows indicate signals highlighted by *r*PLS. (a) STOCSY plot using the signal at 6.390 ppm as driver. (b) STOCSY plot using the signal at 6.399 ppm as driver. Signals are colored according to their squared correlation.

TABLE 2 | Chemical shifts (ppm), J-coupling (Hz), and multiplicity of signals identified by STOCSY and standard addition.

Compound	Chemical shift (ppm) (multiplicity and J-coupling [Hz])
Ferulic acid	3.915 (s)[b], 6.390[a] (d, J = 15.94 Hz), 6.945[a] (d, J = 8.16), 7.152 (dd, J = 8.16, 1.90 Hz), 7.281 (d, J = 1.91 Hz)[b], 7.340 (d, J = 15.94 Hz)
p-Coumaric acid	6.399[a] (d, J = 16.0 Hz), 6.934 (d, J = 8.60 Hz), 7.357 (d, J = 15.97 Hz), 7.537 (d, J = 8.60 Hz)

Note: Signals characteristic of ferulic acid and *p*-coumaric acid are shown with their respective splitting patterns. Keys: s: singlet; d: doublet; dd: double doublet.
[a]Highlighted by *r*PLS.
[b]Could only be identified after standard addition.

7.357 ppm (d, J = 15.97 Hz), and 7.537 ppm (d, J = 8.60 Hz). These chemical shifts and coupling patterns are very characteristic of *p*-coumaric acid, and this was confirmed by standard addition.

3.6 | Quantitative Comparison of Ferulic and *p*-Coumaric Acid Across Origin and Bee Species

To enable a direct comparison of ferulic and *p*-coumaric acid levels across different origins and bee species, these compounds were quantified from the ^{1}H NMR spectra of the hydrophilic extracts of propolis and cerumen.

Despite large variation, the quantitative NMR analysis revealed substantially higher levels of both ferulic acid and *p*-coumaric acid in Scandinavian *A. mellifera* propolis compared to Australian samples (Figure 8). Australian *A. mellifera* propolis contained lower amounts of these compounds, while cerumen from *T. carbonaria* exhibited only trace levels, if detected at all. Notably, in both Scandinavian and Australian propolis, average *p*-coumaric acid concentrations were considerably higher than those of ferulic acid.

4 | Discussion

4.1 | Resin and Beeswax Are Origin- and Species-Specific

PCA highlighted clear differences associated with both geographic origin and bee species. Notably, cerumen samples exhibited a markedly more aliphatic profile than propolis, tentatively assigned to terpenoids. Although the ^{1}H NMR-based assignment of these aliphatic signals remains tentative, the pattern is consistent with previous analyses showing that *T. carbonaria* cerumen is rich in terpenoids such as pimaric and abietic acids, β-amyrin, and multiple sterols [45]. The presence of such compounds is also consistent with the documented resin-foraging behavior of stingless bees, which rely on olfactory cues from terpenes and preferentially collect terpenoid-rich resins [46]. These terpenoids contribute to nest defense through the release of antimicrobial volatiles [47], an effect further amplified by the elevated nest temperatures typical of tropical and subtropical climates where these bees thrive. In contrast, *A. mellifera*, native to cooler regions, produced propolis with a lower relative proportion of terpenoids and a higher content of phenolic compounds, reflecting different foraging strategies and a reliance on less volatile chemical defenses. The low levels of aromatic compounds in Australian propolis may be due to the limited availability of poplar trees (e.g., *Populus nigra*) [48], favored by *A. mellifera*, which are not native to Australia, thereby compelling bees to utilize resins from less phenolic-rich plant sources. The differences in resins available for foraging could also explain the increased contents of carbohydrates in both Australian propolis and cerumen. Furthermore, the seemingly different carbohydrate profile observed between Australian propolis and cerumen highlights differences in resins foraging. Interestingly, our previous vibrational spectroscopy study on this same sample set [44] proposed that the Australian samples differed from the Scandinavian ones due to variations in carbohydrate and/or terpenoid content. The present results confirm this result, demonstrating that Australian propolis contained higher levels of carbohydrates, while cerumen samples exhibited elevated levels of both carbohydrates and terpenoids.

Both PCA and subsequent beeswax analysis highlighted differences in wax content between propolis and cerumen. The higher wax content observed in Australian propolis likely reflects both limited access to preferred resin-producing flora and the influence of higher temperatures, as resins are softer and more fluid

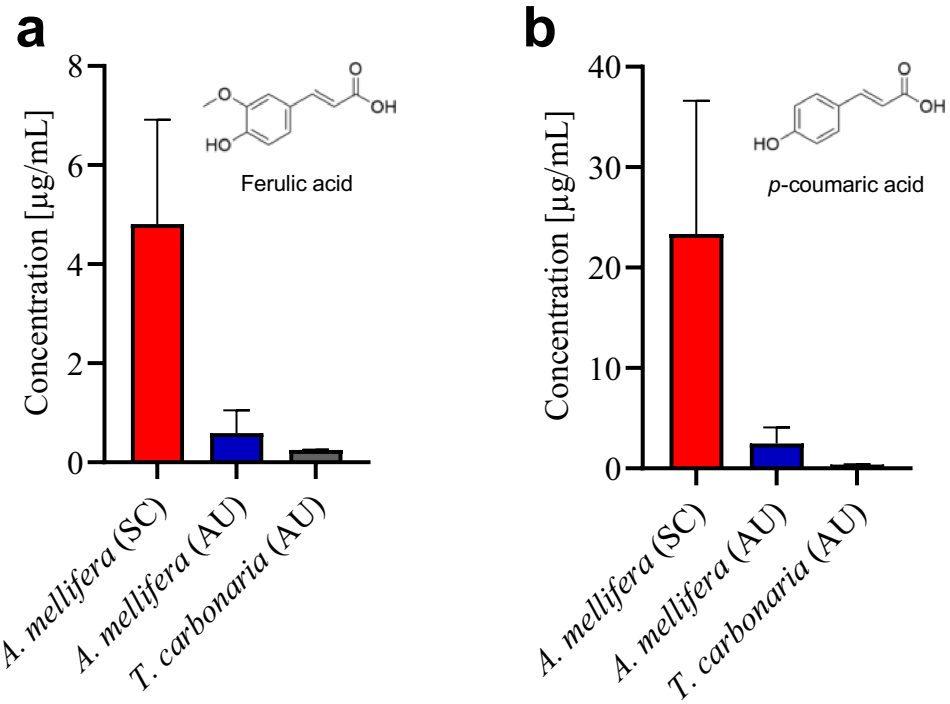

FIGURE 8 | Bar plots showing the quantitative comparison of (a) ferulic acid and (b) *p*-coumaric acid in hydrophilic extracts of propolis from Scandinavia (SC, $n = 41$) and Australia (AU, $n = 5$) *A. mellifera* and cerumen from *T. carbonaria* ($n = 3$). Bars and vertical lines indicate mean + standard deviation (SD).

in warmer climates. Incorporating additional wax may thus enhance stiffness and structural integrity, helping bees maintain the necessary consistency and cohesion of propolis. In contrast, Scandinavian bees live in cooler climates and have abundant access to poplar resins, resulting in propolis with a higher resin-to-wax ratio and richer phenolic composition. This hypothesis also helps explain why *T. carbonaria* cerumen contains even less wax, as stingless bees collect large quantities of resin used not only for antimicrobial defense but also as a primary structural material in nest construction, reducing reliance on wax as a binder [49].

While the beeswax content in propolis varied with geographic origin, the wax structure of *A. mellifera*, assessed by chain length as well as degrees of esterification and acidification, remained relatively consistent. In contrast, *T. carbonaria* wax exhibited shorter chain lengths, a lower degree of esterification, and a higher proportion of free fatty acids. The shorter wax chains observed in stingless bees have previously been described [50] and may be attributed to their nesting behavior, where increased flexibility is advantageous for the construction and maintenance of nest structures. The higher proportion of free fatty acids relative to esters in *T. carbonaria* may similarly enhance antimicrobial protection within their resin-rich nests, although this functional role remains speculative.

4.2 | *r*PLS Identified Important Metabolites Linked RSA in the Hydrophilic Extracts of Propolis

*r*PLS regression was employed to model the relationship between signals in the aromatic region of the hydrophilic phase ^{1}H NMR spectra and RSA. Based on MCCV, the *r*PLS model yielded a mean $RMSE_{test}$ of 8.0% relative to a mean RSA of 42.6%, which indicates only moderate predictive strength. This outcome is not unexpected given that the analysis was limited to the hydrophilic phase, as substantial aromatic overlap in the hydrophobic phase hindered precise variable identification by *r*PLS, while many compounds with radical scavenging potential, such as flavonoids, were likely concentrated in the hydrophobic phase and were therefore not captured by the model. Despite the moderate overall predictive strength, the *r*PLS highlighted signals attributable to ferulic acid as positively associated with RSA, suggesting that this compound serves as an important marker of anti-oxidative capacity within these hydrophilic extracts. This interpretation is further supported by literature demonstrating that hydroxycinnamic acids bearing multiple electron-donating groups, such as the methoxy-hydroxy substitution in ferulic acid, enhance radical stabilization [51]. In contrast, signals from *p*-coumaric acid were negatively associated with RSA in the PLS models, consistent with lower intrinsic antioxidant potency reported in literature [51], due to its structure bearing only a single para-positioned hydroxyl group, offering less effective radical stabilization. Although ferulic acid was detected in only modest amounts in the hydrophilic phase, its methoxy substitution may favor partitioning into the hydrophobic fraction, which may partially explain its lower representation in the hydrophilic phase. Nonetheless, the identification of ferulic acid signals despite these concentrations suggests that it contributes to the antioxidant activity of propolis, while also serving as a useful marker for compounds or pathways associated with enhanced radical scavenging activity. These findings also indicate that hydrophilic extracts of propolis can still retain significant antioxidant capacity, suggesting that high ethanol concentrations may not always be necessary for effective extraction of compounds of interest, which could be advantageous in food, cosmetic, or

pharmaceutical formulations for pediatric use where ethanol is undesirable. Furthermore, these results demonstrate the utility of *r*PLS in spectroscopic analysis of complex mixtures by effectively pinpointing relevant variables through recursive weighting.

In line with the PCA results, Scandinavian propolis contained considerably higher levels of both ferulic acid and *p*-coumaric acid compared to Australian propolis and cerumen. Within Scandinavia, Danish and Norwegian samples showed broadly similar concentrations, although *p*-coumaric acid appeared slightly lower on average in the Norwegian samples. As several Danish samples overlapped with the Norwegian range and the Norwegian group was smaller, this apparent difference was deemed too weak to draw firm conclusions. Consistently, Danish and Norwegian propolis exhibited comparable RSA, and both showed substantially higher antioxidant activity than the Australian sample [44]. Notably, within the hydrophilic extracts of propolis, *p*-coumaric acid was present at higher concentrations than ferulic acid. However, given the greater lipophilicity of ferulic acid and the resulting tendency to partition into the hydrophobic phase, it remains unclear whether *p*-coumaric acid is truly more abundant overall. Nevertheless, since the partitioning behavior would be consistent across samples, these observations support the broader conclusion from the PCA that resins collected by Scandinavian *A. mellifera* are generally richer in aromatic compounds, including both ferulic and *p*-coumaric acids, with ferulic acid emerging as a key contributor to the hydrophilic extractable antioxidant capacity of propolis.

5 | Conclusions

This study demonstrates the advantages of ^{1}H NMR coupled with advanced multivariate data analysis for detailed characterization of propolis and cerumen and for identifying metabolites associated with RSA. Geographic origin and bee species strongly influenced chemical composition, with Scandinavian propolis showing higher levels of aromatic constituents compared to Australian propolis and stingless bee cerumen. The application of *r*PLS, combined with STOCSY, enabled the identification of specific RSA-related signals, highlighting ferulic acid as an important marker within the hydrophilic extracts. Hydrophilic and hydrophobic extracts displayed clear chemical differences, underscoring the impact of extraction liquid choice in which bioactive constituents are captured.

Overall, these findings emphasize the complementarity of spectroscopic approaches for chemotyping and bioactivity assessment and the importance of extraction strategy and provenance in shaping the chemical and functional diversity of propolis.

Author Contributions

All authors contributed to the conception and design of the study. Material preparation, data collection, and data analysis were performed by Jonas Pordel Vind, Violetta Aru, Knud Josefsen, and Søren Balling Engelsen. Jonas Pordel Vind prepared the first draft of the manuscript. All authors contributed to manuscript review and editing and approved the final version of the manuscript.

Acknowledgments

This work was funded by the European Union and Landbrugsstyrelsen (the Danish Agricultural Agency) under the national implementation of the Apiculture Support Scheme 2023–2026. Data were generated through accessing research infrastructure at the University of Copenhagen, including FOODHAY (Food and Health Open Innovation Laboratory, Danish Roadmap for Research Infrastructure).

Conflicts of Interest

The authors declare no conflicts of interest.

Data Availability Statement

The data that support the findings of this study are available from the corresponding author upon reasonable request.

References

1. E. L. Ghisalberti, "Propolis: A Review," *Bee World* 60 (1979): 59–84.

2. R. Hossain, C. Quispe, R. A. Khan, et al., "Propolis: An Update on Its Chemistry and Pharmacological Applications," *Chinese Medicine* 17 (2022): 100.

3. A. K. Balasubramaniam, A. Elangovan, M. A. Rahman, et al., "Propolis: A Comprehensive Review on the Nature's Polyphenolic Wonder," *Fitoterapia* 183 (2025): 106526.

4. W. Gao, L. Pu, J. Wei, et al., "Serum Antioxidant Parameters Are Significantly Increased in Patients With Type 2 Diabetes Mellitus After Consumption of Chinese Propolis: A Randomized Controlled Trial Based on Fasting Serum Glucose Level," *Diabetes Therapy* 9 (2018): 101–111.

5. F. Afsharpour, M. Javadi, S. Hashemipour, Y. Koushan, and H. K. Haghighian, "Propolis Supplementation Improves Glycemic and Antioxidant Status in Patients With Type 2 Diabetes: A Randomized, Double-Blind, Placebo-Controlled Study," *Complementary Therapies in Medicine* 43 (2019): 283–288.

6. E. Rendueles, E. Mauriz, J. Sanz-Gómez, et al., "Biochemical Profile and Antioxidant Properties of Propolis From Northern Spain," *Food* 12 (2023): 4337.

7. A. Kurek-Górecka, Y. Kara, K. Pokajewicz, et al., "Phenolic Content, Volatile Compounds and Antioxidant Activity in Pooled Propolis Samples From Turkey and Poland," *European Food Research and Technology* 251 (2025): 2199–2210.

8. M. A. Sanches, A. M. S. Pereira, and J. E. Serrão, "Pharmacological Actions of Extracts of Propolis of Stingless Bees (Meliponini)," *Journal of Apicultural Research* 56 (2017): 50–57.

9. M. Shanahan and M. Spivak, "Resin Use by Stingless Bees: A Review," *Insects* 12 (2021): 719.

10. R. F. A. Moritz, S. Härtel, and P. Neumann, "Global Invasions of the Western Honeybee (*Apis mellifera*) and the Consequences for Biodiversity," *Écoscience* 12 (2005): 289–301.

11. E. Toledo-HernÁNdez, G. PeÑA-Chora, V. M. HernÁNdez-VelÁZquez, et al., "The Stingless Bees (Hymenoptera: Apidae: Meliponini): A Review of the Current Threats to Their Survival," *Apidologie* 53 (2022): 8.

12. A. S. Rozman, N. Hashim, B. Maringgal, and K. Abdan, "A Comprehensive Review of Stingless Bee Products: Phytochemical Composition and Beneficial Properties of Honey, Propolis, and Pollen," *Applied Sciences* 12 (2022): 6370.

13. S. I. Anjum, A. Ullah, K. A. Khan, et al., "Composition and Functional Properties of Propolis (Bee Glue): A Review," *Saudi Journal of Biological Sciences* 26, no. 7 (2019): 1695–1703.

14. U. Layek, N. Das, S. Kumar De, and P. Karmakar, "The Botanical Origin of Cerumen and Propolis of Indian Stingless Bees (*Tetragonula*

iridipennis Smith): Pollen Spectrum Does Not Accurately Indicate Latex and Resin Sources," *Apidologie* 54, no. 2 (2023): 18.

15. M. Dobrosielska, R. Dobrucka, P. Kozera, et al., "Beeswax as a Natural Alternative to Synthetic Waxes for Fabrication of PLA/Diatomaceous Earth Composites," *Scientific Reports* 13, no. 1 (2023): 1161.

16. A. Bucio, R. Moreno-Tovar, L. Bucio, J. Espinosa-Dávila, and F. Anguebes-Franceschi, "Characterization of Beeswax, Candelilla Wax and Paraffin Wax for Coating Cheeses," *Coatings* 11, no. 3 (2021): 261.

17. L. Szwajkowska-Michałek, A. Przybylska-Balcerek, T. Rogoziński, and K. Stuper-Szablewska, "Phenolic Compounds in Trees and Shrubs of Central Europe," *Applied Sciences* 10, no. 19 (2020): 6907.

18. A. Baştürk and B. Yavaş, "Antioxidant Activity, Total Phenolic Content, and Volatile Component Profiles of Propolis From Eight Turkish Regions," *Chemistry & Biodiversity* 22, no. 4 (2025): e202402269.

19. V. D. Wagh, "Propolis: A Wonder Bees Product and Its Pharmacological Potentials," *Advances in Pharmacological and Pharmaceutical Sciences* 2013, no. 1 (2013): 308249.

20. D. Kasote, V. Bankova, and A. M. Viljoen, "Propolis: Chemical Diversity and Challenges in Quality Control," *Phytochemistry Reviews* 21, no. 6 (2022): 1887–1911.

21. D. C. Woods, M. A. Olsson, T. A. Heard, H. M. Wallace, and T. D. Tran, "Quality Assessment and Chemical Diversity of Australian Propolis From *Tetragonula carbonaria* and *Tetragonula hockingsi* Stingless Bees," *Scientific Reports* 15 (2025): 17928.

22. E. Guzelmeric, P. I. Yuksel, B. K. Yaman, et al., "Comparison of Antioxidant and Anti-Inflammatory Activity Profiles of Various Chemically Characterized Turkish Propolis Sub-Types: Which Propolis Type Is a Promising Source for Pharmaceutical Product Development?," *Journal of Pharmaceutical and Biomedical Analysis* 203 (2021): 114196.

23. G. Grassi, G. Capasso, E. Gambacorta, and A. M. Perna, "Chemical and Functional Characterization of Propolis Collected From Different Areas of South Italy," *Food* 12, no. 18 (2023): 3481.

24. M. Woźniak, A. Sip, L. Mrówczyńska, J. Broniarczyk, A. Waśkiewicz, and I. Ratajczak, "Biological Activity and Chemical Composition of Propolis From Various Regions of Poland," *Molecules* 28, no. 1 (2022): 141.

25. A. S. Ayad, M. P. Hébert, J. A. Doiron, et al., "Algerian Propolis From Distinct Geographical Locations: Chemical Profiles, Antioxidant Capacity, Cytotoxicity and Inhibition of 5-Lipoxygenase Product Biosynthesis," *Chemistry & Biodiversity* 21, no. 4 (2024): e202301758.

26. A. K. Helmy, N. M. Sidkey, M. M. Abdel-Aziz, and A. A. El-Hela, "Chemical Composition of Egyptian Propolis and Studying Its Antimicrobial Activity and Synergistic Action With Honey Against Some Multidrug-Resistant Uropathogens," *Scientific Reports* 15 (2025): 17484.

27. F. Azonwade, B. B. Mabanza-Banza, A. M. Le Ray, et al., "Chemodiversity of Propolis Samples Collected in Various Areas of Benin and Congo: Chromatographic Profiling and Chemical Characterization Guided by ^{13}C NMR Dereplication," *Phytochemical Analysis* 34, no. 4 (2023): 461–475.

28. D. S. Ghallab, M. M. Mohyeldin, E. Shawky, A. M. Metwally, and R. S. Ibrahim, "Chemical Profiling of Egyptian Propolis and Determination of Its Xanthine Oxidase Inhibitory Properties Using UPLC–MS/MS and Chemometrics," *LWT* 136 (2021): 110298.

29. Z. Huang, T. Bi, H. Jiang, and H. Liu, "Review on NMR as a Tool to Analyse Natural Products Extract Directly: Molecular Structure Elucidation and Biological Activity Analysis," *Phytochemical Analysis* 35 (2024): 5–16.

30. B. Khakimov, G. Gürdeniz, and S. Engelsen, "Trends in the Application of Chemometrics to Foodomics Studies," *Acta Alimentaria* 44 (2015): 4–31.

31. K. Bingol, "Recent Advances in Targeted and Untargeted Metabolomics by NMR and MS/NMR Methods," *High-Throughput* 7 (2018): 9.

32. S. B. Engelsen, F. Savorani, and M. A. Rasmussen, *Encyclopedia of Magnetic Resonance*, vol. 2, eds. R. K. Harris and R. Wasylishen (John Wiley & Sons Ltd, 2013), 267–278.

33. O. Fiehn, "Metabolomics—The Link Between Genotypes and Phenotypes," *Plant Molecular Biology* 48 (2002): 155–171.

34. X. Du, L. Yang, L. Kong, et al., "Metabolomics of Various Samples Advancing Biomarker Discovery and Pathogenesis Elucidation for Diabetic Retinopathy," *Frontiers in Endocrinology* 13 (2022): 1037164.

35. D. K. Pratami, A. Mun'im, M. Sahlan, et al., "A Systematic Review of Metabolomics Studies on Metabolite Profiling and Phytogeographical Discrimination of Propolis," *Journal of Functional Foods* 123 (2024): 106602.

36. M. S. Blois, "Antioxidant Determinations by the Use of a Stable Free Radical," *Nature* 181 (1958): 1199–1200.

37. Å. Rinnan, M. Andersson, C. Ridder, and S. B. Engelsen, "Recursive Weighted Partial Least Squares (rPLS): An Efficient Variable Selection Method Using PLS," *Journal of Chemometrics* 28 (2014): 439–447.

38. O. Cloarec, M.-E. Dumas, A. Craig, et al., "Statistical Total Correlation Spectroscopy: An Exploratory Approach for Latent Biomarker Identification From Metabolic ^{1}H NMR Data Sets," *Analytical Chemistry* 77 (2005): 1282–1289.

39. J. Folch, M. Lees, and G. H. Sloane Stanley, "A Simple Method for the Isolation and Purification of Total Lipides From Animal Tissues," *Journal of Biological Chemistry* 226 (1957): 497–509.

40. J. Forsberg, C. T. Rasmussen, F. W. J. van den Berg, S. B. Engelsen, and V. Aru, "Fermentation Analytical Technology (FAT): Monitoring Industrial *E. coli* Fermentations Using Absolute Quantitative ^{1}H NMR Spectroscopy," *Analytica Chimica Acta* 1311 (2024): 342722.

41. F. Savorani, G. Tomasi, and S. B. Engelsen, "icoshift: A Versatile Tool for the Rapid Alignment of 1D NMR Spectra," *Journal of Magnetic Resonance* 202 (2010): 190–202.

42. S. Wold, K. Esbensen, and P. Geladi, "Principal Component Analysis," *Chemometrics and Intelligent Laboratory Systems* 2 (1987): 37–52.

43. D. Bertelli, G. Papotti, L. Bortolotti, G. L. Marcazzan, and M. Plessi, "^{1}H-NMR Simultaneous Identification of Health-Relevant Compounds in Propolis Extracts," *Phytochemical Analysis* 23 (2012): 260–266.

44. J. P. Vind, V. Aru, H. M. Jørgensen, et al., "Manuscript Submitted for Publication," (2025).

45. F. C. Massaro, P. R. Brooks, H. M. Wallace, and F. D. Russell, "Cerumen of Australian Stingless Bees (*Tetragonula carbonaria*): Gas Chromatography-Mass Spectrometry Fingerprints and Potential Anti-Inflammatory Properties," *Naturwissenschaften* 98 (2011): 329–337.

46. S. D. Leonhardt, S. Zeilhofer, N. Blüthgen, and T. Schmitt, "Stingless Bees Use Terpenes as Olfactory Cues to Find Resin Sources," *Chemical Senses* 35 (2010): 603–611.

47. T. Siddiqui, M. U. Khan, V. Sharma, and K. Gupta, "Terpenoids in Essential Oils: Chemistry, Classification, and Potential Impact on Human Health and INDUSTRY," *Phytomedicine Plus* 4 (2024): 100549.

48. D. De Rigo, C. M. Enescu, T. Houston Durrant, and G. Caudullo, "*Populus nigra* in Europe: Distribution, Habitat, Usage and Threats," European Atlas of Forest Tree Species, 2016, 136–137.

49. S. Wang, B. Wittwer, T. A. Heard, J. Q. D. Goodger, and M. A. Elgar, "Nonvolatile Chemicals Provide a Nest Defence Mechanism for Stingless Bees *Tetragonula carbonaria* (Apidae, Meliponini)," *Ethology* 124 (2018): 633–640.

50. D. Koedam, H. Jungnickel, J. Tentschert, G. R. Jones, and E. D. Morgan, "Production of Wax by Virgin Queens of the Stingless Bee

Melipona bicolor (Apidae, Meliponinae)," *Insectes Sociaux* 49 (2002): 229–233.

51. T. Takahashi and M. Miyazawa, "Tyrosinase Inhibitory Activities of Cinnamic Acid Analogues," *Die Pharmazie* 65 (2010): 913–918.

Supporting Information

Additional supporting information can be found online in the Supporting Information section. **Figure S1:** Correlation between IR absorbance signals at 1710 cm^{-1} (fatty acids) and 1736 cm^{-1} (fatty esters) to the ^1H NMR region of interest containing the multiplet (2.15–2.25 ppm). ^1H NMR signals were aligned with *i*coshift [1]. **Figure S2:** mrc70082-sup-0001-Supporting_Information.docx. ^1H NMR and IR region of interest in relation to fatty esters and fatty acids. **Figure S3:** Development of variable weights across recursive iterations in the three component *r*PLS model. ^1H NMR data were Pareto-scaled, while RSA data were mean-centered. The grayscale lines in the main panel represent the evolution of normalized weights for each spectral variable over 25 iterations, illustrating how variable influence changes through recursive weighting. The red line overlays the average ^1H NMR spectrum (6.0–8.0 ppm) of the hydrophobic phase extracts for reference. The blue stippled horizontal line marks the iteration with the lowest $RMSE_{CV.}$ The right-side plot shows the $RMSE_{CV}$ at each iteration, confirming model stability across the recursive process. The scale indicates normalized weights, where a value of 1 corresponds to high importance in the model. **Table S1:** Overview of the geographical origin of propolis and cerumen.

Supporting information

Comparative ^{1}H NMR Metabolomics between Scandinavian Propolis and Australian Propolis: The Quest to Identify Radical Scavenging Compounds

Jonas Vind[1], Søren Balling Engelsen[2], Henrik Munch Jørgensen[1], Julie Christine Antvorskov[3], Knud Josefsen[1], Violetta Aru[2].

Affiliations:

[1]Department of Pathology, The Bartholin Institute, Copenhagen University Hospital, Copenhagen, Denmark

[2]Department of Food Science, University of Copenhagen, Rolighedsvej 26, 1958 Frederiksberg C, Denmark

[3]Department of Clinical Research, Steno Diabetes Center Copenhagen, Translational Type 1 Diabetes Research, Herlev, Denmark

Table S1. Overview of the geographical origin of propolis and cerumen

Sample ID	Geographic location		Species
	Country	Region	
1	Denmark	Region Zealand	*Apis mellifera*
2	Denmark	Region Zealand	*Apis mellifera*
3	Denmark	Region Zealand	*Apis mellifera*
4	Denmark	Region Zealand	*Apis mellifera*
5	Denmark	Region Zealand	*Apis mellifera*
6	Denmark	Region Southern Denmark	*Apis mellifera*
7	Denmark	Region Northern Denmark	*Apis mellifera*
9	Denmark	The Capital Region	*Apis mellifera*
10	Denmark	Region Southern Denmark	*Apis mellifera*
11	Denmark	Region Southern Denmark	*Apis mellifera*
12	Denmark	Region Southern Denmark	*Apis mellifera*
13	Denmark	Region Southern Denmark	*Apis mellifera*
14	Denmark	Central Denmark Region	*Apis mellifera*
15	Denmark	Central Denmark Region	*Apis mellifera*
16	Denmark	Region Zealand	*Apis mellifera*
17	Denmark	Central Denmark Region	*Apis mellifera*
18	Denmark	Region Southern Denmark	*Apis mellifera*
19	Denmark	Central Denmark Region	*Apis mellifera*
20	Denmark	Region Northern Denmark	*Apis mellifera*
21	Denmark	Region Zealand	*Apis mellifera*
22	Denmark	Region Southern Denmark	*Apis mellifera*
23	Denmark	Region Southern Denmark	*Apis mellifera*
24	Denmark	Region Southern Denmark	*Apis mellifera*
25	Denmark	Region Northern Denmark	*Apis mellifera*
26	Denmark	Central Denmark Region	*Apis mellifera*
27	Denmark	Region Northern Denmark	*Apis mellifera*
28	Denmark	Region Northern Denmark	*Apis mellifera*
29	Denmark	Region Zealand	*Apis mellifera*
33	Denmark	Region Southern Denmark	*Apis mellifera*
34	Denmark	Region Southern Denmark	*Apis mellifera*
35	Denmark	Region Zealand	*Apis mellifera*
36	Denmark	The Capital Region	*Apis mellifera*
37	Denmark	Region Zealand	*Apis mellifera*
38	Denmark	Region Northern Denmark	*Apis mellifera*
39	Denmark	Central Denmark Region	*Apis mellifera*
40	Denmark	Central Denmark Region	*Apis mellifera*
41	Norway	Viken	*Apis mellifera*
42	Norway	Viken	*Apis mellifera*

44	Norway	Vestland	*Apis mellifera*
45	Norway	Vestland	*Apis mellifera*
46	Norway	Agder	*Apis mellifera*
47	Norway	Agder	*Apis mellifera*
48	Australia	New South Wales	*Apis mellifera*
49	Australia	New South Wales	*Apis mellifera*
50	Australia	New South Wales	*Apis mellifera*
51	Australia	New South Wales	*Apis mellifera*
52	Australia	New South Wales	*Apis mellifera*
53	Australia	New South Wales	*Tetragonula carbonaria*
54	Australia	New South Wales	*Tetragonula carbonaria*
55	Australia	New South Wales	*Tetragonula carbonaria*

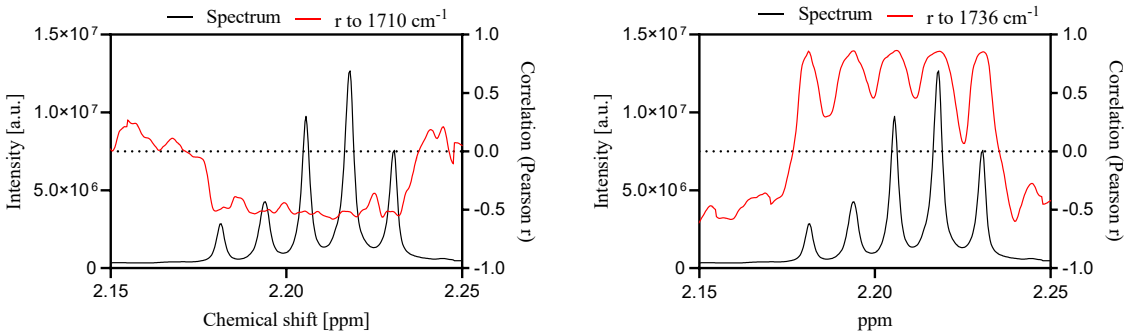

Figure S1. Correlation between IR absorbance signals at 1710 cm^{-1} (fatty acids) and 1736 cm^{-1} (fatty esters) to the ^{1}H NMR region of interest containing the multiplet (2.15–2.25 ppm). ^{1}H NMR signals were aligned with *i*coshift [1].

A. mellifera (SC):

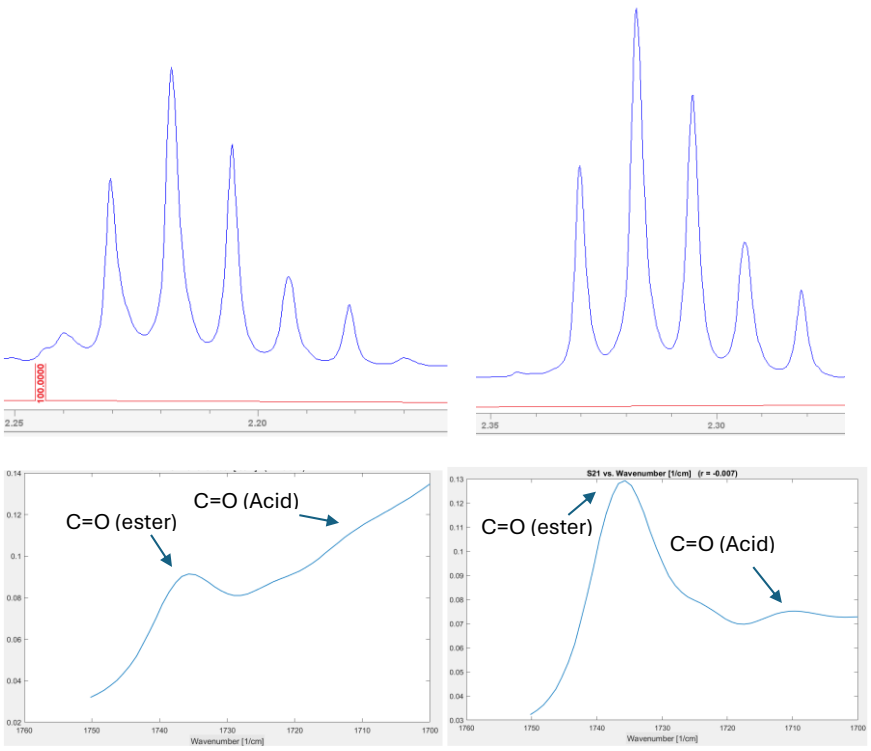

A. mellifera (AU):

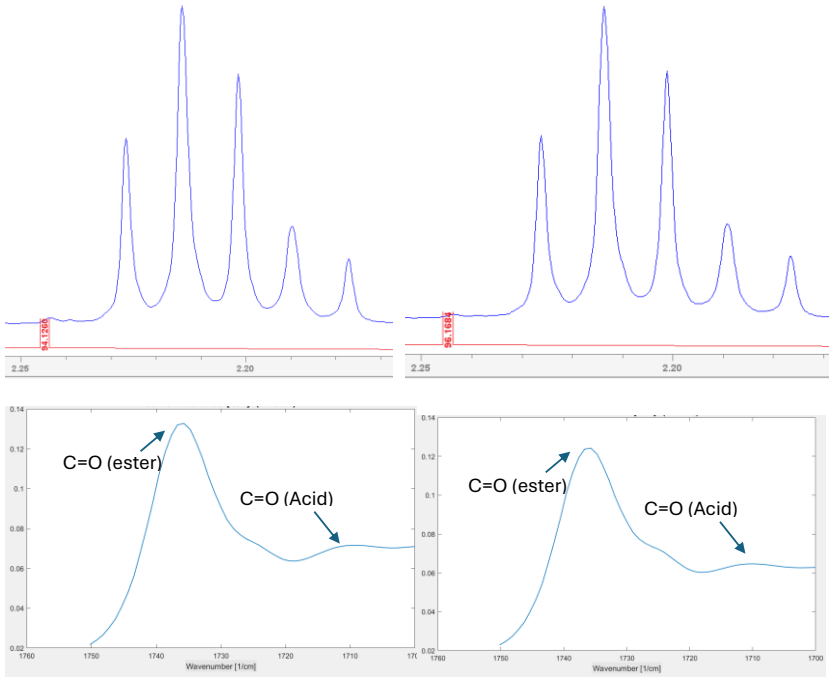

T. carbonaria (AU):

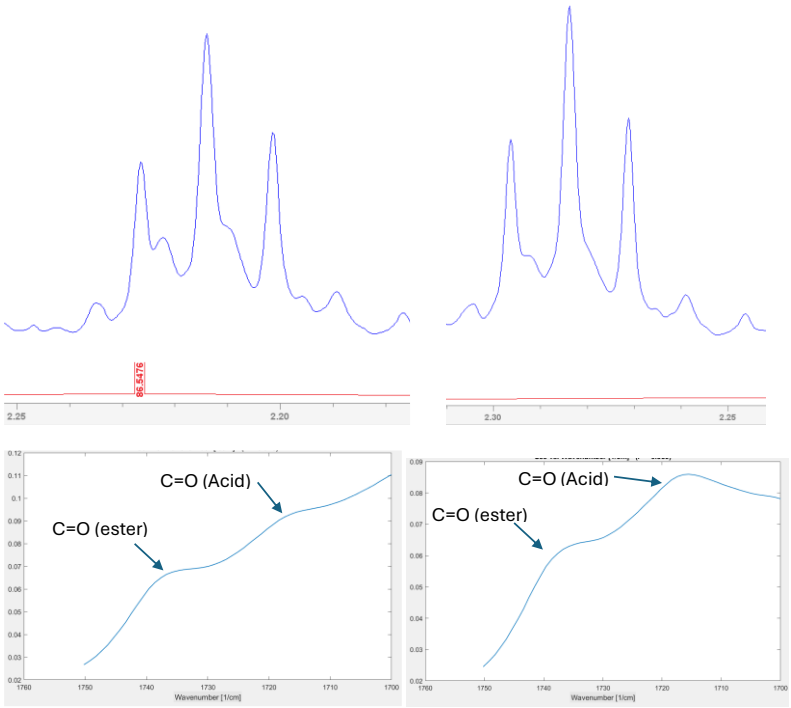

Figure S2. ^{1}H NMR and IR region of interest in relation to fatty esters and fatty acids.

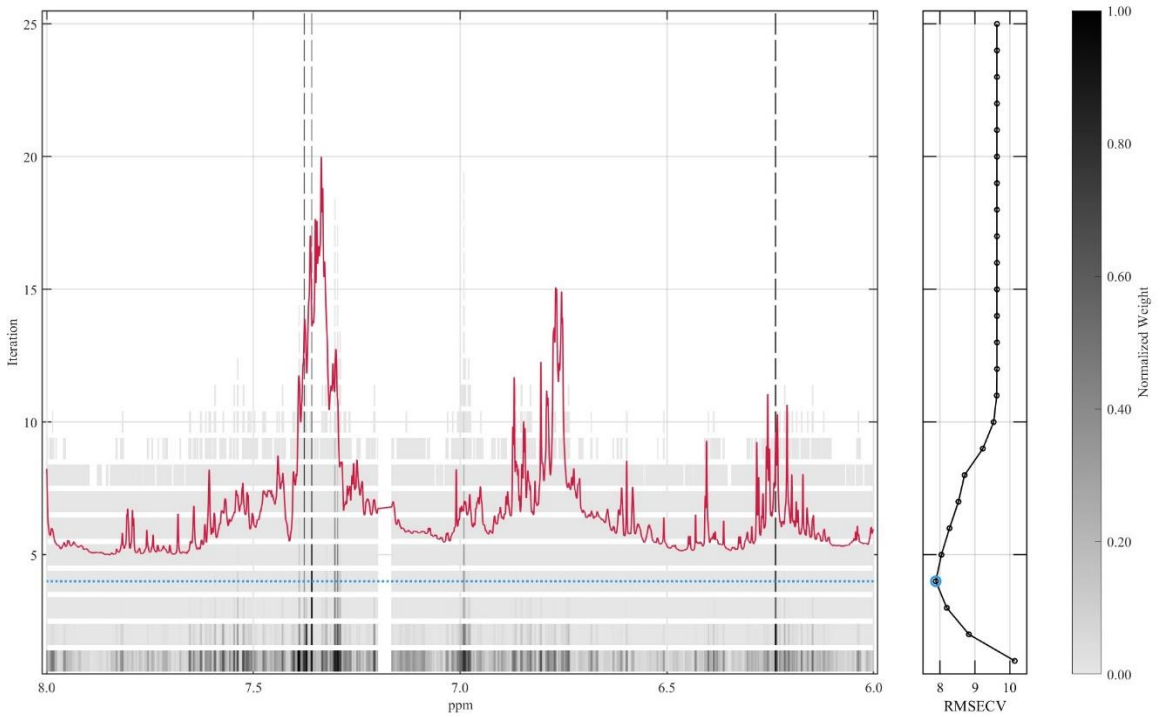

Figure S3 Development of variable weights across recursive iterations in the three component *r*PLS model. ^{1}H NMR data was Pareto-scaled, while RSA data was mean-centered. The grayscale lines in the main panel represent the evolution of normalized weights for each spectral variable over 25 iterations, illustrating how variable influence changes through recursive weighting. The red line overlays the average ^{1}H NMR spectrum (6.0-8.0 ppm) of the hydrophobic phase extracts for reference. The blue stippled horizontal line marks the iteration with the lowest $RMSE_{CV}$. The right-side plot shows the $RMSE_{CV}$ at each iteration, confirming model stability across the recursive process. The scale indicates normalized weights, where a value of 1 corresponds to high importance in the model.

References

[1] F. Savorani, G. Tomasi, S. B. Engelsen, *J Magn Reson* **2010**, *202*, 190-202.

Manuscript III

Journal of Ethnopharmacology 368 (2026) 121867

Contents lists available at ScienceDirect

Journal of Ethnopharmacology

journal homepage: www.elsevier.com/locate/jethpharm

Linking propolis chemical composition and geographical origin to immunomodulatory effects in human immune cells

Magni Steintún [a,1], Jonas Vind [a,*,1], Camilla Hartmann Friis Hansen [b], Jesper Larsen [c], Lars Duelund [d], Rime Bahij [d], Henrik Munch Jørgensen [a], Julie Christine Antvorskov [e], Bo Markussen [f], Violetta Aru [g], Søren Balling Engelsen [g], Knud Josefsen [a]

[a] Bartholin Institute, Rigshospitalet Copenhagen Biocenter, Ole Maaløes Vej 5, 2200, Copenhagen N, Denmark
[b] Department of Veterinary and Animal Sciences, University of Copenhagen, Ridebanevej 9, 1870, Frederiksberg C, Denmark
[c] Bioneer A/S, Kogle Alle 2, 2970, Hørsholm, Denmark
[d] Department of Green Technology, University of Southern Denmark, Campusvej 55, 5230, Odense M, Denmark
[e] Steno Diabetes Center, Herlev Hospital, Borgmester Ib Juuls Vej 1, Herlev, 2730, Denmark
[f] Department of Mathematical Sciences, University of Copenhagen, Universitetsparken 5, 2100, Copenhagen OE, Denmark
[g] Department of Food Science, University of Copenhagen, Rolighedsvej 26, 1958, Frederiksberg C, Denmark

ARTICLE INFO

Keywords:
Propolis
Immunomodulation
Anti-inflammation
Polyphenols
Chemometrics
Peripheral blood mononuclear cells (PBMCs)

ABSTRACT

Ethnopharmacological relevance: Propolis is a resinous bee product traditionally used for its anti-inflammatory activity; however, its chemical complexity limits standardization and ethnopharmacological validation. This study integrated chemical profiling with functional immune assays to identify compounds underlying its anti-inflammatory effects.

Methods: 52 ethanolic propolis extracts from Australia (N = 7), Denmark (N = 38), and Norway (N = 7) were analysed by high-performance liquid chromatography (HPLC). 8 polyphenols with reported anti-inflammatory activity were used as reference standards. Human peripheral blood mononuclear cells (PBMCs) were stimulated with lipopolysaccharide (LPS) or phytohemagglutinin-L (PHA), and effects of propolis extracts and individual polyphenols on interleukin-1β (IL-1β) secretion were quantified by ELISA. Log_{10}-transformed HPLC fingerprints and IL-1β data were analysed using multivariate methods, including partial least squares (PLS) regression, selectivity ratios (SRs), forward stepwise selection (FSS), and corrected Akaike's Information Criterion (AICc). Additional cytokines were measured using a mesoscale multiplex immunoassay.

Results: HPLC-analysis showed that propolis from Denmark and Norway contained higher levels of aromatic compounds than Australian samples. Propolis extracts reduced IL-1β secretion by 13%, 41%, and 37% for samples from Australia, Denmark, and Norway, respectively. Chemometric modelling identified the total extract load as key for anti-inflammatory effect, however, following log_{10}-transformation, the chrysin-associated peak emerged as the most consistently supported candidate for independent, compound-specific IL-1β suppression. Multiplex cytokine profiling further demonstrated that propolis decreased IL-1β, IL-10, and IFN-γ while increasing IL-4, IL-6, and TNF-α, indicating a multifaceted immunomodulatory effect, including a Th1-to-Th2 shift.

Conclusion: Propolis demonstrated anti-inflammatory and immunomodulatory properties supporting its traditional use. Geographic variation in chemistry was associated with differences in IL-1β suppression. Chemometric

Abbreviations: **AICc**, corrected Akaike's Information Criterion; **ANOVA**, analysis of variance; **CAPE**, caffeic acid phenethyl ester; **CV**, cross-validation; **DAD**, diode array detector; **DAPI**, 4′,6-diamidino-2-phenylindole; **DMSO**, dimethyl sulfoxide; **ELISA**, enzyme-linked immunosorbent assay; **ESI**, electrospray ionization; **FBS**, fetal bovine serum; **FSS**, forward stepwise selection; **HPLC**, high-performance liquid chromatography; **IFN-γ**, interferon gamma; **IL**, interleukin; **LC-QTOF-MS**, liquid chromatography–quadrupole time-of-flight mass spectrometry; **LPS**, lipopolysaccharide; **LV**, latent variable; **MSD**, Meso Scale Discovery; **NF-κB**, nuclear factor kappa B; **PBMCs**, peripheral blood mononuclear cells; **PHA**, phytohemagglutinin-L; **PLS**, partial least squares; **RMSECV**, root mean square error of cross-validation; **RPMI**, Roswell Park Memorial Institute medium; **SD**, standard deviation; **SR**, selectivity ratio; **TCA**, total chromatographic area; **TLR4**, Toll-like receptor 4; **UV-VIS**, ultraviolet-visible spectroscopy.

* Corresponding author. Bartholin Institute, Rigshospitalet, Copenhagen Biocenter, Ole Maaløes Vej 5, 2200, Copenhagen N, Denmark.
E-mail address: Jonas.Pordel.Vind@regionh.dk (J. Vind).

[1] Shared first authorship.

https://doi.org/10.1016/j.jep.2026.121867
Received 13 February 2026; Received in revised form 5 May 2026; Accepted 14 May 2026
Available online 15 May 2026

analysis identified overall composition and the chrysin-associated signal as the most consistently supported putative candidate for compound-specific anti-inflammatory activity, while cytokine profiling further indicated that propolis acts as a complex immunomodulator rather than a broad immunosuppressant.

1. Introduction

Propolis is a natural resinous substance produced by honeybees through the collection and amalgamation of plant resins combined with various bee-derived secretions (Simone-Finstrom and Spivak, 2010; Anjum et al., 2019). Within the hive, it serves to seal cracks and protect the colony from environmental threats and microbial invasion, functioning both as a physical barrier and an antimicrobial defence (Simone-Finstrom and Spivak, 2010). Propolis has been used in traditional medicine to treat a variety of conditions, including upper respiratory infections, oral inflammations, and wounds (Rojczyk et al., 2020, Ożarowski and Karpiński, 2023; López-Valverde et al., 2021). Due to its chemical complexity, propolis remains incompletely characterized, and its therapeutic effects are not yet rigorously documented in clinical settings. The international standard for bee propolis (ISO 24381:2023) has aimed to provide chemical benchmarks, but the complexity of propolis, influenced by regional flora and geography (El Menyiy et al., 2021), continues to challenge uniform classification. More than 300 distinct compounds have been identified to date (Huang et al., 2014), where many of these constitute bioactive compounds with diverse pharmacological effects, including immunomodulatory properties (Zulhendri et al., 2022; Magnavacca et al., 2022). Polyphenols are believed to be among the main contributors to these effects (Hossain et al., 2022). However, the variability and complexity of propolis make it difficult to pinpoint the specific compounds responsible for its biological activity, and increasing evidence suggests that these effects likely result from the synergistic actions of multiple constituents (Ramata-Stunda et al., 2022). While ISO 24381:2023 includes apigenin, caffeic acid, caffeic acid phenethyl ester (CAPE), p-coumaric acid, chrysin, ferulic acid, galangin, and pinocembrin as benchmark compounds with reported anti-inflammatory properties, it remains uncertain which of these, if any, are the primary drivers of the anti-inflammatory activity, or if other yet unidentified compounds may play a more significant role.

The aim of this study was to characterize the anti-inflammatory effects of propolis by integrating chemical profiling with immune functional assays. This included comparative analysis of samples from Australia, Denmark, and Norway using high-performance liquid chromatography (HPLC), followed by cytokine measurements in stimulated peripheral blood mononuclear cells (PBMCs). To identify compounds independently associated with biological activity, multivariate data analysis was applied to relate HPLC-based chemical fingerprints to IL-1β. This study introduces a methodological framework not previously applied in propolis research, combining HPLC fingerprinting with multivariate model selection and immune functional readouts. This approach enables disentangling of matrix effects from compound-specific contributions, providing a more precise understanding of the constituents driving the anti-inflammatory activity than previously presented.

2. Methods

2.1. Chemicals

Apigenin (≥95%, HPLC grade), caffeic acid (≥95%, HPLC grade), caffeic acid phenethyl ester (CAPE), p-coumaric acid (≥98%, HPLC grade), chrysin (≥98%, HPLC grade), ethanol (70 %), ferulic acid (99%), galangin (≥95%, HPLC grade), pinocembrin (≥95%, HPLC grade), dimethyl sulfoxide (DMSO, >99.9%), formic acid (>98%), acetonitrile (≥99.9%, HPLC grade), lipopolysaccharides (LPS) from *Escherichia coli*, and phytohemagglutinin-L (PHA) were purchased from Sigma-Aldrich (Copenhagen, Denmark). Milli-Q water (18.2 MΩ cm) was produced using a Milli-Q purification system from Merck Millipore (Burlington, MA, USA). 10x spectral 4′,6-diamidino-2-phenylindole (DAPI) was obtained from BD Biosciences (CA, USA). Lymphoprep™ was acquired from STEMCELL Technologies (Vancouver, Canada). GlutaMAX™ and fetal bovine serum (FBS, qualified, Brazil origin) were purchased from Gibco, Thermo Fisher Scientific (MA, USA).

2.2. Collection of propolis

In total, 52 propolis samples were collected and analysed, comprising 38 samples from across Denmark, 7 samples from Australia (New South Wales), and 7 samples from southern Norway. Upon collection, the samples were stored at 4 °C until analysis.

2.3. Preparation of propolis ethanolic extractions

Raw propolis samples were frozen in liquid nitrogen and subsequently ground into a fine powder using a pestle and mortar. For each extraction, 100 mg of the powdered propolis was combined with 5 mL of 70% ethanol in round-bottom glass tubes and homogenized for 30 s using a T10 Basic ULTRA-TURRAX ® (IKA-Werke, Germany). The mixture was then stored in the dark for 1 h before being centrifuged at 3600 RPM for 15 min at 4 °C. Following centrifugation, 4 mL of the supernatant was collected into 15 mL Falcon™ conical centrifuge tubes and kept in a dark cooling room at 4 °C until further analysis.

2.4. HPLC analysis of ethanolic extracts

Chromatographic separation of the ethanolic extracts was performed using reverse-phase HPLC on an HP Agilent HPLC system Series 1100. The mobile phase consisted of two solvents: (A) Milli-Q water with 0.1% (v/v) formic acid and (B) acetonitrile. The flow rate was set to 1.0 mL/min. The elution gradient began at 20% B for 6 min. B then gradually shifted to 30% by t = 10 min, followed by a transition to 40% B by over 30 min. Between t = 40 min and t = 70 min, B increased to 77.5% B. At t = 70.1 min, B increased to 90%. At t = 80 min B returned to 20% for 10 min throughout the run. The column (Phenomenex Jupiter, 5 μm C18, 300 Å, 250 × 4.60 mm) was maintained at room temperature, and the injection volume was 10 μL. Chromatograms were acquired using a diode array detector (DAD), which recorded full UV-VIS spectra (190–400 nm). For quantitative analysis, data at 280 nm were extracted and used. Based on the international standard for bee propolis (ISO 24381:2023), the polyphenols apigenin, caffeic acid, CAPE, p-coumaric acid, chrysin, ferulic acid, galangin, and pinocembrin were selected as benchmark polyphenols. To identify selected polyphenols, 20 μL of a 1 mg/mL standard solution was spiked into 200 μL of ethanolic extract and the retention time of each polyphenol was recorded for identification.

2.5. PBMC isolation

Buffy coats were obtained from a healthy volunteer, diluted 1:1 in isotonic saline, and isolated according to the manufacturer's instructions. Aliquots were resuspended in RPMI 1640, 40% serum, 10 % DMSO, frozen at 1°/min and stored in liquid nitrogen vapor until use. The same donor was used for all experiments.

2.6. PBMC stimulation

PBMCs were thawed in a 37 °C water bath, washed once, and resuspended in RPMI 1640 medium supplemented with GlutaMAX™, HEPES, and pyruvate. The cells (1.45×10^5/well) were seeded into Corning® 96-well clear flat-bottom plates and incubated with 6.25 ng/mL LPS and 25 μg/mL propolis or test substance in a total volume of 200 μL for 24 h at 37 °C, 5% CO_2, and 100% humidity. The propolis concentration of 25 μg/mL was selected based on the concentration-response profiles of three randomly selected Danish propolis samples, tested in dilution series ranging from 400 to 0.024 μg/mL (400, 100, 25, 6.25, 1.56, 0.39, 0.098, and 0.024 μg/mL) following LPS or PHA stimulation. As Australian and Norwegian samples were included to enable direct geographic comparison with Danish propolis, the same concentration was applied uniformly across all samples. Propolis treatment produced a consistent anti-inflammatory response across PBMCs from four independent donors; therefore, one donor was selected for all subsequent experiments. Based on the similar inhibition patterns observed for LPS and PHA, as well as comparable cytokine responses in the mesoscale multiplex assay, the anti-inflammatory effect of all samples were assessed using LPS stimulation only. Supernatants were harvested, centrifuged at 200 × g for 5 min, and stored at -20 °C until analysis. IL-1β was quantified by ELISA (Proteintech, IL, USA) at a 1:30 dilution. Pure polyphenols were dissolved in 70% ethanol, except for chrysin and galangin, which were dissolved in DMSO.

2.7. Multiplex cytokine analysis

Cytokine concentrations in PBMC supernatants were measured using the V-PLEX Proinflammatory Panel 1 Human Kit (Meso Scale Discovery (MSD), Rockville, MD, USA) according to the manufacturer's protocol. This electrochemiluminescence-based assay allows simultaneous quantification of multiple cytokines. Briefly, 50 μL of a 1:15 dilution of PBMC supernatant was added to pre-coated plates and incubated for 2 h with gentle shaking. After washing, SULFO-TAG-labelled detection antibodies were added and incubated for an additional 2 h. Plates were washed again and read buffer was added before detection using an MESO QuickPlex SQ120MM (MSD). Cytokine concentrations were calculated using standard curves generated from duplicate standards, and data were processed using MSD Workbench software v4.0. For these analyses 3 randomly selected Danish propolis samples were used and measured in triplicates and compared to dexamethasone.

2.8. Cell viability

PBMC viability was assessed before and after 24 h of incubation. Samples (90 μL) were mixed with 10 μL of 10× Spectral DAPI and analysed on a BD FACSCelesta™ flow cytometer (BD Biosciences, CA, USA). Single cells were gated in the forward scatter.

2.9. Mass spectrometry analysis

Mass spectrometry was used to validate the HPLC spiking experiments, ensuring correct peak assignment and enabling identification of additional, unidentified compounds. For this purpose, one Danish sample was analysed by liquid chromatography coupled to quadrupole time-of-flight mass spectrometry (LC-QTOF-MS). Analyses were performed on an Agilent 1290 Infinity HPLC system (G4226A autosampler with G1330B thermostat, G4220A binary pump, G1316C column oven, and G1315C photodiode array detector) coupled to a G6550A quadrupole time-of-flight (Q-TOF) mass spectrometer with a dual Agilent Jet Stream electrospray ionization (Dual AJS ESI) source. The chromatographic column and HPLC parameters were identical to those described above. The mass spectrometer source was operated with a drying gas temperature of 225 °C, a sheath gas temperature of 400 °C, and a fragmentor voltage of 100 V. Data were acquired in both positive and negative ionization modes.

2.10. Statistical analysis

All statistical analyses were performed using GraphPad Prism (version 8.4.3, GraphPad Software, San Diego, CA, USA) unless otherwise specified. For experiments assessing concentration-dependent inhibition of IL-1β release by propolis and dexamethasone, data were analysed using two-way repeated measures ANOVA with Geisser-Greenhouse correction, followed by Sidak's post hoc test to compare treatments at individual concentrations. Differences in IL-1β inhibition between propolis samples of different geographical origin were assessed using one-way ANOVA with Tukey's post hoc test. The effects of individual polyphenols were compared to the LPS-stimulated control using one-way ANOVA with Dunnett's post hoc test. Data are presented as mean ± SD, and statistical significance was defined as $p < 0.05$.

2.11. Chemometric analyses

To investigate associations between chromatographic profiles and IL-1β responses, a chemometric workflow was performed in MATLAB R2023b (MathWorks, Natick, MA, USA). Initially, chromatograms were aligned using *icoshift* (Savorani et al., 2010; Tomasi et al., 2011), and peak intensities were extracted as local maxima. For each sample, the total chromatographic area (TCA) was calculated to assess overall associations between compound abundance and IL-1β. Both raw and $\log_{10}$-transformed HPLC and IL-1β data were evaluated, with $\log_{10}$-transformation applied to stabilise variance, reduce dominance of large peaks, and improve linearity.

Partial least squares (PLS) regression (Wold et al., 1983; Martens and Dardenne, 1998) was performed on $\log_{10}$-transformed data using mean-centering and two latent variables (LVs), as this provided the lowest cross-validated prediction error. Selectivity ratios (SRs) (Kvalheim, 2010) were computed using 20-times repeated Venetian-blinds 10-fold cross-validation (CV) to quantify each signal's contribution. Subsequently, forward stepwise selection (FSS) (Norgaard et al., 2000) was applied to the $\log_{10}$-transformed, mean-centered data. At each step, models with up to two LVs were optimised via internal 5-fold Venetian CV and evaluated by an outer 5-fold Venetian CV. The signal yielding the greatest reduction in cross-validated root mean square error (RMSECV) was retained, along with its univariate Pearson correlation with IL-1β. Iterations continued until no remaining signal improved RMSECV. The 31.00 min signal was excluded because it showed a moderately strong positive correlation with IL-1β, suggesting a potential pro-inflammatory association that could confound identification of negatively correlated anti-inflammatory markers This exclusion was further motivated by its dominant influence on the variance structure, which could mask detection of independent compound-specific contributors to anti-inflammatory activity regardless of correlation direction. To evaluate variable robustness, all subsets (255 models) of the eight FSS-retained signals were assessed using the corrected Akaike Information Criterion (AICc). Variable inclusion frequencies among the top 10 AICc-ranked models were recorded.

2.12. Ethical approval

The experiments using human immune cells were approved by The Danish Health Research Ethics Committee system under approval number H-25003840.

3. Results

3.1. Comparative HPLC analysis of the propolis samples

Average HPLC chromatograms for each geographical region are shown in Fig. 1, with identified polyphenols indicated. Peak assignments

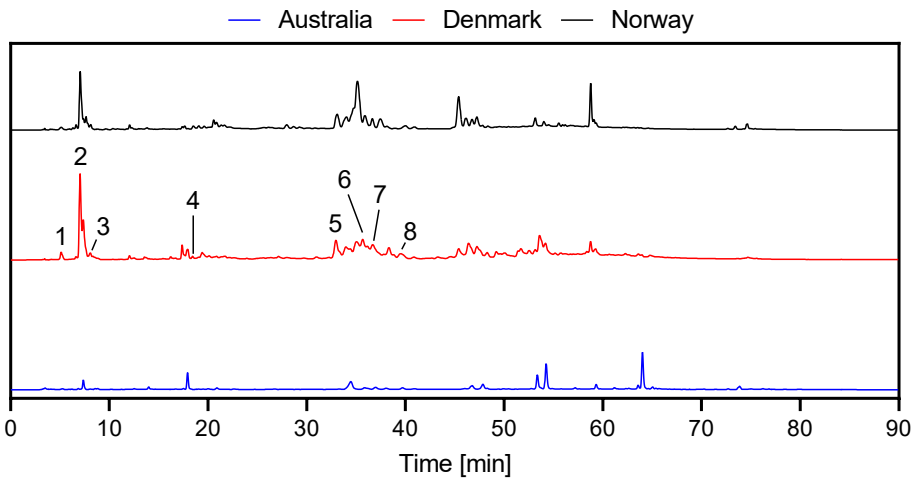

Fig. 1. Average HPLC chromatograms of ethanolic propolis extracts from Australia (N = 7), Denmark (N = 38), and Norway (N = 7). Peaks corresponding to identified polyphenols are indicated: (1) Caffeic acid, (2) *p*-Coumaric acid, (3) Ferulic acid, (4) Apigenin, (5) Chrysin, (6) Pinocembrin, (7) Galangin, and (8) CAPE.

were further supported by LC-QTOF-MS analysis (Supplementary Table 1). The labelled peaks correspond to: (1) caffeic acid, (2) p-coumaric acid, (3) ferulic acid, (4) apigenin, (5) chrysin, (6) pinocembrin, (7) galangin, and (8) caffeic acid phenethyl ester (CAPE).

The chromatograms of Danish and Norwegian propolis exhibited relatively similar chromatographic profiles, characterized by a wide range of signals with comparable retention times but varying intensities. In both Danish and Norwegian samples, the most intense peak, corresponding to *p*-coumaric acid, appeared at approximately 7 min. In contrast, the chromatograms of Australian samples displayed fewer and less intense signals, with the most prominent peak eluting after 64 min.

3.2. Concentration dependent inhibition of stimulated IL-1β release in PBMC

Three Danish propolis samples were randomly selected to assess their concentration-dependent effects on IL-1β release from PBMCs stimulated with LPS or PHA (Fig. 2). Cell viability remained high across the tested concentration range, with no evidence of cytotoxicity (Supplementary Table 2). The anti-inflammatory activity of propolis was compared to dexamethasone. In LPS-stimulated PBMCs, both treatments reduced IL-1β release in a concentration-dependent manner. Two-way repeated measures ANOVA showed that IL-1β release was strongly influenced by concentration, and that the effect of increasing concentrations differed between propolis and dexamethasone. Post hoc test revealed that dexamethasone suppressed IL-1β more effectively than propolis at 100 μg/mL, whereas no other concentrations showed significant differences.

In PHA-stimulated PBMCs, both treatments again reduced IL-1β in a concentration-dependent manner, and the effect of concentration differed between treatments. However, post hoc testing did not identify significant differences between propolis and dexamethasone at individual concentrations, consistent with greater variability under PHA stimulation. Overall, dexamethasone was more potent at lower concentrations, while propolis achieved comparable inhibitory effects at higher concentrations.

3.3. Inhibition of LPS-induced IL-1β release of propolis

Based on the concentration-dependent inhibition curve of LPS-induced IL-1β release, a concentration of 25 μg/mL propolis was selected to assess the anti-inflammatory effects of all samples (N = 52). The results are presented in Fig. 3.

No significant difference was observed between the Danish and Norwegian samples, which showed mean IL-1β levels of 59.5% ± 14.5% and 63.6% ± 11.1%, respectively, relative to the positive control (LPS stimulation without propolis). IL-1β release in the Australian samples was 86.7% ± 14.5%.

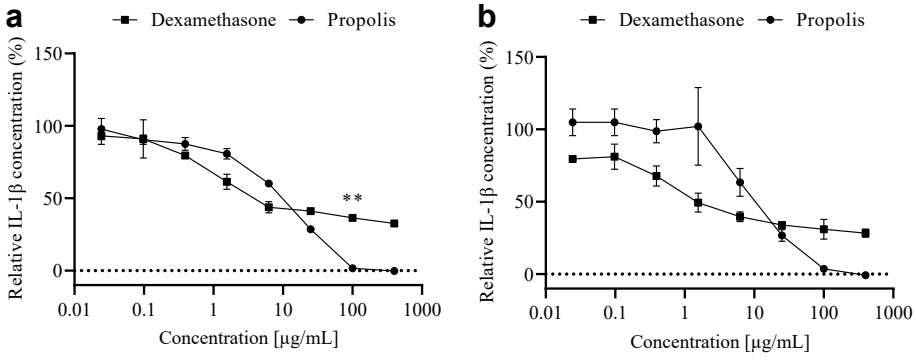

Fig. 2. Concentration-dependent effect of propolis and dexamethasone on IL-1β release from stimulated PBMCs. Cells were stimulated with (a) LPS or (b) PHA and treated with increasing concentrations of propolis (three randomly selected Danish samples, N = 3) or dexamethasone (N = 2). IL-1β concentrations in culture supernatants were quantified and expressed relative to the stimulated, untreated control. Data represent mean ± SD. Statistical analysis was performed using two-way repeated measures ANOVA followed by Sidak's post hoc tests. Only significant differences between treatments are indicated (**p < 0.01).

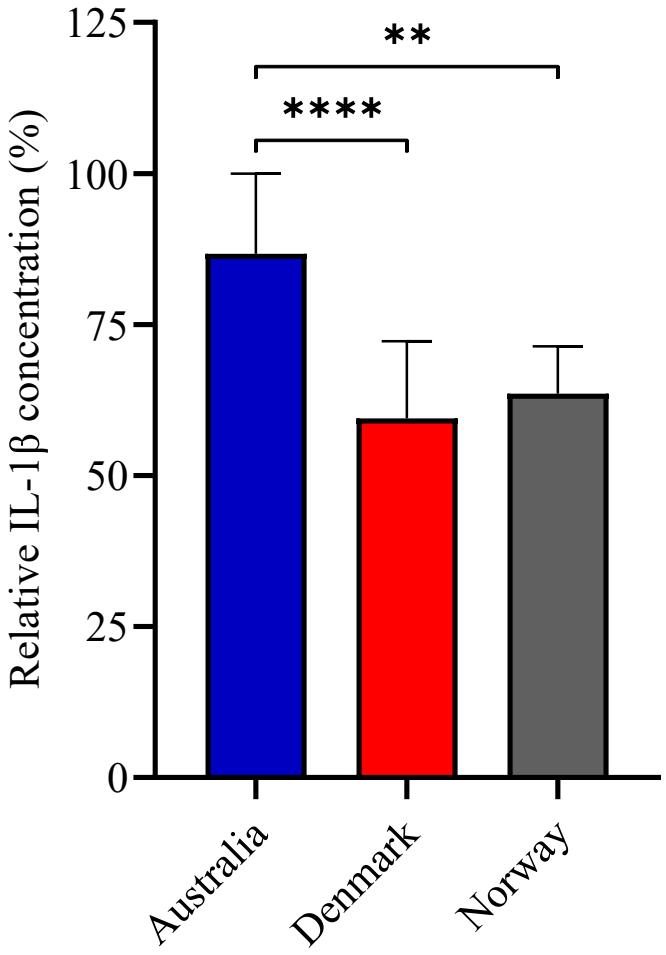

Fig. 3. Inhibition of IL-1β release by Danish (N = 38), Norwegian (N = 7), and Australian (N = 7) propolis samples (25 μg/mL) in LPS-stimulated PBMCs. Values are expressed as IL-1β release relative to LPS stimulated PBMS with no added treatment. PBMCs were stimulated with 6.25 ng/mL LPS, and IL-1β levels in the culture supernatants were measured by ELISA. All samples were tested in triplicate. Data represent mean ± SD. Statistical comparisons were performed between each experimental group and the positive control (**p < 0.01, ****p < 0.0001).

3.4. Log_{10}-transformation effect on compound abundance on IL-1β correlation

The percentage of variance in IL-1β explained by the TCA was compared between raw and log_{10}-transformed data (Fig. 4a). For the raw data, the TCA explained roughly 48% of the variation in IL-1β, whereas this dropped to 6% after log_{10}-transformation. A PLS model was then built using the log_{10}-transformed data, and SRs were calculated for each signal. The chrysin-associated peak at 32.99 min showed the strongest contribution (SR = 0.73), whereas peaks at 5.14 min (caffeic acid), 8.38 min, and 31.00 min followed with more modest contributions (SR = 0.50, 0.48, and 0.47, respectively).

3.5. Identification of compounds linked to anti-inflammatory effect

Forward stepwise selection (FSS) was applied to the log_{10}-transformed data to identify the most complementary descriptive compounds of IL-1β. FSS selected eight signals, of which the chrysin peak at 32.99 min and a peak at 13.51 min were the only features with significant negative correlations to the IL-1β concentration (r = −0.35 and −0.39, respectively) (see Table 1).

Subsequent AICc-based model selection, based on the 8 FSS-selected signals, highlighted three peaks, 12.02 min (r = −0.21), 28.64 min (r = +0.24), and 32.99 min (r = −0.35), which appeared in 100% of the top 10-ranked models, confirming them as the most consistent predictors of IL-1β (see Fig. 5).

In summary, although the TCA initially explained a large proportion of the IL-1β variation, this effect was largely removed by log_{10}-

Table 1
Forward stepwise selection PLS on log_{10}-transformed, mean-centered data. At each step, up to 2 latent variables were tuned using an internal 5-fold venetian CV, and model performance was evaluated by an outer 5-fold venetian CV. The signal providing the largest reduction in RMSECV was added. Pearson correlation (r) with IL-1β is shown for each signal (*p < 0.05).

Signal added to model	r (IL-1β)	RMSECV
Intercept	-	0.0913
32.99 min (Chrysin)	−0.35*	0.0892
12.02 min	−0.21	0.0877
28.64 min	0.24	0.0847
16.19 min	−0.29	0.0827
39.56 min (CAPE)	−0.11	0.0814
35.08 min	0.11	0.0812
51.41 min	0.12	0.0802
13.51 min	−0.39*	0.0790

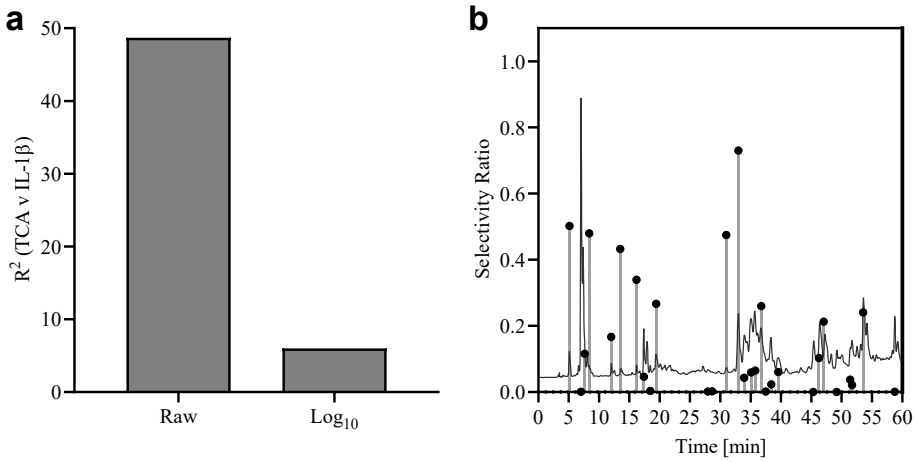

Fig. 4. (a) The percentage variance in IL-1β concentration explained by the TCA for on raw data and log_{10}-transformed data. (b) SRs of PLS model on log-transformed data. The PLS model used 2 LVs and 20 times repeated venetian blinds 10-fold CV.

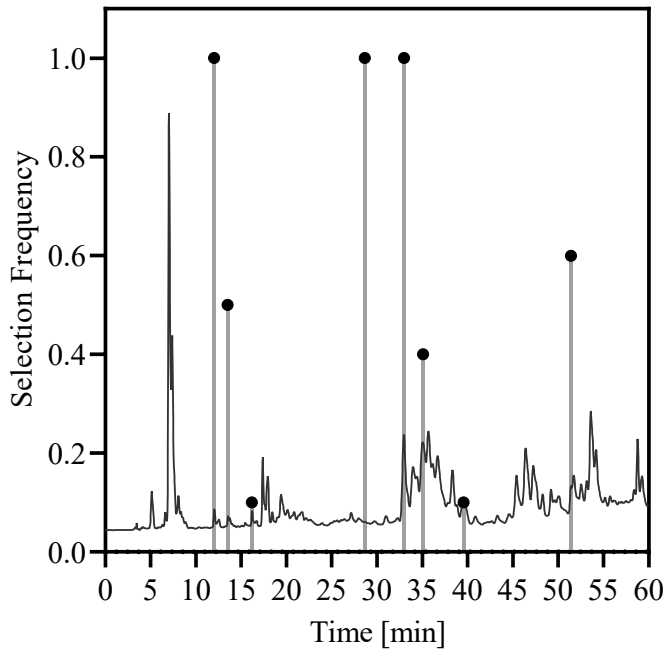

Fig. 5. Variable inclusion frequency among the top AICc models, based on HPLC signals pre-selected by FSS.

transformation. Across multiple multivariable analyses, the 32.99 min peak (chrysin) was the only signal combining a significant individual correlation with complete stability across the top AICc-selected models, identifying it as the most consistently supported putative candidate for independent, compound-specific IL-1β suppression. The signals at 12.02 and 28.64 min also exhibited complete stability across the top AICc-selected models but did not show significant individual associations with IL-1β and were not highlighted by the SR ranking.

3.6. In vitro assessment of polyphenol effects on IL-1β

To evaluate the potency of chrysin compared to other reference polyphenols in the applied immune functional assay, compounds were tested individually using the same experimental setup as in Fig. 3. IL-1β concentrations were expressed relative to the positive control (LPS stimulation without polyphenol).

Chrysin showed the strongest and saturated inhibitory effect reducing IL-1β to 0.3 % of control levels (Table 2). Caffeic acid also showed great potency reducing IL-1b levels to 2.4 %. CAPE also markedly reduced IL-1β (39.1% of control), whereas galangin and p-coumaric acid produced more moderate inhibition (83.7% and 75.2%, respectively). Ferulic acid seemingly reduced IL-1β secretion, although this effect did not reach statistical significance.

3.7. Propolis is immunomodulatory rather than only supressing

To assess the immunomodulatory effects of propolis beyond IL-1β, multiple cytokines were measured following stimulation of PBMCs with either LPS or PHA, using a Meso Scale multiplex immunoassay. Fig. 6 shows cytokine concentrations relative to the positive control (LPS- or PHA-stimulated PBMCs without treatment).

The well-established immunosuppressant, dexamethasone, was included as a reference treatment. Similar patterns were observed across both LPS- and PHA-stimulated conditions. Dexamethasone generally reduced cytokine levels, although some effects did not reach statistical significance. In contrast, propolis treatment resulted in both increased and decreased cytokine concentrations. Consistent with the ELISA findings, propolis significantly reduced IL-1β levels. In addition, IL-10 and IFN-γ were also significantly decreased. Conversely, increases were observed in IL-4, IL-6, and TNF-α levels following propolis treatment. These results thus indicate that propolis exhibits immunomodulatory activity rather than only immunosuppressive.

4. Discussion

HPLC chromatograms of the 52 propolis samples revealed clear geographical differences, with Australian extracts displaying considerably fewer signals at 280 nm compared with Danish and Norwegian samples, indicating lower levels of UV-absorbing aromatic compounds. This is consistent with complementary spectroscopic analyses (J. P. Vind et al., 2026; J. Vind et al., 2026). These compositional differences likely reflect variation in the botanical resin sources available to the bees. However, the botanical origins of the collected propolis were not directly identified or characterized in this study, and the specific plant-derived constituents underlying the observed geographic differences therefore remain unresolved.

Functionally, the Danish and Norwegian samples showed comparable IL-1β inhibition despite internal variation and both suppressed IL-1β more effectively than the Australian samples. Although Australian propolis has previously been reported to exert anti-inflammatory effects in vitro (Bhuyan et al., 2021), this study is, to our knowledge, the first to compare it directly with Scandinavian propolis. While the geographic distribution of samples was uneven, with Danish samples comprising the majority of the dataset (N = 38) compared to Australian and Norwegian samples (N = 7 each), group differences were assessed using one-way ANOVA with Tukey's post hoc test, which is robust to unequal group sizes.

The observed anti-inflammatory effect of propolis is likely to derive from modulation of NF-κB activation, which regulates pro-IL-1β transcription (Liu et al., 2017), or selective reduction of monocytes (Hougee et al., 2005), since monocytes are the primary IL-1β-producing cells in PBMC cultures (Hadadi et al., 2016); however, no mechanistic experiments were conducted to directly test these pathways, and these interpretations therefore remain hypothetical. Furthermore, the strong association between TCA and IL-1β initially suggested that the observed inhibition was dominated by overall extract load, consistent with a matrix-driven mechanism. However, following $\log_{10}$-transformation, this influence was greatly reduced, allowing compound-specific effects to emerge. Across the multivariate workflow, the chrysin-associated signal was the most consistently supported putative candidate for independent, compound-specific IL-1β suppression, being the only signal to combine a significant negative individual correlation, the highest selectivity ratio, first entry in FSS, and complete stability across all top AICc-ranked models. While the modest correlation coefficient and limited sample size preclude formal causal inference (Peters et al., 2016), the convergence of evidence across independent analytical approaches supports chrysin as a meaningful contributor beyond overall extract load rather than an incidental finding. Future studies with larger and more geographically diverse sample sets will be needed to establish the robustness of this association. It should be noted that although the HPLC method follows ISO 24381:2023, complete chromatographic

Table 2
Inhibition of IL-1β release by selected polyphenols (25 μg/mL) in peripheral blood mononuclear cells (PBMCs) stimulated with 6.25 ng/mL LPS. Values are expressed relative to LPS-stimulated controls (set to 100%) and shown as mean ± SD (n = 3) (**p < 0.01, ****p < 0.0001).

Compound	Caffeic acid	CAPE	Chrysin	p-Coumaric acid	Ferulic acid	Galangin
Relative IL-1β concentration (%), Mean ± SD	2.35 ± 0.50****	39.14 ± 3.83****	0.30 ± 0.72****	83.70 ± 3.29**	93.46 ± 3.77	75.19 ± 10.20****

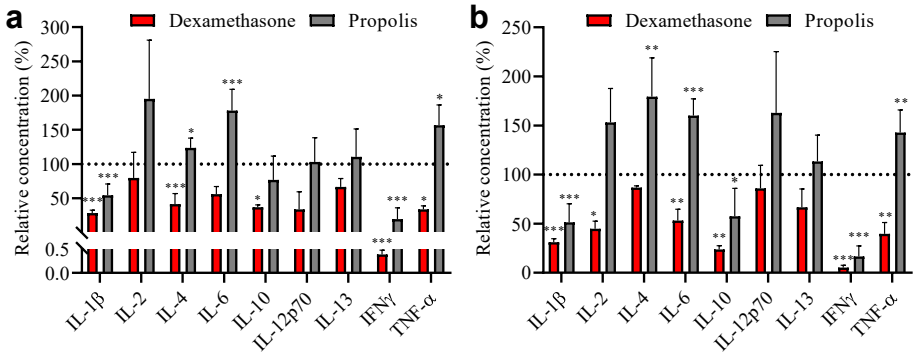

Fig. 6. Cytokine secretions from in PBMCs treated with propolis or dexamethasone following immune stimulation. PBMCs were stimulated with either (a) LPS or (b) PHA and treated with propolis (three randomly selected Danish samples, N = 3) or dexamethasone (N = 3). Cytokine concentrations are shown as percentages relative to the positive control (stimulated PBMCs without treatment; indicated by a dashed line at 100%). Bars represent mean ± SD. Statistical comparisons were performed between each experimental group and the positive control (*p < 0.05, **p < 0.01, ***p < 0.001).

separation cannot be guaranteed given the chemical complexity of the propolis matrix. Consequently, co-elution may contribute to peak areas attributed to individual polyphenols, and compound-specific associations should therefore be interpreted with caution. However, independent in vitro testing of selected polyphenols supported the chemometric findings, as chrysin exhibited the strongest IL-1β-reducing effect. These experiments were performed at uniform concentrations that do not reflect their abundance within the extract, but they nonetheless provide insight into relative potency. Considering the matrix-dependent nature of the overall response, the in vitro results cannot establish chrysin as the dominant mediator of propolis activity, although both modelling and functional assays suggest it to be an important contributor.

Cytokine profiling further demonstrated that propolis does not act as a broadly immunosuppressive agent. Unlike dexamethasone, which uniformly decreased all measured cytokines, propolis selectively increased or decreased specific cytokines. IL-1β, IL-10, and IFN-γ were significantly reduced, whereas TNF-α, IL-6, and IL-4 were increased. This pattern suggests that propolis primarily interferes with the inflammasome-dependent activation of IL-1β, while the upstream NF-κB-driven priming is not uniformly suppressed. This interpretation is consistent with the two-step mechanism of IL-1β production (Hadadi et al., 2016). Although TNF-α is often reported to decrease after propolis treatment, other studies have documented increased TLR4 expression and NF-κB activation (Conti et al., 2016), emphasizing the influence of chemical composition and experimental context. The consistent reduction of IFN-γ also suggests interference with Th1 polarisation, potentially through disruption of IL-12-dependent STAT4 signalling (Trinchieri, 2003), despite unchanged IL-12p70 levels.

Notably, the decrease in IL-10, an anti-inflammatory cytokine, was unexpected and may reflect broader modulation of regulatory immune responses, although the mechanism cannot be determined from the present data. Increased IL-4 and decreased IFN-γ suggest a potential shift toward Th2-associated signalling, while concurrent increases in TNF-α and IL-6 are consistent with intact or enhanced NF-κB-driven activity. However, definitive mechanistic conclusions regarding these patterns remain beyond the scope of the present study.

Taken together, these findings suggest that propolis exerts its effects through a combination of matrix-driven and compound-specific mechanisms. Chrysin represents a candidate marker of anti-inflammatory potency warranting further investigation. The cytokine data further indicate that propolis functions as a complex immunomodulator, selectively dampening some inflammatory pathways while enhancing others rather than acting as a broad immunosuppressant. However, as the cytokine profiling was based on a limited number of samples, these observations should be interpreted as preliminary. Future research incorporating larger and more chemically diverse samples, alongside mechanistic experiments and comprehensive LC-MS profiling, will be essential for clarifying causal relationships and establishing robust markers of activity to support consistent, reliable formulations.

CRediT authorship contribution statement

Magni Steintún: Writing – review & editing, Writing – original draft, Visualization, Validation, Resources, Project administration, Methodology, Investigation, Formal analysis, Data curation, Conceptualization. **Jonas Vind:** Writing – review & editing, Writing – original draft, Visualization, Resources, Methodology, Investigation, Formal analysis, Data curation, Conceptualization. **Camilla Hartmann Friis Hansen:** Writing – review & editing, Writing – original draft, Resources, Methodology, Investigation, Formal analysis, Conceptualization. **Jesper Larsen:** Writing – review & editing, Writing – original draft, Methodology, Investigation. **Lars Duelund:** Writing – review & editing, Writing – original draft, Methodology, Investigation. **Rime Bahij:** Writing – review & editing, Writing – original draft, Methodology, Investigation. **Henrik Munch Jørgensen:** Writing – review & editing, Writing – original draft, Methodology, Investigation, Conceptualization. **Julie Christine Antvorskov:** Writing – review & editing, Writing – original draft, Methodology, Investigation, Conceptualization. **Bo Markussen:** Writing – review & editing, Writing – original draft, Validation, Methodology, Investigation, Conceptualization. **Violetta Aru:** Writing – review & editing, Writing – original draft, Methodology, Investigation. **Søren Balling Engelsen:** Writing – review & editing, Writing – original draft, Methodology, Investigation. **Knud Josefsen:** Writing – review & editing, Writing – original draft, Validation, Supervision, Resources, Project administration, Methodology, Investigation, Funding acquisition, Formal analysis, Conceptualization.

Funding

This work was funded by the European Union and the Danish Agricultural Agency under the national implementation of the Apiculture Support Scheme 2023–2026.

Declaration of competing interest

The authors declare that they have no financial or personal conflicts of interest that could have affected the research reported in this paper.

Appendix A. Supplementary data

Supplementary data to this article can be found online at https://doi.org/10.1016/j.jep.2026.121867.

Data availability

Data will be made available on request.

References

Anjum, S.I., Ullah, A., Khan, K.A., Attaullah, M., Khan, H., Ali, H., Bashir, M.A., Tahir, M., Ansari, M.J., Ghramh, H.A., Adgaba, N., Dash, C.K., 2019. Composition and functional properties of propolis (bee glue): a review. Saudi J. Biol. Sci. 26, 1695–1703.

Bhuyan, D.J., Alsherbiny, M., Low, M., Zhou, X., Kaur, K., Li, G., Li, C.-G., 2021. Broad-spectrum pharmacological activity of Australian propolis and metabolomic-driven identification of marker metabolites of propolis samples from three continents. Food Funct.

Conti, B.J., Santiago, K.B., Cardoso, E.O., Freire, P.P., Carvalho, R.F., Golim, M.A., Sforcin, J.M., 2016. Propolis modulates miRNAs involved in TLR-4 pathway, NF-κB activation, cytokine production and in the bactericidal activity of human dendritic cells. J. Pharm. Pharmacol. 68, 1604–1612.

El Menyiy, N., Bakour, M., El Ghouizi, A., El Guendouz, S., Lyoussi, B., 2021. Influence of geographic origin and plant source on physicochemical properties, mineral content, and antioxidant and antibacterial activities of Moroccan propolis. International Journal of Food Science 2021, 5570224.

Hadadi, E., Zhang, B., Baidžajevas, K., Yusof, N., Puan, K.J., Ong, S.M., Yeap, W.H., Rotzschke, O., Kiss-Toth, E., Wilson, H., Wong, S.C., 2016. Differential IL-1β secretion by monocyte subsets is regulated by Hsp27 through modulating mRNA stability. Sci. Rep. 6, 39035.

Hossain, R., Quispe, C., Khan, R.A., Saikat, A.S.M., Ray, P., Ongalbek, D., Yeskaliyeva, B., Jain, D., Smeriglio, A., Trombetta, D., Kiani, R., Kobarfard, F., Mojgani, N., Saffarian, P., Ayatollahi, S.A., Sarkar, C., Islam, M.T., Keriman, D., Uçar, A., Martorell, M., Sureda, A., Pintus, G., Butnariu, M., Sharifi-Rad, J., Cho, W.C., 2022. Propolis: an update on its chemistry and pharmacological applications. Chin. Med. 17, 100.

Hougee, S., Sanders, A., Faber, J., Graus, Y.M., Van Den Berg, W.B., Garssen, J., Smit, H. F., Hoijer, M.A., 2005. Decreased pro-inflammatory cytokine production by LPS-stimulated PBMC upon in vitro incubation with the flavonoids apigenin, luteolin or chrysin, due to selective elimination of monocytes/macrophages. Biochem. Pharmacol. 69, 241–248.

Huang, S., Zhang, C.P., Wang, K., Li, G.Q., Hu, F.L., 2014. Recent advances in the chemical composition of propolis. Molecules 19, 19610–19632.

Kvalheim, O.M., 2010. Interpretation of partial least squares regression models by means of target projection and selectivity ratio plots. J. Chemometr. 24, 496–504.

Liu, T., Zhang, L., Joo, D., Sun, S.-C., 2017. NF-κB signaling in inflammation. Signal Transduct. Targeted Ther. 2, 17023.

López-Valverde, N., Pardal-Peláez, B., López-Valverde, A., Flores-Fraile, J., Herrero-Hernández, S., Macedo-De-Sousa, B., Herrero-Payo, J., Ramírez, J.M., 2021. Effectiveness of propolis in the treatment of periodontal disease: updated systematic review with meta-analysis. Antioxidants (Basel) 10.

Magnavacca, A., Sangiovanni, E., Racagni, G., Dell'agli, M., 2022. The antiviral and immunomodulatory activities of propolis: an update and future perspectives for respiratory diseases. Med. Res. Rev. 42, 897–945.

Martens, H.A., Dardenne, P., 1998. Validation and verification of regression in small data sets. Chemometr. Intell. Lab. Syst. 44, 99–121.

Norgaard, L., Saudland, A., Wagner, J., Nielsen, J.P., Munck, L., Engelsen, S.B., 2000. Interval partial least-squares regression (iPLS): a comparative chemometric study with an example from near-infrared spectroscopy. Appl. Spectrosc. 54, 413–419.

Ożarowski, M., Karpiński, T.M., 2023. The effects of propolis on viral respiratory diseases. Molecules 28.

Peters, J., Bühlmann, P., Meinshausen, N., 2016. Causal inference by using invariant prediction: identification and confidence intervals. J. Roy. Stat. Soc. B Stat. Methodol. 78, 947–1012.

Ramata-Stunda, A., Petriņa, Z., Valkovska, V., Borodušķis, M., Gibnere, L., Gurkovska, E., Nikolajeva, V., 2022. Synergistic effect of polyphenol-rich complex of plant and green propolis extracts with antibiotics against respiratory infections causing bacteria. Antibiotics (Basel) 11.

Rojczyk, E., Klama-Baryła, A., Łabuś, W., Wilemska-Kucharzewska, K., Kucharzewski, M., 2020. Historical and modern research on propolis and its application in wound healing and other fields of medicine and contributions by Polish studies. J. Ethnopharmacol. 262, 113159.

Savorani, F., Tomasi, G., Engelsen, S.B., 2010. Icoshift: a versatile tool for the rapid alignment of 1D NMR spectra. J. Magn. Reson. 202, 190–202.

Simone-Finstrom, M., Spivak, M., 2010. Propolis and bee health: the natural history and significance of resin use by honey bees. Apidologie 41, 295–311.

Tomasi, G., Savorani, F., Engelsen, S.B., 2011. Icoshift: an effective tool for the alignment of chromatographic data. J. Chromatogr. A 1218, 7832–7840.

Trinchieri, G., 2003. Interleukin-12 and the regulation of innate resistance and adaptive immunity. Nat. Rev. Immunol. 3, 133–146.

Vind, J.P., Aru, V., Jørgensen, H.M., Antvorskov, J.C., Tekin, H., Josefsen, K., Engelsen, S.B., 2026. Comparative spectroscopic analysis of bee propolis: NIR, FT-IR, FT-Raman and 1H NMR. Focus on provenance and antioxidative correlation. Pharmacological Research - Natural Products 10, 100578.

Vind, J., Engelsen, Søren b., Jørgensen, Henrik m., Antvorskov, Julie c., Josefsen, K., Aru, V., 2026. Comparative 1H NMR metabolomics between Scandinavian propolis and Australian propolis: the quest to identify radical scavenging compounds. Magn. Reson. Chem. 64, 438–450.

Wold, S., Martens, H., Wold, H. The multivariate calibration problem in chemistry solved by the PLS method. *In:* KÅGSTRÖM, B. & RUHE, A., eds. Matrix Pencils, 1983//1983 Berlin, Heidelberg. Springer Berlin Heidelberg, 286-293.

Zulhendri, F., Lesmana, R., Tandean, S., Christoper, A., Chandrasekaran, K., Irsyam, I., Suwantika, A.A., Abdulah, R., Wathoni, N., 2022. Recent update on the anti-inflammatory activities of propolis. Molecules 27.

Supplementary Table 1. LC-QTOF-MS (negative ionization mode) confirmation of benchmark polyphenols in a representative Danish propolis sample. RT, retention time; $[M-H]^-$, deprotonated molecular ion.

Compound	RT (min)	Theoretical $[M-H]^-$	Observed $[M-H]^-$	Mass error (ppm)
Caffeic acid	5.14	179.0350	179.0397	2.6
p-Coumaric acid	7.04	163.0401	163.0445	2.7
Ferulic acid	7.65	193.0506	193.0458	-2.5
Apigenin	18.45	269.0455	269.0527	2.7
Chrysin	32.99	253.0506	253.0581	3
Pinocembrin	35.75	255.0663	255.0719	2.2
Galangin	36.74	269.0455	269.0519	2.4
CAPE	39.56	283.0972	283.1050	2.8

Supplementary Table 2. Cell viability (%) of PBMCs following stimulation with LPS (6.25 µg/mL) in the presence of propolis or dexamethasone across a concentration range.

Concentration (µg/mL)	Propolis + LPS (%viable cells)	Dexamethasone + LPS (%viable cells)	LPS only (%viable cells)
400	99.1	54.8	-
100	93.2	72.2	-
25	87.2	74.4	-
6.25	79.5	70	70.25
1.56	95.8	75	-
0.39	89.2	85.1	-
0.098	84.6	71.8	-
0.024	89.2	65.7	-

Manuscript IV

Immunomodulatory Effects of Dietary Propolis in Autoimmune Diabetes: A Preclinical Study in NOD Mice

Jonas Vind[1], Camilla Hartmann Friis Hansen[2], Magni Steintún[1], Lukasz Krych[3], Henrik Munch Jørgensen[1], Julie Christine Antvorskov[4], Violetta Aru[3], Søren Balling Engelsen[3], Knud Josefsen[1].

Affiliations:

[1]Department of Pathology, The Bartholin Institute, Copenhagen University Hospital, Copenhagen, Denmark

[2]Department of Veterinary and Animal Sciences, University of Copenhagen, Ridebanevej 9, 1870 Frederiksberg C, Denmark

[3]Department of Food Science, University of Copenhagen, Rolighedsvej 26, 1958 Frederiksberg C, Denmark

[4]Department of Clinical Research, Steno Diabetes Center Copenhagen, Translational Type 1 Diabetes Research, Herlev, Denmark

Corresponding author:
Jonas Vind,
Bartholin Institute, Rigshospitalet,
Copenhagen Biocenter,
Ole Maaløes Vej 5, 2200 Copenhagen N, Denmark
E-mail: Jonas.Pordel.Vind@regionh.dk

Abstract

Background: Propolis is a honey bee derived bioactive with immunomodulatory properties. The influence of dietary propolis supplementation on autoimmune diabetes development in non-obese diabetic (NOD) mice was investigated.

Methods: Female NOD mice (n = 66) received standard chow or chow supplemented with 1.8% or 3.6% (w/w) raw propolis from 4-30 weeks of age. Diabetes incidence was monitored longitudinally. At 14 weeks, pancreatic insulitis, T cell subsets in pancreatic lymph nodes and spleen, serum cytokines, and gut microbiota composition were assessed.

Results: Propolis delayed diabetes onset, significantly reducing incidence at 17 weeks, although cumulative incidence converged by 30 weeks. High-dose propolis reduced pancreatic immune infiltration, decreased $CD4^+$ T helper cells in pancreatic lymph nodes, and increased total splenic T cells. Serum interleukin (IL)-4 decreased, whereas IL-10 and interferon-γ increased. *Akkermansia muciniphila* abundance was elevated.

Conclusion: Long-term dietary propolis modulates the immune-microbiota axis and transiently delays autoimmune diabetes onset, supporting its potential as a functional dietary immunomodulator.

Keywords: Propolis, Type 1 diabetes, Immunomodulation, NOD mouse, Gut microbiota

1 Background

Propolis is a resinous substance produced by honey bees, rich in polyphenols such as flavonoids and phenolic acids (Zhu et al., 2023), which contribute to its well-documented anti-inflammatory properties (Bhatti et al., 2024; Hossain et al., 2022). These effects have primarily been attributed to propolis' inhibition of nuclear factor kappa-light-chain-enhancer of activated B cells (NF-κB) (Búfalo et al., 2013), a central transcription factor involved in regulating immune and inflammatory gene expression (Liu, Zhang, Joo, & Sun, 2017). Polyphenols can interfere with NF-κB signaling at several levels, including inhibition of inhibitor of κB kinase activity, stabilization of inhibitor of κB alpha, and prevention of NF-κB nuclear translocation and DNA binding, thereby reducing the transcription of pro-inflammatory mediators (Yu, Wang, Yang, & Wang, 2022). Propolis flavonoids have also been demonstrated to cause decreased pro-inflammatory cytokine production through selective elimination of monocytes and macrophages (Hougee et al., 2005).

Interestingly, propolis may also exert immunostimulatory effects and has been reported to increase pro-inflammatory cytokine levels in mice (Rifa'i & Widodo, 2014; H. Zhu et al., 2024), suggesting that its immunological actions are context-dependent, and thus capable of both dampening excessive inflammation and enhancing immune responsiveness. While the immunosuppressive effects are linked to NF-κB inhibition, the immune-enhancing effects are thought to involve pattern recognition receptors, through the upregulation of Toll-like receptor 4 (TLR4), which is primarily expressed on cells of myeloid origin, including monocytes, macrophages, and dendritic cells (Orsatti & Sforcin, 2012; Vaure & Liu, 2014; H. Zhu et al., 2024). TLR4 activation triggers downstream NF-κB signaling, leading to the production of pro-inflammatory cytokines such as tumor necrosis factor (TNF)-α, interleukin (IL)-1β, IL-6, and IL-12p40 (Liu et al., 2017). Upon TLR4 activation, IL-12p40 combines with the p35 subunit of IL-12 to form the bioactive heterodimer IL-12p70 (Gilmour, Corthay, & Øynebråten, 2024). This cytokine promotes IFN-γ secretion by T cells and natural killer (NK) cells through activation of STAT4 (Wang, Ritz, & Frank, 1999), thereby supporting Th1 differentiation and activation. Thus, propolis may modulate immune responsiveness in both directions through the TLR4-NF-κB pathway, acting either suppressively or stimulatory depending on context. However, due to its complex and variable chemical composition (Šturm & Ulrih, 2020), delineating the precise cellular mechanisms remains challenging, and its dual immunomodulatory effects likely reflect this biochemical diversity.

Nonetheless, given these properties, propolis may hold therapeutic potential for autoimmune diseases such as type 1 diabetes (T1D), a chronic T cell-mediated condition characterized by the progressive inactivation and destruction of insulin-producing pancreatic β-cells (Burrack, Martinov, & Fife, 2017). This immune-driven β-cell loss results in insulin deficiency and necessitates lifelong exogenous insulin therapy. A characteristic feature of T1D is insulitis, defined as the infiltration of autoreactive immune cells into the islets of Langerhans (Pugliese, 2016). In humans, insulitis is observed primarily at or near disease onset, whereas it is more consistently present and progressive in animal models such as Non-Obese Diabetic (NOD) mice (In't Veld, 2014). This local immune response is typically accompanied by dysregulated cytokine signaling that promotes pro-inflammatory, Th1-skewed immune activity within the pancreas (Pilström, Björk, & Böhme, 1995).

The NOD mouse is a widely used and well-characterized preclinical model of spontaneous autoimmune diabetes. Female NOD mice develop disease in a manner that resembles human T1D, both immunologically and pathologically, whereas the male are more resistant to disease (Chen, Mathews, & Driver, 2018). Disease onset is marked by early lymphocytic infiltration of the pancreatic islets, followed by gradual β-cell destruction and eventual hyperglycemia (Chen et al., 2018). Given these parallels, the NOD mouse provides a robust and relevant system for exploring the immunopathogenesis of autoimmune diabetes and assessing the therapeutic potential of immunomodulatory interventions such as propolis.

In this study, it is investigated whether dietary administration of propolis modulates immune responses and alters the progression of autoimmune diabetes in female NOD mice. Specifically, immune infiltration in pancreatic islets, systemic cytokine profiles, and T cell subset distribution in lymphoid organs are evaluated. To our knowledge, this is the first study to evaluate the immunological and disease-modifying effects of propolis in the NOD mouse model.

2 Methods

2.1 Collection of Propolis

Raw propolis was obtained from two Danish organic beekeepers located in North Jutland and North Zealand. Propolis from these beekeepers has been evaluated in previous studies (J. Vind et al., 2026; J. P. Vind et al., 2026). To ensure sample freshness, propolis was harvested within the same year the study started. Upon receipt, the raw propolis was promptly shipped for incorporation into the mice diets.

2.2 Study design

2.2.1 Housing and assignment to experimental groups

Sixty-six female NOD mice were housed in a rodent barrier facility at the Department of Veterinary and Animal Sciences, University of Copenhagen, with the sample size determined based on feasibility and ethical considerations for this exploratory study. The environment was maintained at a temperature of 20-24 °C with a relative humidity of 55 % ± 10 %, and a 12-hour light-dark cycle (lights on from 6 a.m. to 6 p.m.). Mice were kept in open cages with a maximum of six animals per cage (grouped as 6, 5, and 5 animals per cage, respectively). Housing and health monitoring followed the guidelines of the Federation of European Laboratory Animal Science Associations (FELASA) (Nicklas et al., 2010). The mice were four weeks old upon arrival. Immediately after arrival, mice were randomly assigned to three dietary groups (n = 22 per group). The control group received standard Altromin 1324 pellets, while the low-dose and high-dose groups received modified Altromin 1324 pellets containing 1.8% and 3.6% (w/w) raw propolis, respectively. All diets were prepared by Brogaarden (Lage, Germany). At the start of the dietary intervention, six mice from each group were randomly selected for sacrifice at 14 weeks of age to assess early diabetes progression. These animals were housed separately in cages of three per group prior to sacrifice. This time point was selected to capture the prediabetic stage, as NOD mice are typically in the early phases of autoimmune development at this age, but with immune infiltrations in most islets (Chen et al., 2018). The pancreas was harvested for histological evaluation of insulitis, while the spleen and pancreatic lymph nodes (PLNs) were collected for analysis of T cell subsets distribution. Blood samples were obtained via retro-orbital sinus puncture under anesthesia for cytokine profiling. Feces were also collected for gut microbiota analysis. All samples were immediately placed on ice. One mouse in the high-dose group was diagnosed with diabetes on the day of sacrifice and was therefore excluded from data analysis.

However, its fecal sample was retained for gut microbiota analysis, as this outcome was assessed independently of immunological status. A timeline of the experimental design is presented in Fig. 1.

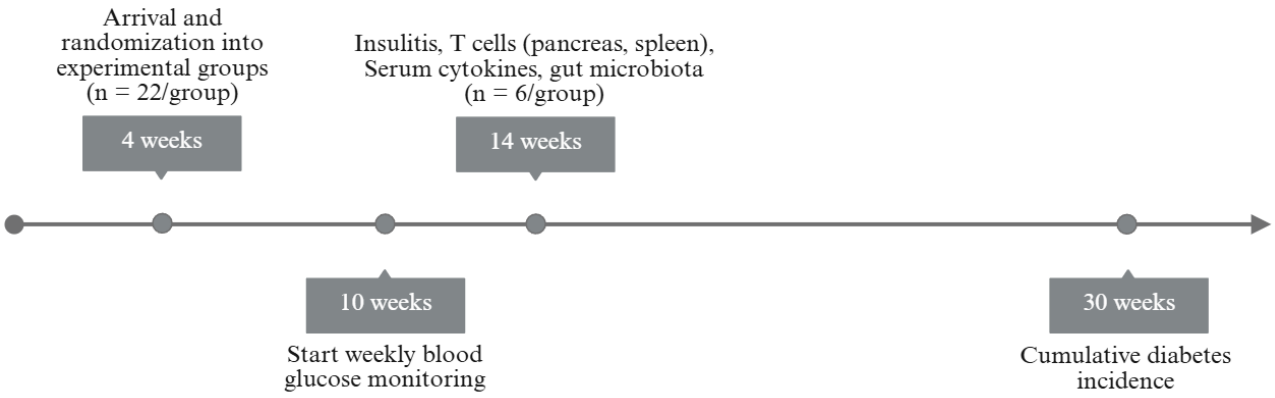

Fig. 1 Timeline of experimental design. Female NOD mice were randomized into dietary groups at 4 weeks of age (n = 22 per group). From 10 weeks of age, diabetes monitoring was initiated, and at 14 weeks of age, six mice per group were sacrificed for immunological and microbiota analyses. Cumulative diabetes incidence was recorded up to 30 weeks of age.

2.2.2 Diabetes onset monitoring

Diabetes monitoring of the remaining mice (n=16 per group) began when the mice reached 10 weeks of age, with blood glucose levels measured weekly by tail vein puncture using a handheld glucometer. If a mouse exhibited blood glucose levels exceeding 12.0 mmol/L, a confirmatory measurement was taken the following day. Mice with confirmed hyperglycemia (>12.0 mmol/L on two consecutive days) were classified as diabetic and euthanized. Monitoring continued until 30 weeks of age. To ensure nutritional adequacy, feed and water intake were recorded weekly on a per-cage basis from 11 to 14 weeks of age.

2.3 Histological Assessment of Insulitis

Insulitis was assessed on twenty islets per 14-week-old mouse from hematoxylin and eosin (H&E)-stained pancreatic sections (5 μm thick), cut at 100 μm intervals. Islets were classified based on the degree of immune cell infiltration into the following categories: no insulitis, peri-insulitis, mild insulitis (<25% infiltration), moderate insulitis (25-75% infiltration), and severe insulitis (>75% infiltration or complete islet destruction). An insulitis index was then calculated for each mouse by assigning numerical values to these categories (from 0 for no insulitis to 4 for severe insulitis) and

averaging the scores across the 20 islets, providing a single quantitative measure of insulitis severity. Scoring was performed blindly, and islets were evaluated in random order.

2.4 Cell Isolation and Flow Cytometry Analysis

Single-cell suspensions were prepared from spleen and PLNs by mechanically dissociating freshly isolated organs through a 100 μm nylon mesh into cold PBS. Cells were then washed and resuspended in PBS with 1% FC-block CD16/CD32 (eBioscience, San Diego, USA).

For flow cytometric analysis, cells were stained with fluorophore-conjugated antibodies targeting surface and intracellular markers according to the manufacturer's instructions (eBioscience,). T cells were defined as $CD3^+CD45^+$, helper T cells (Th) as $CD3^+CD4^+$, and regulatory T cells (Tregs) as $CD3^+CD4^+FoxP3^+$. The following antibodies were used: CD3-FITC, CD4-PerCP-Cy5.5, FoxP3-PE, CD45-APC. Intracellular FoxP3 staining was performed following fixation and permeabilization as per the manufacturer's protocol (eBioscience).

Samples were acquired using an Accuri C6 flow cytometer (BD Biosciences, Franklin Lakes, NJ, USA), and data were analyzed in the BD Accuri C6 software to determine the percentage of T cell subsets per organ. The total number cells were counted using the TC20 Automated Cell Counter (Bio-Rad, Hercules, CA, USA).

2.5 Cytokine Measurement

Serum levels of IFN-γ, IL-1β, IL-2, IL-4, IL-5, IL-6, C-X-C motif ligand 1 (CXCL1), IL-10, IL-12p70, and TNF-α were measured using the V-PLEX Proinflammatory Panel 1 Mouse Kit (Meso Scale Diagnostics, Rockville, MD, USA) on a MESO QuickPlex SQ 120MM platform and analyzed using Discovery Workbench software (MSD).

2.6 Gut microbiota analysis

Genomic DNA was extracted from fecal samples using the DNeasy PowerSoil Pro Kit (Qiagen, Venlo, The Netherlands) on a QIAcube automated platform, following mechanical lysis with a TissueLyser II. All procedures were carried out according to the manufacturer's protocols. The DNA library was prepared using a custom protocol involving two PCR steps for the amplification of near full-length 16S rRNA genes. The pooled library was sequenced on a PromethION 2 Solo platform (Oxford Nanopore Technologies, Oxford, UK) using an R10.4.1 flow cell.

Sequencing data were collected and basecalled in super-accurate mode using the MinKNOW GUI (version 24.06.10; Oxford Nanopore Technologies, Oxford, UK). Raw data processing, including filtering, trimming, and taxonomic assignment, was performed using the LACA pipeline (Hui, Sandris Nielsen, & Krych, 2025). The resulting feature table was further analyzed using QIIME2 (Bolyen et al., 2019). Beta diversity was assessed using Bray-Curtis and Jaccard distance metrics, calculated from rarefied feature tables (20,000 reads per sample). Differences in beta diversity were tested using Permutational Multivariate Analysis of Variance (PERMANOVA). The differences in bacterial relative distribution was evaluated using Analysis of Compositions of Microbiomes (Lin & Peddada, 2020) implemented in QIIME2.

2.7 Statistical Analysis

GraphPad Prism version 8 (GraphPad Software, San Diego, CA, USA) and MATLAB version R2023b (MathWorks Inc., Natick, MA, USA) were used for statistical analyses. A p-value < 0.05 was considered statistically significant.

Cumulative diabetes incidence curves were analyzed using the Kaplan-Meier method, and group differences were assessed using the log-rank test for trend. Insulitis scores were compared across groups using the χ^2 test, with pairwise comparisons between individual score categories performed using Fisher's exact test. Holm correction was applied to adjust for multiple testing.

Differences in T cell subset distributions, serum cytokine concentrations and insulitis indexes were analyzed using either one-way ANOVA for normally distributed data or the Kruskal-Wallis test for non-normally distributed data. Normality was assessed using the Shapiro-Wilk test. For multiple comparisons following ANOVA, Tukey's test was applied; in cases of unequal variances, the Brown-Forsythe test was used. For post hoc comparisons following the Kruskal-Wallis test, Dunn's test was employed.

2.8 Ethical Approval

The experiment complied with the Danish Act on Animal Experimentation which implements the Directive 2010/63/EU on the Protection of Animals used for Scientific Purposes. It was approved by the Danish Animal Experiments Inspectorate at Ministry of Food, Agriculture, and Fisheries of Denmark (License number: 2021-15-0201-00847).

2.9 Data and Resource Availability

All datasets and critical resources generated and/or analyzed during the current study are available from the corresponding author upon reasonable request.

3 Results

3.1 Perorally administered propolis delays diabetes onset in NOD mice

To investigate the effect of perorally administered propolis on the development of autoimmune diabetes, female NOD mice were fed either standard chow (control) or chow supplemented with a low (1.8% w/w) or high (3.6% w/w) dose of propolis starting at 4 weeks of age. Cumulative diabetes incidence was monitored until 30 weeks and is presented in Fig. 2a.

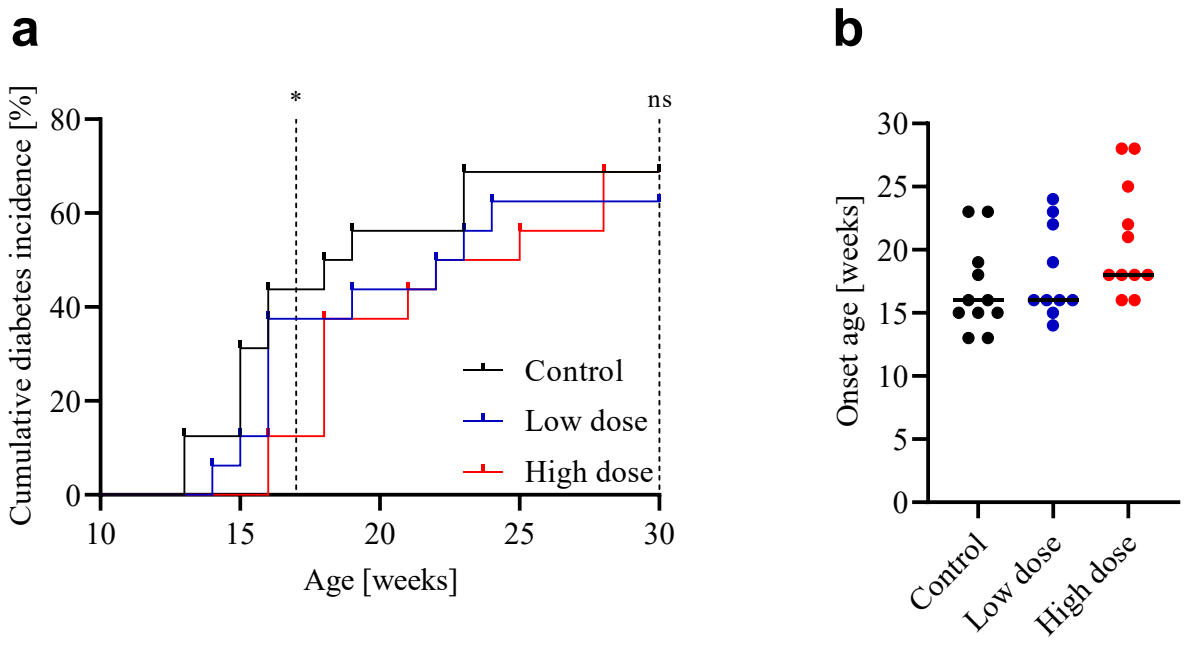

Fig. 2 (a) Cumulative diabetes incidence in female Non-Obese Diabetic (NOD) mice. Diabetes incidence was monitored over time. Groups were compared using the log-rank test for trend. Statistical significance was last observed at 17 weeks of age, with no differences at the study endpoint (30 weeks). Statistically significant pairwise comparisons are shown. $p < 0.05$*, *ns*: not significant. (b) Age of diabetes onset in NOD mice. Lines indicate the median onset age for each group.

The earliest onset of diabetes was observed in the control group (13 weeks), with slightly later onsets in the low-dose (14 weeks) and high-dose (16 weeks) groups. At 17 weeks, a log-rank test for trend indicated a statistically significant difference in diabetes onset across treatment groups, with more incidents observed in the control (n = 7) and low-dose (n = 6) groups compared to the high-dose group (n = 2). The control group reached a cumulative diabetes incidence of 50% at 18 weeks of age, whereas the low and high-dose groups reached this threshold at 22 weeks. However, by the end of the study, cumulative diabetes incidence was similar across all groups.

Fig. 2b shows the onset age of diabetes for each mouse. While the onset age was not statistically different between the groups, the median age of onset was higher in the high-dose group (18 weeks), relative to the control and low-dose groups (16 weeks).

3.2 Higher dose of propolis reduced immune infiltrations of islets of Langerhans

To examine the protective effects of propolis on immune infiltration in the pancreatic islets of Langerhans, insulitis was assessed in H&E-stained pancreatic sections from NOD mice at 1 weeks of age. Each islet was scored on a 5-point scale ranging from no infiltration to severe insulitis (>75% infiltration or complete islet destruction).

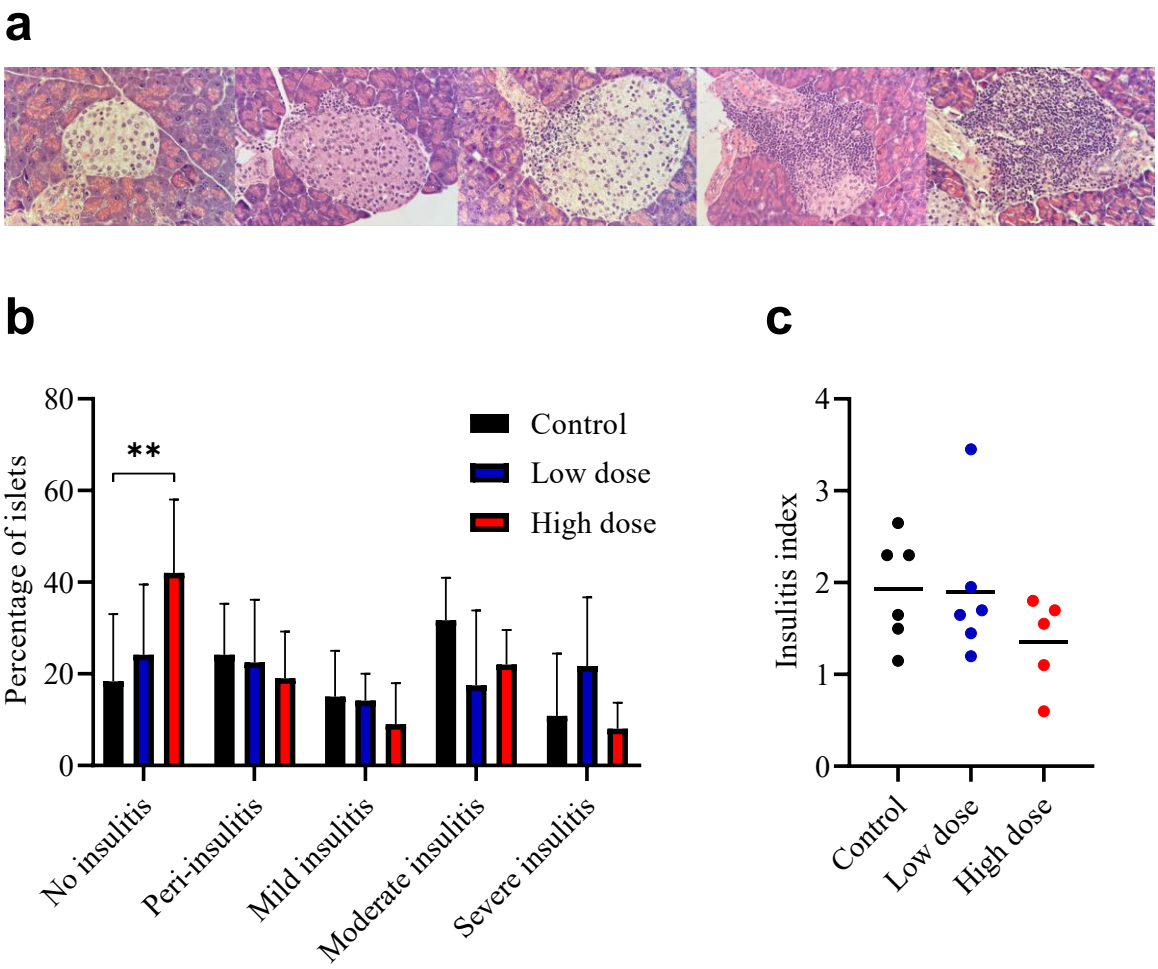

Fig. 3 Insulitis scoring in pancreatic islets of female non-obese diabetic (NOD) mice. Insulitis was assessed in hematoxylin and eosin (H&E)-stained pancreatic sections from NOD mice in the control, low-dose, and high-dose propolis groups at 14 weeks of age (n = 5 or 6 per group). Each islet was graded on a 5-point scale according to the extent of immune cell infiltration: no insulitis, peri-insulitis, mild insulitis (<25% infiltration),

moderate insulitis (25-75% infiltration), or severe insulitis (>75% infiltration or complete islet destruction). (a) Representative images illustrating increasing insulitis severity from left to right. (b) Percentage of islets exhibiting each insulitis grade in the different treatment groups. Bars indicate mean ± SD. (c) Insulitis index calculated for each mouse, with lines indicating group means. Statistically significant differences are indicated in the figure. Statistically significant pairwise comparisons are shown; lines indicate group means. $p < 0.01$**.

Representative images of each insulitis score are shown in Fig. 3a, and the distribution of insulitis scores is presented in Fig. 3b. In the control group, 17.5% of islets showed no infiltration, while approximately 43% exhibited moderate or severe insulitis. In contrast, 43.0% of islets in the high-dose group demonstrated no insulitis, and only 29% were scored as moderate or severe. The low-dose group displayed a relatively even distribution across all scoring categories. A χ^2 test confirmed a significant difference in the overall distribution of insulitis scores between groups ($p = 0.001$). Subsequent pairwise comparisons revealed that the proportion of islets without insulitis was significantly higher in the high-dose group compared to the control group ($p < 0.01$). To better illustrate the insulitis status of each mouse, an insulitis index was calculated (Fig. 3c). Although no statistically significant differences were observed between the experimental groups, the high-dose group displayed a lower mean insulitis index (1.35) compared to the control (1.93) and low-dose (1.90) groups. It is worth noting that one mouse in the low-dose group exhibited a markedly higher insulitis index than the other individuals in this group.

These findings suggest that propolis may reduce immune infiltration in pancreatic islets during the prediabetic stage.

3.3 Propolis affects the distribution of T cell subsets in the pancreatic lymph nodes and spleen

To investigate whether propolis supplementation influences immune cell composition, T cell subsets were quantified in the pancreatic lymph nodes and spleens of female NOD mice at 1 weeks of age. Single-cell suspensions were analyzed by flow cytometry, and the total number of T cells, $CD4^+$ T helper cells, and $CD4^+Foxp3^+$ regulatory T cells were measured.

In the pancreatic lymph nodes (Fig. 4a-c), a trend toward decreasing cell counts across all T cell subsets was observed with increasing propolis dose. In contrast, an opposite pattern emerged in the spleen (Fig. 4d-f), where higher propolis doses appeared to elevate T cell subset counts. Substantial intragroup variability was noted for all T cell subsets examined.

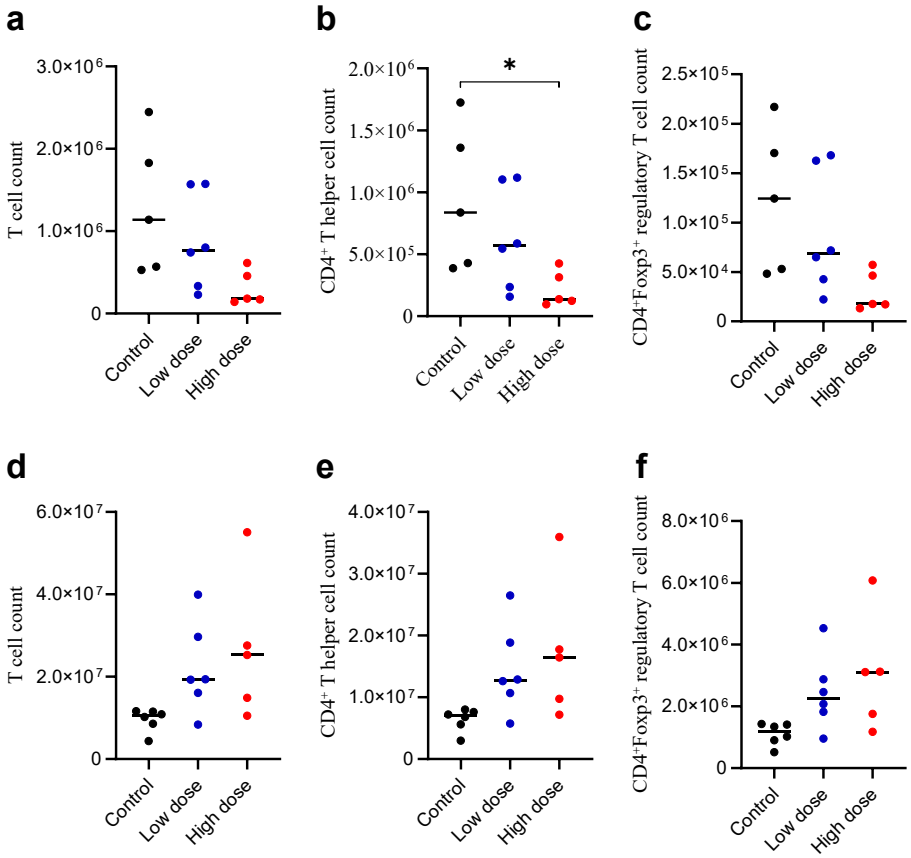

Fig. 4 T cell subset counts in pancreatic lymph nodes and spleen from female NOD mice in the control, low-dose, and high-dose propolis groups at 1 weeks of age (n = 5 or 6 per group). Total T cell counts (a), $CD4^+$ T helper cells (b), and $CD4^+Foxp3^+$ regulatory T cells (c) in the pancreatic lymph nodes. (d-f) The same T cell subsets measured in the spleen. Statistically significant pairwise comparisons are shown; lines indicate group means. $p < 0.05$*.

Among all T cell subsets analyzed in both the pancreatic lymph nodes and spleen, only the lymphatic $CD4^+$ T helper cells demonstrated statistically significant differences between experimental groups ($p < 0.05$). Post hoc pairwise analysis further revealed that this difference was attributable to a significant reduction in $CD4^+$ T helper cell counts between the control and high-dose groups ($p < 0.05$). Notably, although absolute numbers of T cell subsets were altered, no significant differences were found in their relative distributions

These findings suggest that propolis may modulate local T cell populations in the pancreatic draining lymph nodes during the prediabetic stage.

3.4 Propolis influences serum cytokines

To assess systemic immune signaling, cytokine concentrations were measured in serum from female NOD mice at 14 weeks of age. Serum levels of IL-1β, IL-4, IL-6, IL-10, IFN-γ, and TNF-α are shown in Fig. 5(a-f).

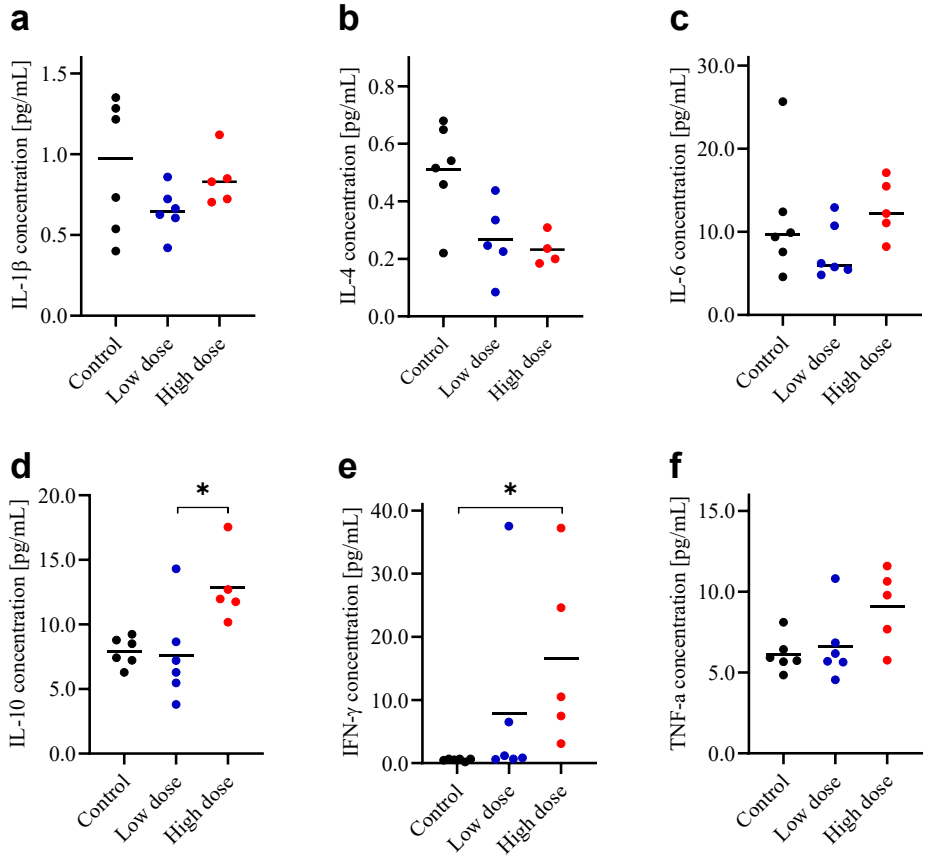

Fig. 5 Serum concentrations of IL-1β (a), IL-4 (b), IL-6 (c), IL-10 (d), IFN-γ (e), and TNF-α (f) in NOD mice in the control, low-dose, and high-dose propolis groups at 14 weeks of age (n=5 or 6 per group). Statistically significant pairwise comparisons are shown; lines indicate group means. $p < 0.05$*.

Significant group-level differences were detected for IL-4, IL-10, and IFN-γ ($p < 0.05$). Although IL-4 levels differed across groups in the global test, no pairwise comparison reached significance after post-hoc testing, and the apparent reduction in the high-dose group should therefore be considered a non-significant trend. By contrast, IL-10 concentrations were significantly elevated in the high-dose group compared to the low-dose group, and IFN-γ levels were significantly higher in the high-dose group than in controls.

Serum IL-1β, IL-6, and TNF-α did not differ significantly between groups, although TNF-α levels appeared slightly higher in the high-dose group without reaching statistical significance.

These findings suggest that propolis modulates systemic cytokine responses in NOD mice by enhancing Th1-type activity accompanied by increased IL-10-mediated regulatory signaling, while exerting minimal effects on classical pro-inflammatory cytokines such as TNF-α, IL-1β, and IL-6.

3.5 Propolis changes the microbiomics of NOD mice

Beta diversity analysis, based on weighted (Bray-Curtis) and unweighted (Jaccard) distance matrices, revealed significant differences among all tested groups (Fig. 6a,b), suggesting both qualitative and quantitative alterations in gut microbial composition between the high-dose, low-dose, and control groups.

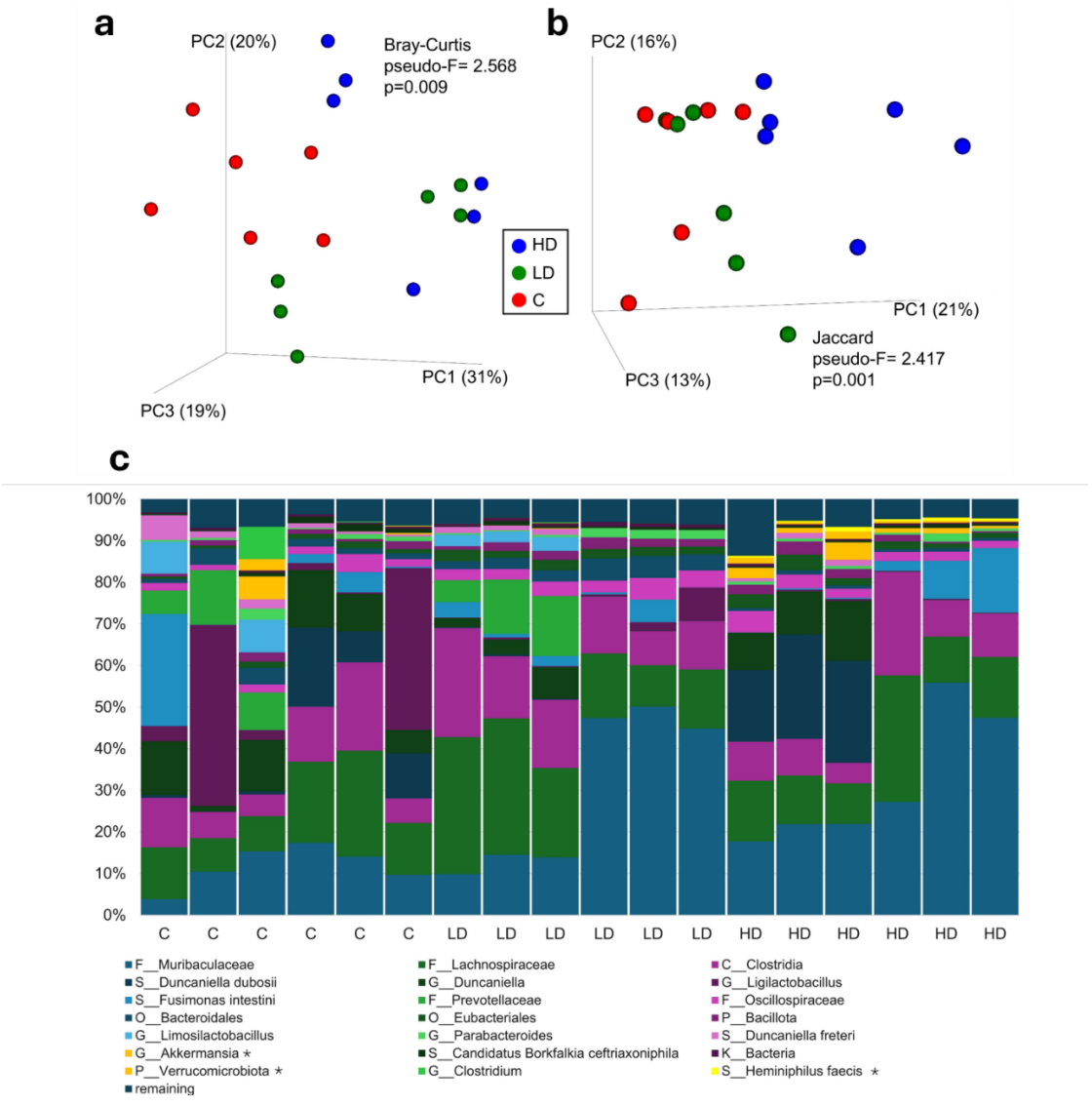

Fig. 6 Gut microbiota composition in female non-obese diabetic (NOD) mice following propolis administration. (a) Principal coordinates analysis (PCoA) based on Bray-Curtis dissimilarity, with each point representing an individual mouse colored by treatment group. (b) PCoA based on the Jaccard index. (c) Stacked bar plot showing the relative abundances of bacterial taxa in fecal samples from control (C), low-dose propolis (LD), and high-dose propolis (HD) groups at 1 weeks of age. Each bar represents an individual mouse, and taxa are colored by family, genus, or species as indicated in the legend.

Further examination using ANCOM identified *Akkermansia muciniphila* and *Heminiphilus faecis* as significantly enriched in the high-dose propolis group compared to the control group (Fig. 6c). Moreover, although not reaching statistical significance, the family Muribaculaceae exhibited a trend toward increased relative abundance in both treatment groups, with some individual mice showing levels approaching 50%.

Collectively, these data indicate that oral administration of propolis modulates gut microbiota composition in NOD mice.

4 Discussion

The purpose of this study was to investigate the effect of dietary propolis on the development of autoimmune diabetes in NOD mice. The findings suggest that propolis exerts a dual immunomodulatory effect, influencing both the activation and regulation of immune responses. Although the final cumulative diabetes incidence was not altered, diabetes onset was delayed in both the low and high-dose groups, with the most pronounced effect observed in the high-dose group. This delay may reflect immunological modulation during the prediabetic phase. Supporting this interpretation, reduced immune infiltration in the islets of Langerhans, altered distribution of T cells between immune compartments, significant changes in systemic cytokine levels, and changes in the gut microbiota were observed.

The cytokine profile in the high-dose group, characterized by increased IFN-γ and IL-10 together with a non-significant trend toward reduced IL-4, suggests a shift toward a Th1-skewed immune response with accompanying regulatory mechanisms. Although IFN-γ is classically pro-inflammatory, the concomitant increase in IL-10 suggests that propolis treatment counterbalances this activity, resulting in reduced islet infiltration and limiting tissue injury. Interestingly, IL-10 was significantly elevated in the high-dose group compared to the low-dose group, whereas the difference between high-dose and control groups did not reach significance, likely reflecting variability rather than a true absence of effect. However, substantial intragroup variability was present, particularly in IFN-γ levels within the low- and high-dose groups, which may reflect individual differences in responsiveness to propolis.

Mechanistically, the observed cytokine profile is consistent with partial activation of the TLR4-NF-κB signaling pathway, which drives IL-12p40 production. IL-12p40 can heterodimerize with the p35 subunit to form bioactive IL-12 (IL-12p70), a key cytokine promoting the differentiation of naïve $CD4^+$ T cells into IFN-γ-producing Th1 cells and enhancing IFN-γ secretion NK cells. Elevated IFN-γ levels in the high-dose group may therefore reflect IL-12-mediated activation of both Th1 and NK cell responses. Direct quantification of IL-12p70 was not feasible, as this heterodimer is typically expressed at very low levels under non-stimulated conditions and often falls below the detection limit of multiplex cytokine assays. TNF-α levels showed a modest, non-significant increase in the high-dose group, which may indicate partial engagement of TLR4-NF-κB signaling without triggering broad inflammatory cascades. The absence of increases in IL-1β and IL-6, together with the known

NF-κB-inhibitory activity of several propolis constituents, further suggests that propolis induces a selective rather than generalized immune activation.

Flow cytometric analysis provided further insights into the immune-modulatory effects of propolis. In the high-dose group, T cell numbers were reduced in the pancreatic lymph nodes but increased in the spleen. Because pancreatic lymph nodes drain the pancreas, lower T cell numbers in this compartment likely reflect reduced immune activity in pancreatic tissue rather than altered trafficking. This interpretation aligns with the attenuated insulitis observed in high-dose propolis-treated mice. The presence of systemic Th1 polarization, without excessive local immune activation, suggests that propolis fosters a functional yet non-pathogenic immune profile. This kind of immune regulation is particularly relevant in T1D, where maintaining immune vigilance without exacerbating autoimmunity is a key therapeutic goal. However, notable intragroup variability was observed in T cell counts across all subsets and tissues. The only significant difference detected in post hoc analysis was a reduction in $CD4^+$ T helper cells in pancreatic lymph nodes of the high-dose group compared with controls. This highlights the variability of the immune response to propolis and calls for caution in interpretation. Although absolute numbers of T cell subsets were altered, their relative distributions did not differ significantly, suggesting that propolis does not strongly influence T cell differentiation but rather modulates immune responses through changes in the activity or localization of existing cell populations.

These findings are consistent with previous studies. Zhu et al. demonstrated that supercritical CO_2-extracted propolis activates the TLR4-NF-κB signaling cascade and enhances pro-inflammatory cytokine production in immunosuppressed mice (H. Zhu et al., 2024). Orsatti and Sforcin also found that propolis upregulates TLR4 expression in spleen cells and can protect against stress-induced immunosuppression (Orsatti & Sforcin, 2012). Sy et al. likewise demonstrated that oral propolis administration increased IFN-γ secretion and promoted a Th1-skewed response in an OVA-sensitized asthma model, thereby ameliorating asthma and supporting its role in enhancing cell-mediated immunity (Sy, Wu, Chiang, Wang, & Wu, 2006). Together, these findings support the notion that propolis activates Th1-associated pathways, likely involving TLR4 and IL-12, without promoting harmful inflammation under steady-state or prediabetic conditions.

In addition to the observed immunological changes, analysis of fecal samples indicated that propolis administration was associated with alterations in gut microbiota composition. Although the functional significance of these shifts remains to be determined, it is plausible that modulation of the gut

microbial environment contributes to the observed immunomodulatory effects of propolis. Previous studies in NOD mice have demonstrated that manipulating gut microbiota can influence autoimmune diabetes development. Hansen et al. reported that early-life vancomycin treatment markedly altered the microbiota, leading to an expansion of *Akkermansia muciniphila*and a reduced incidence of diabetes (Hansen et al., 2012). Likewise, Hänninen et al. found that direct administration of *A. muciniphila* altered microbial composition, enhanced mucus production, modulated innate immune signaling, and delayed diabetes onset (Hänninen et al., 2018). Notably, *Heminiphilus faecis*, a recently described member of the *Muribaculaceae* family, was also significantly enriched in the high-dose propolis group, whereas the *Muribaculaceae* family as a whole showed a non-significant trend toward increased abundance in propolis-treated groups. While *H. faecis* has not previously been linked to T1D, members of the *Muribaculaceae* have been associated with gut-restorative effects in metabolic disease models (Y. Zhu et al., 2024).

These findings support the view that changes in gut microbial communities may play a complementary role in shaping systemic immune responses, offering a potential additional mechanism by which propolis affects autoimmune diabetes.

To our knowledge, this is the first study to evaluate the immunological and disease-modifying effects of propolis in the NOD mouse model. The findings provide new insights into how complex bioactive mixtures such as propolis can shape systemic and tissue-specific immune responses in autoimmunity, as well as influence the gut microbiome. Future work should delineate the underlying cellular and molecular mechanisms, with particular attention to antigen-presenting cells, TLR signaling, and cell trafficking. It will also be important to assess whether propolis can be combined with other immunomodulatory interventions to enhance prophylactic strategies for T1D.

5 Conclusion

In conclusion, dietary supplementation with propolis delayed the onset of autoimmune diabetes in female NOD mice without affecting the final cumulative disease incidence. This delay was accompanied by reduced immune infiltration of pancreatic islets, modulation of T cell distribution between pancreatic lymph nodes and spleen, and alterations in systemic cytokine profiles characterized by increased IFN-γ and IL-10 levels in the high-dose group. In addition, dietary propolis intake was associated with significant shifts in gut microbiota composition, including enrichment of *Akkermansia muciniphila* and *Heminiphilus faecis*, suggesting that modulation of the intestinal microbial environment may contribute to the observed immunological effects.

Collectively, these findings demonstrate that propolis, when administered as a dietary component, exerts dose-dependent immunomodulatory effects during the prediabetic stage. The data support the concept that bioactive constituents in propolis can influence systemic immune responses and gut microbiota composition in a manner consistent with functional food-mediated immune modulation. Further research is needed to elucidate the underlying molecular mechanisms and to determine the translational relevance of dietary propolis supplementation in the context of autoimmune disease

6 Declarations

6.1 Conflicts of Interest

None to be declared.

6.2 Acknowledgements

This work was funded by the European Union and the Danish Agricultural Agency under the national implementation of the Apiculture Support Scheme 2023-2026.

6.3 Author Contributions

J.P.V. and K.J. generated data, performed data analysis, and contributed to study design. C.H.F.H., M.S., and L.K. contributed to data collection and/or data analysis. J.P.V., K.J., C.H.F.H., M.S., L.K., H.M.J., J.C.A., S.B.E., and V.A. contributed to study design and interpretation. J.P.V. wrote the first draft of the manuscript. All authors reviewed and edited the manuscript and approved the final version. J.P.V. is the guarantor of this work and, as such, had full access to all the data in the study and takes responsibility for the integrity of the data and the accuracy of the data analysis.

7 References

Bhatti, N., Hajam, Y. A., Mushtaq, S., Kaur, L., Kumar, R., & Rai, S. (2024). A review on dynamic pharmacological potency and multifaceted biological activities of propolis. *Discover Sustainability, 5*(1), 185. doi: 10.1007/s43621-024-00375-3

Bolyen, E., Rideout, J. R., Dillon, M. R., Bokulich, N. A., Abnet, C. C., Al-Ghalith, G. A., . . . Caporaso, J. G. (2019). Reproducible, interactive, scalable and extensible microbiome data science using QIIME 2. *Nat Biotechnol, 37*(8), 852-857. doi: 10.1038/s41587-019-0209-9

Búfalo, M. C., Ferreira, I., Costa, G., Francisco, V., Liberal, J., Cruz, M. T., . . . Sforcin, J. M. (2013). Propolis and its constituent caffeic acid suppress LPS-stimulated pro-inflammatory response by blocking NF-κB and MAPK activation in macrophages. *J Ethnopharmacol, 149*(1), 84-92. doi: 10.1016/j.jep.2013.06.004

Burrack, A. L., Martinov, T., & Fife, B. T. (2017). T Cell-Mediated Beta Cell Destruction: Autoimmunity and Alloimmunity in the Context of Type 1 Diabetes. [Review]. *Frontiers in Endocrinology, Volume 8 - 2017*. doi: 10.3389/fendo.2017.00343

Chen, Y. G., Mathews, C. E., & Driver, J. P. (2018). The Role of NOD Mice in Type 1 Diabetes Research: Lessons from the Past and Recommendations for the Future. *Front Endocrinol (Lausanne), 9*, 51. doi: 10.3389/fendo.2018.00051

Gilmour, B. C., Corthay, A., & Øynebråten, I. (2024). High production of IL-12 by human dendritic cells stimulated with combinations of pattern-recognition receptor agonists. *npj Vaccines, 9*(1), 83. doi: 10.1038/s41541-024-00869-1

Hänninen, A., Toivonen, R., Pöysti, S., Belzer, C., Plovier, H., Ouwerkerk, J. P., . . . De Vos, W. M. (2018). Akkermansia muciniphila induces gut microbiota remodelling and controls islet autoimmunity in NOD mice. *Gut, 67*(8), 1445-1453. doi: 10.1136/gutjnl-2017-314508

Hansen, C. H., Krych, L., Nielsen, D. S., Vogensen, F. K., Hansen, L. H., Sørensen, S. J., . . . Hansen, A. K. (2012). Early life treatment with vancomycin propagates Akkermansia muciniphila and reduces diabetes incidence in the NOD mouse. *Diabetologia, 55*(8), 2285-2294. doi: 10.1007/s00125-012-2564-7

Hossain, R., Quispe, C., Khan, R. A., Saikat, A. S. M., Ray, P., Ongalbek, D., . . . Cho, W. C. (2022). Propolis: An update on its chemistry and pharmacological applications. *Chinese Medicine, 17*(1), 100. doi: 10.1186/s13020-022-00651-2

Hougee, S., Sanders, A., Faber, J., Graus, Y. M., van den Berg, W. B., Garssen, J., . . . Hoijer, M. A. (2005). Decreased pro-inflammatory cytokine production by LPS-stimulated PBMC upon in vitro incubation with the flavonoids apigenin, luteolin or chrysin, due to selective elimination of monocytes/macrophages. *Biochem Pharmacol, 69*(2), 241-248. doi: 10.1016/j.bcp.2004.10.002

Hui, Y., Sandris Nielsen, D., & Krych, L. (2025). De novo clustering of long-read amplicons improves phylogenetic insight into microbiome data. *Gut Microbes, 17*(1), 2516703. doi: 10.1080/19490976.2025.2516703

In't Veld, P. (2014). Insulitis in human type 1 diabetes: a comparison between patients and animal models. *Semin Immunopathol, 36*(5), 569-579. doi: 10.1007/s00281-014-0438-4

Lin, H., & Peddada, S. D. (2020). Analysis of compositions of microbiomes with bias correction. *Nature Communications, 11*(1), 3514. doi: 10.1038/s41467-020-17041-7

Liu, T., Zhang, L., Joo, D., & Sun, S.-C. (2017). NF-κB signaling in inflammation. *Signal Transduction and Targeted Therapy, 2*(1), 17023. doi: 10.1038/sigtrans.2017.23

Nicklas, W., Deeny, A., Diercks, P., Gobbi, A., Illgen-Wilcke, B., & Seidelin, M. (2010). FELASA guidelines for the accreditation of health monitoring programs and testing laboratories involved in health monitoring. *Lab Animal, 39*(2), 43-48. doi: 10.1038/laban0210-43

Orsatti, C. L., & Sforcin, J. M. (2012). Propolis immunomodulatory activity on TLR-2 and TLR-4 expression by chronically stressed mice. *Nat Prod Res, 26*(5), 446-453. doi: 10.1080/14786419.2010.482049

Pilström, B., Björk, L., & Böhme, J. (1995). Demonstration of a TH1 cytokine profile in the late phase of NOD insulitis. *Cytokine, 7*(8), 806-814. doi: 10.1006/cyto.1995.0097

Pugliese, A. (2016). Insulitis in the pathogenesis of type 1 diabetes. *Pediatr Diabetes, 17 Suppl 22*(Suppl Suppl 22), 31-36. doi: 10.1111/pedi.12388

Rifa'i, M., & Widodo, N. (2014). Significance of propolis administration for homeostasis of CD4(+)CD25(+) immunoregulatory T cells controlling hyperglycemia. *Springerplus, 3*, 526. doi: 10.1186/2193-1801-3-526

Šturm, L., & Ulrih, N. P. (2020). Advances in the Propolis Chemical Composition between 2013 and 2018: A Review. *eFood, 1*(1), 24-37. doi: 10.2991/efood.k.191029.001

Sy, L. B., Wu, Y. L., Chiang, B. L., Wang, Y. H., & Wu, W. M. (2006). Propolis extracts exhibit an immunoregulatory activity in an OVA-sensitized airway inflammatory animal model. *Int Immunopharmacol, 6*(7), 1053-1060. doi: 10.1016/j.intimp.2006.01.015

Vaure, C., & Liu, Y. (2014). A comparative review of toll-like receptor 4 expression and functionality in different animal species. *Front Immunol, 5*, 316. doi: 10.3389/fimmu.2014.00316

Vind, J., Engelsen, Søren B., Jørgensen, Henrik M., Antvorskov, Julie C., Josefsen, K., & Aru, V. (2026). Comparative 1H NMR Metabolomics Between Scandinavian Propolis and Australian Propolis: The Quest to Identify Radical Scavenging Compounds. *Magnetic Resonance in Chemistry, 64*(4), 438-450. doi: 10.1002/mrc.70082

Vind, J. P., Aru, V., Jørgensen, H. M., Antvorskov, J. C., Tekin, H., Josefsen, K., & Engelsen, S. B. (2026). Comparative spectroscopic analysis of bee propolis: NIR, FT-IR, FT-Raman and 1H NMR. Focus on provenance and antioxidative correlation. *Pharmacological Research - Natural Products, 10*, 100578. doi: 10.1016/j.prenap.2026.100578

Wang, K. S., Ritz, J., & Frank, D. A. (1999). IL-2 Induces STAT4 Activation in Primary NK Cells and NK Cell Lines, But Not in T Cells1. *The Journal of Immunology, 162*(1), 299-304. doi: 10.4049/jimmunol.162.1.299

Yu, C., Wang, D., Yang, Z., & Wang, T. (2022). Pharmacological Effects of Polyphenol Phytochemicals on the Intestinal Inflammation via Targeting TLR4/NF-κB Signaling Pathway. *Int J Mol Sci, 23*(13). doi: 10.3390/ijms23136939

Zhu, H., Li, C., Jia, L., Qiao, J., El-Seedi, H. R., Zhang, Y., & Zhang, H. (2024). Supercritical CO2 extracts of propolis inhibits tumor proliferation and Enhances the immunomodulatory activity via activating the TLR4-MAPK/NF-κB signaling pathway. *Food Research International, 196*, 115137. doi: 10.1016/j.foodres.2024.115137

Zhu, L., Zhang, J., Yang, H., Li, G., Li, H., Deng, Z., & Zhang, B. (2023). Propolis polyphenols: A review on the composition and anti-obesity mechanism of different types of propolis polyphenols. [Review]. *Frontiers in Nutrition, 10*. doi: 10.3389/fnut.2023.1066789

Zhu, Y., Chen, B., Zhang, X., Akbar, M. T., Wu, T., Zhang, Y., . . . Shen, Q. (2024). Exploration of the Muribaculaceae Family in the Gut Microbiota: Diversity, Metabolism, and Function. *Nutrients, 16*(16). doi: 10.3390/nu16162660